OPTIMIZATION OF FLUORESCENCE TECHNIQUES TO STUDY THE AUTOPHAGY PATHWAY AND INVESTIGATION OF KERATIN'S IMPACT ON AUTOPHAGY IN HEK 293 CELLS

A thesis presented to the faculty of the Graduate School of Western Carolina University in partial fulfillment of the requirements for the degree of Master of Science in Biology

By

Melissa Ruth Rogers

Advisor: Dr. Heather Coan, Associate Professor, Biology Department

Committee Members: Dr. Amanda Storm, Associate Professor, Biology Department, & Dr. Robert Youker, Associate Professor, Biology Department

June 2024

ACKNOWLEDGEMENTS

First, I would like to express my appreciation to my primary advisor, Dr. Heather Coan, for helping me with this study. She has been a wonderful mentor to me over these past few years and has played a pivotal role in my success as a student at Western Carolina University. I would also like to thank my committee, Dr. Robert Youker and Dr. Amanda Storm, for teaching me laboratory techniques and helping me troubleshoot my western blots. I would like to thank Dr. Jacob Heiling for providing feedback on the readability of my thesis. I would also like to thank Dr. Joe Bill Mathews for mentoring me during my time at Western Carolina University, as well as Dr. Karen Kandl for being a wonderful TA supervisor. Finally, I would like to thank my friends for cheering me on during all the parts of grad school: Kate and Andrew Donnell, Jessie and Eli Clapp, Anna and Jacob Fletcher, Matthew Dernberger, Missi Bowman, and Griffin Johnson.

TABLE OF CONTENTS

LIST OF FIGURES

LIST OF ABBREVIATIONS

Introduction	
3-MA	3-Methyladenine
AMPK	AMP-Activated Protein Kinase
ATG proteins	Autophagy-Related Proteins
ATG1	Autophagy-Related Protein 1
ATG12	Autophagy-Related Protein 12
ATG13	Autophagy-Related Protein 13
ATG16L1	Autophagy-Related Protein 16L1
ATG29	Autophagy-Related Protein 29
ATG3	Autophagy-Related Protein 3
ATG4	Autophagy-Related Protein 4
ATG5	Autophagy-Related Protein 5
ATG6	Autophagy-Related Protein 6
ATG7	Autophagy-Related Protein 7
ATG8	Autophagy-Related Protein 8
ATG9	Autophagy-Related Protein 9
Aβ peptides	Amyloid-Beta Peptide
BECN1	Beclin-1
CHIP	Carboxyl Terminus of HSC70-Interacting Protein
DEPTOR	DEP Domain-Containing mTOR-Interacting Protein
EGFP	Enhanced Green Fluorescent Protein
ESCRTS	Endosomal Sorting Complexes Required for Transport
FIP200	Fak Family-Interacting Protein of 200 kDa
FYCO1	FYVE and Coiled-Coil Domain-Containing 1
GABARAP	y-aminobutyric acid receptor-associated protein
GAPDH	Glyceraldehyde 3-Phosphate Dehydrogenase
HOP	HSP70-HSP90 Organizing Protein
HOPS	Homotypic Fusion and Protein Sorting Complex
HSC70	Heat-Shock Cognate Protein 70
HSP40	Heat-Shock Protein 40
KAPs	Keratin Associated Proteins
LAMP-2A	Lysosome-Associated Membrane Protein 2A
LC3	Microtubule-Associated Proteins 1A/1B Light Chain 3B
LIR Domain	LC3-Interacting Region Domain

mCherry	Monomeric Cherry
MDC	Monodansylcadaverine
MLST8	mTOR Associated Protein, LST8 Homolog
mTOR	Mammalian Target of Rapamycin
mTORC1/2	mTOR Complex 1/mTOR Complex 2
NBR1	Neighbor of BRCA Gene 1
ORP1L	Oxysterol-Binding Protein-Related Protein 1L
PI3KC3	Phosphatidylinositol 3-Kinase Catalytic Subunit Type 3
PI3P	Phosphatidylinositol 3 Phosphate
PIK3R4	Phosphoinositide 3-Kinase Regulatory Subunit 4
PLEKHM1	Pleckstrin Homology and RUN Domain Containing M1
PRAS40	Proline-Rich Akt Substrate of 40 kDa
qPCR	Quantitative Polymerase Chain Reaction
RAPTOR	Regulatory-Associated Protein of mTOR
RILP	Rab-Interacting Lysosomal Protein
SNAP29	Synaptosome-Associated Protein 29
SNARE	Soluble N-ethylmaleimide Sensitive Factor Attachment Protein Receptor
STX17	Syntaxin 17
TAX1BP1	TAX1-Binding Protein 1
TNFα	Tumor Necrosis Factor α
ULK1	Unc-51-like Kinase 1
UVRAG	UV Radiation Resistance Associated Gene
VAMP8	Vesicle-Associated Membrane Protein 8
WIPI	WD Repeat Domain Phosphoinositide-Interacting

Materials & Methods	
DMSO	Dimethylsulfoxide
DMEM	Dulbecco's Modified Eagle Medium
FBS	Fetal Bovine Serum
PBS/PBST	Phosphate Buffered Saline/Phosphate Buffered Saline Tween
RIPA	Radioimmunoprecipitation Assay
BSA	Bovine Serum Albumin
SDS-PAGE	Sodium Dodecyl Sulfate Polyacrylamide Gel Electrophoresis
TEMED	Tetramethylethylenediamine
SDS	Sodium Dodecyl Sulfate
APS	Ammonium Persulfate
PVDF	Polyvinylidene Fluoride

FIJI	FIJI Is Just ImageJ
ROI	Region of Interest

ABSTRACT

OPTIMIZATION OF FLUORESCENCE TECHNIQUES TO STUDY THE AUTOPHAGY PATHWAY AND INVESTIGATION OF KERATIN'S IMPACT ON AUTOPHAGY IN HEK 293 CELLS

Melissa Rogers, M.S.

Western Carolina University (June 2024)

Advisor: Dr. Heather Coan

Keratin is a class of biomaterial that is isolated from living organisms and is commonly used in the field of tissue engineering as a substrate for cell growth or as a scaffolding material. Studies suggest that keratin may have cytoprotective effects via activation of protein and organelle recycling pathways such as the autophagy pathway. A variety of methods can be used to investigate autophagy in mammalian cells including western blotting, fluorescent imaging, and qPCR. Unfortunately, many of these methods are costly, technical in nature, and can drain lab resources if extensive troubleshooting is required (as is common with western blotting). To address these limitations, the first aim of this thesis was to develop a cheaper, less technical, and easier alternative method of assessing autophagy activity of Human Embryonic Kidney 293 (HEK 293) cells and compare its usability to western blotting and dual-reporter fluorescent imaging. This method uses transfection of a dual reporter fluorescent probe coupled with in-gel fluorescence. The second aim of this thesis was to investigate the relationship between keratin and autophagy in HEK 293 cells. To perform in-gel fluorescence, we transfected HEK 293 cells with a mCherry-EGFP-LC3B plasmid and treated HEK 293 cells with autophagy modulators rapamycin, starvation, and chloroquine. We analyzed the banding pattern of the LC3 protein with in-gel fluorescence in the presence of these modulators by calculating the LC3-II/LC3-I ratios.

For the assessment of keratin's impact on autophagy, we treated nontransfected cells with crude keratin, a fraction containing both structural alpha keratins and keratin accessory proteins, and starvation for 24 hours and analyzed the LC3-II/LC3-I ratios and LC3-II/GAPDH ratios with western blotting. We did not observe that keratin altered the LC3 ratios at 24 hours of treatment. However, we found that in-gel fluorescence allows us to observe statistically significant changes in the LC3-II/LC3-I ratios of negative and positive autophagy controls. This method provides reliable information about autophagy activity via LC3-II/LC3-I ratios and can thus serve as a replacement for western blotting.

CHAPTER ONE: THE AUTOPHAGY PATHWAY

Autophagy is a conserved catabolic process that is essential for the maintenance of cellular homeostasis. During autophagy, cells break down structures such as protein complexes, aggregates, and organelles in order to provide energy, recycle metabolic building blocks, and ameliorate damage due to reactive oxidant species or toxic protein aggregates [1, 2]. Autophagy thus functions as a protective mechanism that can help the cell avoid apoptosis, although this approach is not always successful and sometimes leads to apoptosis and necrosis [3].

Cells are capable of performing three types of autophagy: macroautophagy, microautophagy, and chaperone-mediated autophagy. During macroautophagy, double-membraned vesicles called autophagosomes are assembled by autophagy-related (ATG) proteins. Autophagosomes are capable of engulfing structures that have been marked by the cell for destruction. The autophagosomes fuse with lysosomes, and the low pH of the lysosomal lumen alongside hydrolytic enzymes degrade the contents of the autophagolysosome [4]. Small molecules can then be recycled from the autophagolysosome and used by the cell to complete other processes. During microautophagy, a lysosome or endosome engulfs cargo directly without the intermediate step of fusion to an autophagosome [5]. Microautophagy can be divided into three forms (types I-III). During Type 1 microautophagy, the lysosome protrudes its membrane to surround and engulf structures in the cell. In Type 2 microautophagy, the lysosome engulfs a structure via membrane invagination. In Type 3 microautophagy, an endosome engulfs a structure via membrane invagination. These three types of microautophagy either rely on the soluble *N*-ethylmaleimide sensitive factor attachment protein receptor (SNARE) to engulf cargo (a process termed fusion-type microautophagy), or on the endosomal sorting complexes required

for transport (ESCRTS) (a process termed fission-type microautophagy). The molecular mechanisms of the three types of microautophagy are poorly understood [5]. Microautophagy and macroautophagy can be further subdivided into selective and non-selective autophagy. Non-selective autophagy occurs when a signal such as starvation triggers mass recycling of cytoplasmic material [6]. In contrast, during selective autophagy, specific types of organelles or structures are targeted by the cell and degraded. Examples of selective autophagy include mitochondrial autophagy (mitophagy), protein aggregate autophagy (aggrephagy), and autophagy of invading bacteria (xenophagy) [6].

The third main type of autophagy is chaperone-mediated autophagy. During chaperone-mediated autophagy, individual cytosolic proteins containing the KFERQ amino acid sequence are targeted for lysosomal degradation [4]. About 40% of mammalian proteins contain the KFERQ sequence and can be recycled during this process. The KFERQ sequence allows the chaperone HSC70 heat-shock cognate protein 70 (HSC70) and its cochaperones (carboxyl terminus of HSC70-interacting protein (CHIP), heat-shock protein 40 (HSP40), and HSP70-HSP90 organizing protein (HOP)) to bind the protein in question and deliver it to the lysosome [4]. The lysosome-associated membrane protein 2A (LAMP-2A) contains docking sites for the HSC70-substrate complex and transports the targeted protein directly into the lysosome through a channel [4].

Overview of Macroautophagy

During macroautophagy (hereafter referred to as autophagy), stress signals such as starvation, hypoxia, or rising temperature initiate the formation of double-membraned

compartments called autophagosomes. Figure 1 below illustrates the complexity of this process and the multitude of signaling molecules required for the pathway to occur.

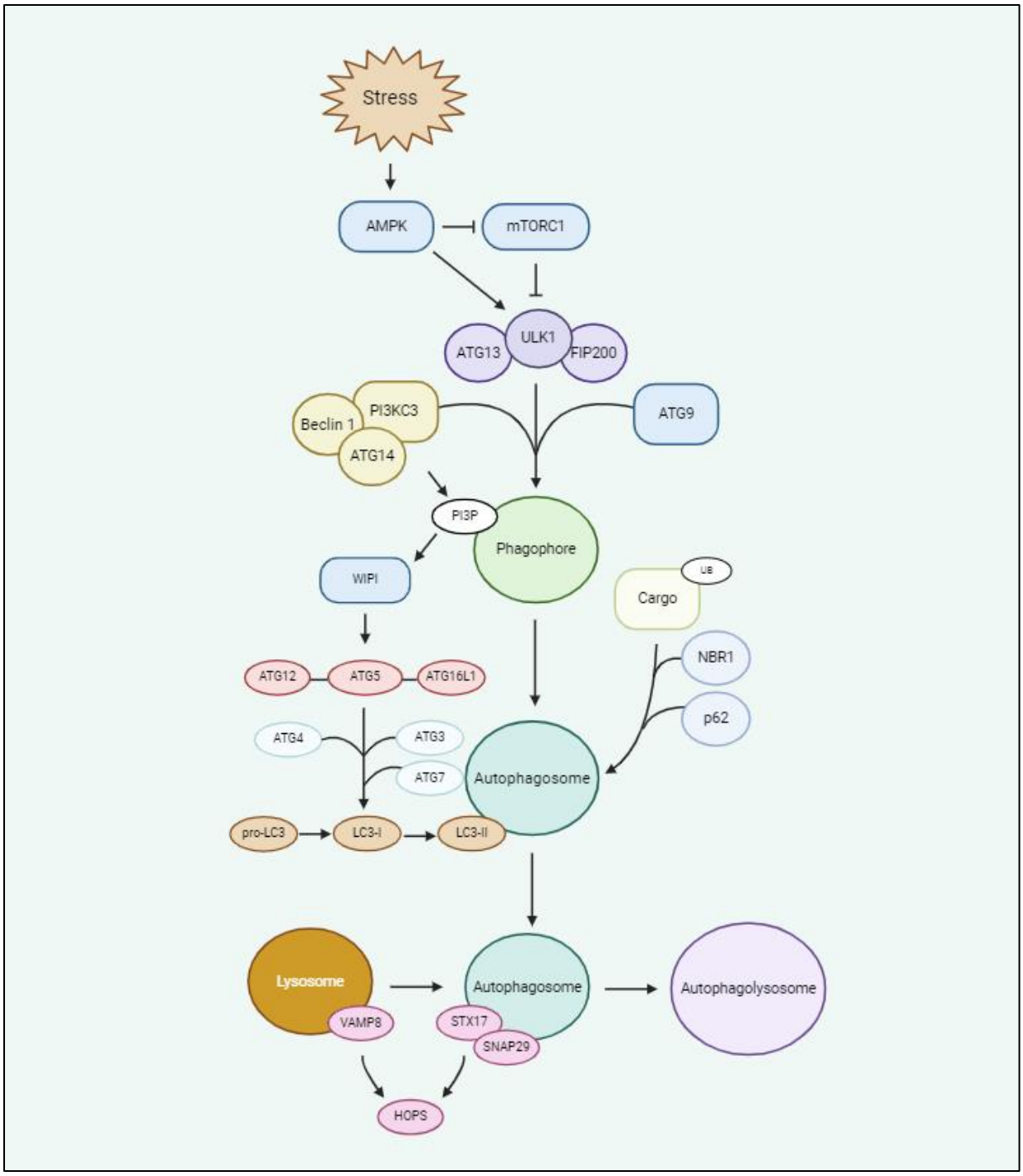
Stress
AMPK
mTORC1
ULK1
ATG13
FIP200
Beclin 1
PI3KC3
ATG14
ATG9
PI3P
Phagophore
WIPI
Cargo
Ub
NBR1
p62
ATG12
ATG5
ATG16L1
ATG4
ATG3
ATG7
Autophagosome
pro-LC3
LC3-I
LC3-II
Lysosome
VAMP8
Autophagosome
STX17
SNAP29
Autophagolysosome
HOPS

Figure 1: The Autophagy Pathway in Mammalian Cells. Stress signals (starvation, heat shock, oxidative stress) trigger the AMP-activated protein kinase (AMPK) to phosphorylate and deactivate the mammalian target of rapamycin (mTOR). AMPK also phosphorylates and activates the unc-51-like kinase (ULK1), which phosphorylates other members of its protein complex: pkt2/fak family-interacting protein of 200 kDa (FIP200) and autophagy-related protein 13 (ATG13). The complex recruits the phosphatidylinositol 3-kinase catalytic subunit type 3 (PI3KC3) complex and autophagy-related protein 9 (ATG9) compartment, which contribute to the development of a young autophagosome, or phagophore. Beclin-1 (BECN1) and PI3KC3 synthesize PI3P on the autophagosome membrane, which recruits the WIPI complex and its downstream effector complex, the ATG12-ATG5-ATG16L1 complex. This complex, alongside the ATG3 and ATG7 proteins, changes the microtubule-associated protein 1A/1B-light chain 3B I (LC3-I) to LC3-II, which joins the membrane of the autophagosome and serves as a docking site for cargo receptors p62 and NBR1. The autophagosome fuses to a lysosome via the combined action of SNARE proteins and tethering factors to create an autophagolysosome, where intracellular cargo can be degraded. *Created with BioRender.com*

In the absence of such stress signals, the mammalian target of rapamycin (mTOR) negatively regulates the autophagy pathway by phosphorylating serine 757 of the Unc-51-like kinase (ULK), a protein essential to the induction of autophagy [7, 8]. Phosphorylation at this site prevents the AMP-activated protein kinase (AMPK) from binding, activating ULK1, and thus initiating autophagy [7, 8].

mTOR is a serine/threonine kinase that belongs to the PI3K-related kinase family and is capable of forming two complexes: mTOR complex 1 (mTORC1) and mTOR complex 2 (mTORC2) [9]. The mTORC1 complex has been implicated in the inhibition of autophagy and contains the mTOR protein, the regulatory-associated protein of mTOR (RAPTOR), the mTOR associated protein, LST8 homolog (MLST8), the proline-rich Akt substrate of 40 kDa (PRAS40), and the DEP domain-containing mTOR-interacting protein (DEPTOR). These accessory proteins serve as scaffolds, docking sites, and stabilizers for downstream effector molecules and have the ability to regulate mTOR activity [9]. When the cell is exposed to a stressor such as amino acid starvation, oxidative stress, hypoxia, heat shock, or protein aggregation, mTORC1 is inhibited by the activation of AMPK and autophagy begins [10]. AMPK inhibits the activity of mTOR by phosphorylating serine 792 of the RAPTOR subunit in the mTORC1 complex [11]. AMPK further stimulates autophagy by phosphorylating serine 317 and 777 of the ULK1 protein [7, 8, 11].

The ULK1 protein belongs to one of five autophagy-related complexes, or ATG proteins. These complexes are a conserved group of proteins that are essential to the formation and growth of autophagosomes. These complexes include the ULK1 complex, the autophagy-related protein 9 (ATG9) complex, the phosphatidylinositol 3-kinase catalytic subunit type 3 (PI3KC3)

complex, the WD repeat domain phosphoinositide-interacting (WIPI) complex, and the ATG12—ATG5–ATG16L complex with its accompanying ATG8 proteins [6, 4, 12].

The ULK1 complex stimulates the formation of the autophagosome after it has been phosphorylated by the AMPK protein. Phosphorylation activates ULK1, causing it to dissociate from mTORC1, autophosphorylate itself, and further phosphorylate two other members of the ULK1 complex: autophagy-related protein 13 (ATG13) and pkt2/fak family-interacting protein of 200 kDa (FIP200) [6]. The ULK complex then localizes to the endoplasmic reticulum at membrane domains termed omegasomes. Omegasomes contain signaling molecules such as phosphatidylinositol 3-phosphate and function as the assembly sites of new autophagosomes called phagophores [6]. The ULK1 complex recruits the second ATG complex (the ATG9 complex) to the phagophore from the Golgi apparatus [6, 13]. The ATG9 proteins travel in recycling endosomes to reach the phagophore, where they then either merge with the phagophore or form a separate “ATG9 compartment” that aids phagophore growth [14]. The ULK1 complex also recruits the third ATG complex, the PI3KC3, to the phagophore via phosphorylation [13]. This complex contains the phosphatidylinositol 3-kinase, phosphoinositide 3-kinase regulatory subunit 4 (PIK3R4), Beclin-1 (BECN1), and autophagy-related protein 14 (ATG14) [14]. These proteins contribute to the movement of the complex to the phagophore, growth of the phagophore, and recruitment of additional ATG complexes. In particular, the ATG14 protein helps the complex find and bind to the phagophore via its amphipathic lipid packing sensor (ALPS) motif. The ALPS motif senses the curvature of the phagophore membrane and binds to it. This binding relocates the ATG14 protein, and thus the rest of the PI3KC3, to the phagophore membrane [13]. PI3KC3 and BECN1 contribute to phagophore growth by creating the lipid

phosphatidylinositol 3-phosphate (PI3P), an essential component of the phagophore [12]. PI3P recruits the fourth ATG complex to the phagophore, called the WIPI complex. The WIPI complex incorporates ATG9 proteins into the phagophore and also recruits the ATG12-ATG5-ATG16L1 complex to the phagophore [6, 7, 13, 14].

The ATG12-ATG5-ATG16L1 complex contributes to the growth of the phagophore by converting ATG8 into a membrane-bound form which is then inserted the membrane of the autophagosome [6]. ATG8 proteins are categorized into two families: the microtubule-associated protein 1A/1B-light chain 3 (LC3) family (containing the LC3A, LC3B, and LC3C proteins) and the y-aminobutyric acid receptor-associated protein family (the GABARAP, GABARAPL1, and GABARAPL2 proteins) [4]. All ATG8 proteins are involved in the process of autophagosome formation and serve as docking sites for the cargo receptors p62 and NBR1 [12, 4].

LC3B (referred to hereafter as LC3) is the best studied of all the LC3 proteins and is frequently used as an indicator of autophagic activity in cells. The LC3 protein exists in a pro-LC3 cytosolic form which is processed at its C-terminal by the cysteine protease autophagy related protein 4 (ATG4). The cleaved product is referred to as LC3-I. This cleavage exposes a glycine residue which is essential for the conversion of LC3-I to its active form, LC3-II. The ATG12-ATG5-ATG16L1 complex works with autophagy-related protein 7 (ATG7) and autophagy-related protein 3 (ATG3) to conjugate LC3-I to a phosphatidylethanolamine (PE) to create LC3-II [6, 7, 13]. LC3-II is then inserted into the autophagosome membrane and serves as a docking site for cargo receptors.

Once the autophagosomes have been formed by the combined effort of the five ATG complexes, they must engulf cargo and migrate towards lysosomes for autophagosome-lysosome

fusion. The engulfment of cargo is mediated by cargo receptors that bind ubiquitin-tagged organelles, escort them to autophagosomes, and dock at the autophagosomes to deliver the cargo [12]. These cargo receptors (such as p62 and NBR1) can interact with both autophagosomes and cargo because they contain LC3 interacting regions that allow them to bind to LC3-II and ubiquitin binding domains that allow them to bind to ubiquitinated cargo.

After the autophagosome has engulfed its cargo, the autophagosome undergoes the removal of LC3 from its outer membrane and the recruitment of kinesin motor proteins to its surface [6]. LC3 proteins, although important to the formation of the autophagosome, must eventually be removed from the outer surface of the autophagosome in order for lysosomal fusion to occur. The recruitment of motor proteins is important for the movement of autophagosomes towards lysosomes so that fusion can occur. The motor proteins attach to the autophagosomes via the help of tethering factors and adaptor proteins. Tethering factors such as the RAB7 protein family of GTPases bind to adaptor proteins FYVE and coiled-coil domain-containing 1 (FYCO1), oxysterol-binding protein-related protein 1L (ORP1L), Rab-interacting lysosomal protein (RILP), and Pleckstrin Homology and RUN Domain Containing M1 (PLEKHM1), facilitating the anchoring of the autophagosomes and lysosomes to motor proteins and microtubules [4]. The motor proteins then carry these vesicles along microtubules, where fusion can occur [14].

Once the autophagosomes and lysosomes are in close proximity, tethering factor proteins facilitate fusion by binding to small GTPases and lipids on the opposing surfaces of autophagosomes and lysosomes in order to bring them together [4, 14]. The autophagosome is equipped with two Q-SNARE proteins (Syntaxin 17 or STX17 and Synaptosome-Associated

Protein 29 or SNAP29) which work to fuse the autophagosome to the lysosome. The STX17 protein is recruited to the membrane of the autophagosome from the endoplasmic reticulum. It recruits the SNAP29 protein to the autophagosome and interacts with a tethering factor needed for fusion (called the homotypic fusion and protein sorting complex, or the HOPS complex) [14]. The HOPS complex coordinates tethering of the autophagosome to the lysosome by facilitating the formation of the *trans*-SNARE complex [14, 15]. STX17 on the autophagosome binds the R-SNARE VAMP8 on the lysosome, thus serving to bring the autophagosome and lysosome together [14, 15]. The activated RAB7 protein acts as a docking site for the HOPS complex [4, 14].

The fusion of the autophagosome to the lysosome results in the degradation of the second lipid bilayer of the autophagosome membrane. The degradation of this membrane by lysosomal hydrolases allows the contents of the lysosome to mix with the autophagosome and degrade its components [14]. LC3-II on the luminal surface of the autophagolysosome is degraded alongside the components of the autophagolysosome. After the contents of the autophagolysosome (such as amino acids and sugars) are degraded, they are released to the cytosol via lysosome efflux transporters [14]. These recycled components can be used to fuel other processes in the cell. The autophagolysosomes are then recycled to create new lysosomes, while the protein ATG4 changes LC3-II found on the cytosolic side of the autophagosome back to LC3-I [16, 17].

Autophagy and Protein Degradation Pathways

Autophagy is a major strategy for the cell to maintain homeostasis during times of stress. In particular, autophagy is used by the cell to regulate the presence of protein aggregates in cells. Protein misfolding and the resulting formation of aggregates can be caused by stressors such as

heat shock and reactive oxygen species [18]. Autophagy can be used to clear these resulting protein aggregates. In this way, autophagy complements two additional mechanisms used by the cell to regulate protein folding and clear protein aggregates: the chaperone system and the ubiquitin-proteasome system [19]. In the chaperone system, chaperone proteins facilitate the folding of client proteins and also bind to misfolded proteins. They recognize hydrophobic stretches of amino acids on partially folded or misfolded proteins and bind to facilitate proper folding [18]. Chaperones mediate the clearance of misfolded proteins by recruiting E3 ligases to transport ubiquitinylated proteins to a complex called the proteasome for destruction.

In the ubiquitin-proteasome system, misfolded substrates are modified by a series of ligases and delivered to the proteasome for destruction. The E1 ligase, or the “ubiquitin activating enzyme”, forms a thio-ester bond with a glycine residue at the C-terminal of a ubiquitin molecule [18]. This interaction allows ubiquitin to be conjugated to the E2 ligase, or the “ubiquitin conjugating enzyme”. The E2 ligase, alongside an E3 ligase termed the “ubiquitin ligase”, binds ubiquitin to lysine residues on a target protein. Ubiquitin molecules linked at the Lysine 48 residue target the protein for destruction via the proteasome, while linkage at other Lysine residues (such as Lysine-63) function as signals for processes such as DNA repair [19]. Polyubiquitination at Lysine-48 signals the recognition of the protein by receptors of the proteasome or by shuttle factors that escort the misfolded proteins to the proteasome [1]. Once the misfolded proteins reach the proteasome, the proteasome senses the ubiquitin molecule with its ubiquitin receptors. The proteasome then uses an AAA+ motor to bind the protein at an unstructured region. The AAA+ motor then unfolds the protein and transports it into the

proteasome [20]. The proteasome then undergoes a series of conformational changes which accommodate the unfolded protein [20].

The proteasome system works on a small scale to degrade individual molecules, while autophagy is capable of degrading larger structures such as aggregates, organelles, and even pathogens [1]. In the event the ubiquitin-proteasome system is overwhelmed, a type of selective autophagy specific for the clearance of protein aggregates (termed “aggrephagy”) can assist with the clearance of proteins [19]. During aggrephagy, cargo receptors p62 and NBR1 recognize and bind to ubiquitinylated protein aggregates by way of their ubiquitin sensing domains. These receptors form hetero-oligomers composed of multiple chains of p62 conjugated to an NBR1. These oligomers surround larger aggregates to assist in their destruction and to signal the formation of the autophagosome directly around the aggregates themselves [19]. The formation of the autophagosome occurs as NBR1 interacts with TAX1 binding protein 1 (TAX1BP1), which in turn recruits FIP200, one of the subunits of the ULK1 complex that assists with autophagosome biogenesis.

There is substantial overlap between the autophagy pathway and the ubiquitin-proteasome system. Both systems rely on ubiquitin as a marker for degradation, as well as receptor proteins to facilitate these processes. For example, the p62 protein has been implicated in both autophagy and the ubiquitin-proteasome system due to its possession of a LC3-interacting region (LIR) domain, an ubiquitin-associated domain, and a proteasome binding domain [1].

Autophagy and Apoptosis

In addition, the autophagy pathway also intersects with apoptosis, or programmed cell death. Apoptosis is characterized by distinct cellular features, such as chromosomal fragmentation and cleavage, membrane blebbing, and cell shrinkage [21]. Apoptosis is activated by two distinct pathways: the extrinsic or death receptor pathway and the intrinsic pathway. In the extrinsic pathway, death ligands bind to death receptors (such as the tumor necrosis factor receptor). This binding promotes the formation of a signaling complex that activates procaspase 8 to activate further caspases [21]. In the intrinsic pathway, stress signals such as radiation, reactive oxygen species, DNA damage, or hypoxia increase the membrane permeability of mitochondria in the cell. This results in the release of cytochrome c into the cytosol of the cell and its subsequent binding to apoptotic protease-activating factor 1 and procaspase 9. This complex is termed the apoptosome complex, and it activates caspases and ultimately results in cell death [21].

Multiple autophagy proteins can be co-opted to enhance the apoptosis response. For example, ATG4, the protein responsible for cleaving pro-LC3 to create LC3-I, is cleaved by caspase 3 during apoptosis, and the resulting ATG4 fragments assist in regulating apoptosis [22]. The N-Terminal fragment of ATG4 functions as a protease, and the C-Terminal fragment is recruited to the mitochondria, where it contributes to cell death by regulating reactive oxygen species. Similarly, the protein BECN1 of the PIKC3 complex is cleaved during apoptosis by caspase 3, where it also goes to the mitochondria and increases the apoptotic response. In contrast, the UVRAG protein of the BECN1 complex inhibits apoptosis by binding to the Bax protein, thus preventing its activation and translocation to the mitochondria [22].

Autophagy in Disease States

Because autophagy is involved in a wide array of cellular stress responses, the dysfunction of the autophagy pathway has been implicated as a causative agent in a diverse array of diseases such as Alzheimer's disease, Parkinson's disease, osteoarthritis, and cancer [23, 24, 25]. As mentioned in the previous section, autophagy is an essential mechanism for the clearance of intercellular protein aggregates, and its dysfunction has been implicated in conditions such as Alzheimer's disease, which involves the buildup of toxic amyloid-beta peptides (Aβ peptides) [25]. In Alzheimer's disease, the abnormal accumulation of amyloid-beta peptides has been observed in autophagosomes and has been attributed to the dysregulation of autophagolysosome maturation [23, 25]. When autophagy is impaired, cells also lack the ability to clear these toxic peptides by secretion [23]. Autophagy functions similarly in Parkinson's disease: it acts as an important quality control mechanism to degrade aggregates of alpha-synuclein and tau. Autophagosome-lysosome fusion is impaired in individuals with Parkinson's disease, contributing to the buildup of these aggregates [26].

Disrupted autophagosome-lysosome fusion has also been implicated in osteoarthritis. Osteoarthritis is characterized by the pathological calcification of cartilage in joints. One study by Yan et al. (2022) observed a failure in the ability of autophagosomes to fuse to lysosomes in osteoarthritic cartilage [24]. This study also reported that extracellular vesicles derived from autophagosomes were the drivers of pathological calcification within joints [24].

Autophagy activity has also been implicated in the development of cancer. It has been documented that cancer cells rely on high background levels of autophagy to maintain their increased metabolic rates and to adapt to environmental stressors. For example, advanced stages

of cancer in mouse models required autophagic activity in order to maintain growth [12]. In addition, blocking autophagy in precancerous cells while simultaneously activating tumor initiators inhibited the ability of cancer cells to reach malignancy [12]. Cancer cells also use autophagy to target specific proteins, such as proteins associated with cellular inflammation, in order to maintain cell viability under less-than-ideal conditions [12].

The principle that autophagy can mediate cancer cell survival during times of stress has garnered the interest of researchers in the field of tissue engineering. Many researchers are investigating how to promote cell survival under less-than-ideal conditions via modulation of the autophagy pathway [3]. One area of interest is how the application of biomaterials can modulate autophagy activity in cells, as will be discussed in chapter two of this thesis.

Techniques for Monitoring Autophagy

Autophagy Modulating Compounds

Changes in autophagy activity are detected by measuring either the ratio between LC3-I and LC3-II in cells or by measuring the ratio between LC3-II and a housekeeping control such as GAPDH. In cells undergoing autophagy, there is generally an increase in the LC3-II protein relative to the LC3-I protein. When the LC3-II/LC3-I ratios are calculated, there is generally a higher ratio in samples undergoing autophagy compared to samples not undergoing autophagy. There is also generally an increase in the LC3-II proteins of samples undergoing autophagy compared to those not undergoing autophagy. This results in a generally increased LC3-II/GAPDH ratio in samples undergoing autophagy compared to those not undergoing autophagy.

Researchers studying autophagy must use an autophagy-stimulating drug such as rapamycin to serve as a positive control. Rapamycin stimulates autophagy by binding to the mTOR protein of the mTOR complex 1. It does so by first forming a complex with the FK506-binding protein in the cytosol of the cell [6, 28]. Together, these proteins bind and inhibit the activity of mTOR. Thus, treatment of rapamycin results in an increase in the cellular levels of LC3-II, resulting in a high LC3-II/LC3-I ratio, or a high LC3-II/GAPDH ratio compared to a negative control. One example of a negative control used to block autophagy is the compound 3-methyladenine, or 3-MA. 3-MA inhibits the ability of the PI3KC3 complex to stimulate the production of the signaling molecule PI3P on the surface of growing autophagosomes [29]. This prevents the growth and maturation of the autophagosome and thus blocks autophagy [29].

In addition to using positive and negative controls, treatment groups for studying autophagy should be compared to control groups dosed with compounds that induce a blockage in autophagosome-lysosome fusion. These controls are necessary because an increase in LC3-II relative to LC3-I can indicate either an increase in autophagic activity or a block in autophagosome-lysosome fusion. One commonly used drug to block autophagosome-lysosome fusion is chloroquine. When chloroquine is used to block autophagy, the LC3-II/LC3-I ratios in the chloroquine group should be higher than the LC3-II/LC3-I ratios in the treatment group [27].

Western Blotting

One of the most common approaches to track autophagic activity in cells involves using western blotting to monitor the expression and modification of the LC3 protein as it goes back and forth between its LC3-I and LC3-II forms. When autophagy levels in a cell are low, LC3 is distributed throughout the cytosol as LC3-I. When autophagy begins, LC3-I is conjugated to a

phosphatidylethanolamine and joins the membrane of autophagosomes as LC3-II [7, 13]. As autophagy progresses, the autophagosomes containing LC3-II will fuse to lysosomes, and LC3-II on the interior of the autophagolysosome will be degraded. At the same time, LC3-II on the exterior of the autolysosome will be recycled, cleaved by the protein ATG-4 to return to its cytosolic form [16, 17]. Western blotting can be used to calculate the ratio of the band densities of LC3-II to LC3-I or LC3-II to a housekeeping protein such as GAPDH. In samples undergoing autophagy, the LC3-II/LC3-I ratio should generally be increased compared to a sample not undergoing autophagy.

Another common protein used to study autophagy via western blotting is p62. p62 is a cargo receptor that is equipped with domains that allow it to bind to both ubiquitinated cargo in the cell and the LC3 protein. This binding allows p62 to sequester cargo marked for destruction, transport it to the membrane of an autophagosome containing LC3-II, bind to LC3-II, and thus deliver cargo to the autophagosome. In the process of delivering cargo to the autophagosome, p62 is also taken up by the autophagosome [27]. When the autophagosome fuses to the lysosome, p62 will be degraded. Thus, a western blot of cells undergoing autophagy should generally demonstrate a decrease in p62 protein banding. Blocked autophagy, on the other hand, should generally result in an increase in p62 protein banding [27].

Other examples of proteins that are probed via western blotting to study autophagy include BECN1, which increases in band size on a western blot due to autophagy stimulation, and the ATG-5 and ATG-12 proteins, which, upon induction of autophagy, form a conjugate that can be visualized at the 50-kDa mark on a western blot [30, 31].

Dual-Reporter Fluorescent Imaging

In addition to western blotting, the autophagy controls mentioned above can be used with a dual-reporter fluorescence imaging technique to detect changes in autophagy activity. In dual-reporter fluorescence imaging, cells are transfected with a plasmid coding for the LC3B protein conjugated to two fluorescent tags (EGFP and mCherry). The EGFP-LC3-mCherry construct allows researchers to observe different stages of autophagy indicated by pH fluctuations in the cell. As the pH changes in the autophagosomes and lysosomes throughout the course of autophagy, the intensity of fluorescence emitted by the GFP-mCherry construct follows a predictable pattern that can yield valuable information about the autophagic state of the cell. For example, when autophagy is not occurring or when cells have been treated with the autophagy inhibitor 3-MA, diffuse red and green fluorescence can be observed in the cytosol of the cell (Figure 2.A). When autophagy has been stimulated by treatment with rapamycin, the diffuse fluorescence is replaced by the formation of red and green puncta (Figure 2.B). This indicates the conversion of LC3-I to autophagosome-bound LC3-II and signals the beginning of autophagy. Overlaid images taken with filters optimized for both GFP and mCherry show yellow puncta. When autophagy progresses to the autophagosome-lysosome fusion stage, the pH of the autophagolysosome drops, the green signal is quenched, and the puncta appear red (Figure 2.C) [27]. If autophagosome-lysosome fusion is inhibited with chloroquine, the green signal will persist, and the puncta will still appear yellow. After taking images of samples at different stages of autophagy, the percentage of cells with green, yellow, and red puncta can be calculated via manual counting to determine whether cells are undergoing low levels of autophagy, the early stages of autophagy, or the late stages of autophagy.

Western blotting and dual-reporter fluorescence imaging are commonly used techniques to evaluate autophagy in cells. The Coan lab has attempted to use western blotting and dual-reporter fluorescence to study keratin's relationship to autophagy, but these techniques present several challenges. Western blotting is expensive, time consuming, and difficult for labs to maintain. In addition, dual-reporter fluorescence techniques to quantify autophagy are subjective and error prone. Typically, many images are required to analyze autophagy and the transfection system cannot be easily automated to count cells and track puncta. Manual counting of dimly fluorescing cells is prone to bias and is time-consuming. This bias can be reduced by having multiple individuals blindly count cells in images or by using software systems to automate cell counting. Despite these options, the high seeding densities required for LC3 plasmid transfection and thus high rates of confluency complicate the ability to accurately count cells manually or successfully use automated cell counting tools. In addition, the dual-reporter fluorescence system does not allow users to distinguish between early autophagy activity and blocked autophagosome-lysosome fusion in cells [32]. With this system, it is difficult to quantify the autophagy response in real time unless autophagy is measured under non-steady-state conditions [32]. Dual-reporter fluorescence techniques are also not quantitative, and while they serve as a complement to other methods of collecting data, a more quantitative system is needed. Thus, the field of autophagy research has need of a less expensive, less time-consuming, and more quantitative method for autophagy analysis.

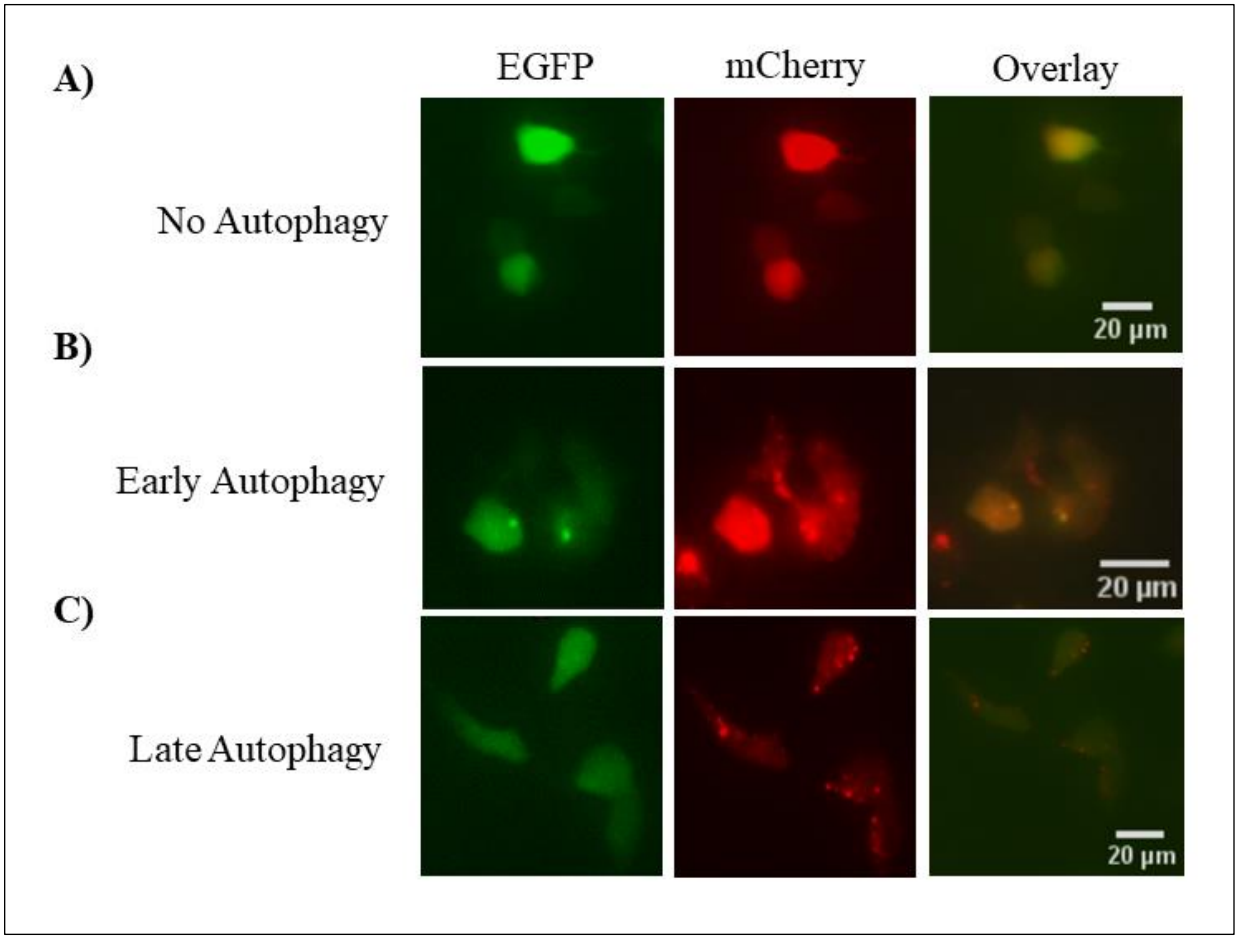

Figure 2: Dual-Reporter Fluorescence to Detect Autophagy. A: Transfected cells without autophagy activity display diffuse fluorescence emanating from the EGFP-mCherry-LC3B protein. B: Transfected cells undergoing early-stage autophagy display red and green puncta. C: Transfected cells undergoing late-stage autophagy display red puncta only.

Quantitative PCR

Another commonly used system for the analysis of cell death-related pathways (autophagy, apoptosis, and necrosis) is quantitative PCR (qPCR). During qPCR, DNA amplification results in the accumulation of a fluorescent signal. The amount of fluorescent signal correlates to the number of DNA copies present. This signal is measured at each PCR cycle number and allows users to quantify the initial number of copies of DNA present from a sample [33]. This system results in a data set which can be used to determine differential gene expression between treatment groups. Genes that may result in increased mRNA levels upon the induction of autophagy include *ATG1, ATG6, ATG7, ATG8/LC3, GABARAPL1, ATG9, ATG12, ATG13, ATG14, p62, ATG29,* and *WIPI1* [25]. Poranki and Van Dyke (2014) used qPCR to study the gene expression of autophagy, apoptosis, and necrosis-related genes in primary mouse fibroblasts exposed to heat shock treatment. Relative up or down regulation of genes was determined by taking the ratio of the gene expression fold change for a treatment group and a control group. A low ratio (less than 1) was considered indicative of higher gene expression of a given gene in the control group, a ratio of 1 or close to 1 was indicative of a similar gene expression change between the treatment group and control group, and a ratio greater than 1 was indicative of a higher gene expression in the treatment group relative to the control (Poranki and Van Dyke, 2014).

CHAPTER TWO: KERATIN BIOMATERIALS

Biomaterials

Biomaterials are natural or synthetically-derived substances that are used to support or replace tissue function in living organisms [34]. Biomaterials can be characterized based upon their chemical structures as either metal, ceramic, polymer, or composite. Metal biomaterials made of magnesium, titanium, cobalt, or steel are used to create structures such as artificial joints, dental implants, and cardiovascular stents [35]. Ceramic biomaterials are made of materials such as glass, clays, whiteware, refractory materials, abrasives, or cements and are used to make similar implants due to their ability to mimic tissues of the body, their biocompatible properties, and their resistance to wear [36]. Polymeric biomaterials are used to create scaffolds, films, and hydrogels for cell attachment, growth, and regeneration [37]. Examples of natural polymeric biomaterials include gelatin, collagen, and keratin, whereas examples of synthetic polymeric biomaterials include polyvinyl alcohol or polylactic acid. Composite biomaterials are engineered with two or more types of biomaterials in order to take advantage of the different qualities of the biomaterials. Typically, composite biomaterials are composed of a matrix surrounding another material called an inclusion [38].

Biomaterials can also be characterized based upon the degree of interaction they maintain with their hosts: as either bioactive or bioinert [36]. Bioactive materials can create and direct a biological response within their hosts. Examples of such biological responses are stem cell differentiation, cell proliferation, or tissue regeneration [39]. Bioinert materials, on the other hand, interact minimally with their hosts and thus do not direct a biological response [40]. A

third characteristic of a biomaterial is its biocompatibility. Materials introduced into the body can invoke an immune response, causing inflammation mediated by macrophages and the development of a fibrous capsule around the material. Biocompatible materials can minimize this response [40]. Biocompatibility can be tested by implanting a material within a tissue and monitoring the immune response to assess the formation of a fibrous capsule around the material. The material is considered to be biocompatible if the capsule is within a given thickness range and there are no signs of an acute inflammatory reaction after a given period of time [41].

Early biomaterial research in the 1960s and 1970s centered on the development of bioinert materials with the goal of minimizing the host immune response to an implant [34]. During the 1980s, the perspective of the field shifted towards the development of bioactive materials that would interact with the surrounding tissue to promote healing as opposed to an inflammatory response [42]. Today, biomaterials are designed to optimize biocompatibility and bioactivity and are used to create a host of devices commonly used in the clinical setting, such as orthopedic joint implants, dental implants, artificial heart valves, and devices to enhance wound healing [42].

Keratin Biomaterials

One priority in the field of biomaterials is to maximize the use of naturally abundant, biodegradable, and inexpensive substances for biomaterials research and applications [43]. To this end, researchers have studied natural polymers with increased attention, and one such polymer is the protein keratin. Keratin is the major structural component of hair, hooves, wool, horns, and feathers [43]. It is abundantly available in nature. For example, the human scalp

contains approximately 10^5 terminal hair strands, and an average of 90g of hair per individual (assuming the individual is maintaining the same hair length) is cut and disposed of each year [44]. The sheer abundance of keratin derived from human hair opens opportunities for its use as a cost-effective, renewable biomaterial for a range of medical applications [44].

The anatomy of the human hair can be divided into three main parts: the cuticle, cortex, and medulla. The cuticle is the outmost layer of the hair fiber. It contains a layer of 5-10 keratinized cells that serve as a protective layer against mechanical and environmental stressors. These cells are bound together by a cell membrane complex [45]. Beneath the cuticle of the hair fiber is the cortex, which comprises the main part of the human hair. Within the cortex is a mixture of cells, intermediate filaments, and keratin proteins. The cortex contains 12 types of keratin proteins and over 100 types of keratin-associated proteins (KAPs). These KAPs, alongside keratins, make up the main structure of the cortex. The middle portion of the hair shaft is the medulla. The medulla contains a mixture of cells and provides tensile strength to the hair shaft [45].

Keratins are part of the intermediate filament superfamily of proteins and are classified into two basic types according to their isoelectric points [46]. Type I keratins are acidic and have an isoelectric point ranging from 4.9-5.4, whereas type II keratins are basic and have their isoelectric points ranging from 6.5-8.5 [46]. All keratins are resistant to degradation when exposed to the proteases pepsin and trypsin. In addition, keratins are insoluble in a range of solutions such as acids, bases, water, or organic solvents. However, keratins can be dissolved in denaturing agents such as urea and can be extracted from tissues by the application of reducing agents [46]. These reducing agents break the disulfide bonds that link keratins together.

Humans have 54 functional keratin genes in their genome [47]. 37 of these genes pertain to epithelial keratin, and 17 of these genes pertain to hair keratin [48]. The secondary structure of a keratin protein is composed of three main domains: an N-Terminal head domain, a rod domain, and a C-Terminal head domain (Figure 3.A). The head domains range from 50-100 amino acids in length and have a positive charge. These domains are globular and contain beta turns. The inner rod domain is negatively charged, contains approximately 310 amino acids, and is divided into four subdomains: 1A, 1B, 2A, and 2B (Figure 3.A) [46, 48]. The rod domain is capable of forming either an alpha helix or a beta sheet in its secondary structure, and keratins can be further classified as alpha or beta keratins based upon the secondary structure of their rod domain. Beta keratins are found in reptiles and birds and compose claws, scales, beaks, and feathers. Alpha keratins are common to all vertebrates [46]. These conserved domains contain repeats of seven amino acids in which the first and fourth amino acids in the pattern are nonpolar. These repeats form the backbone of one turn in the alpha helix and thus contribute to the helical shape of the keratin protein, in addition to the coiled-coil formation of keratin heterodimers [46]. In addition, the four domains of the inner rod domain are separated by non-helical domains, or linkers: L1, L12, and L2 (Figure 3.A) [48]. The organization of keratin fibers found in human hair begins as keratin monomers form secondary structures composed of right-handed alpha-helices stabilized by hydrogen bonds [49]. Two alpha helices associate to form a coiled-coil dimer, and two dimers associate to form a tetramer called a protofilament. Two protofilaments form a protofibril, and two protofibrils form an intermediate filament. The intermediate filaments are themselves the main structural component of keratin [43].

Intermediate filaments can group together to create macrofibrils, which then associate to form keratin fibers (Figure 3.B) [49].

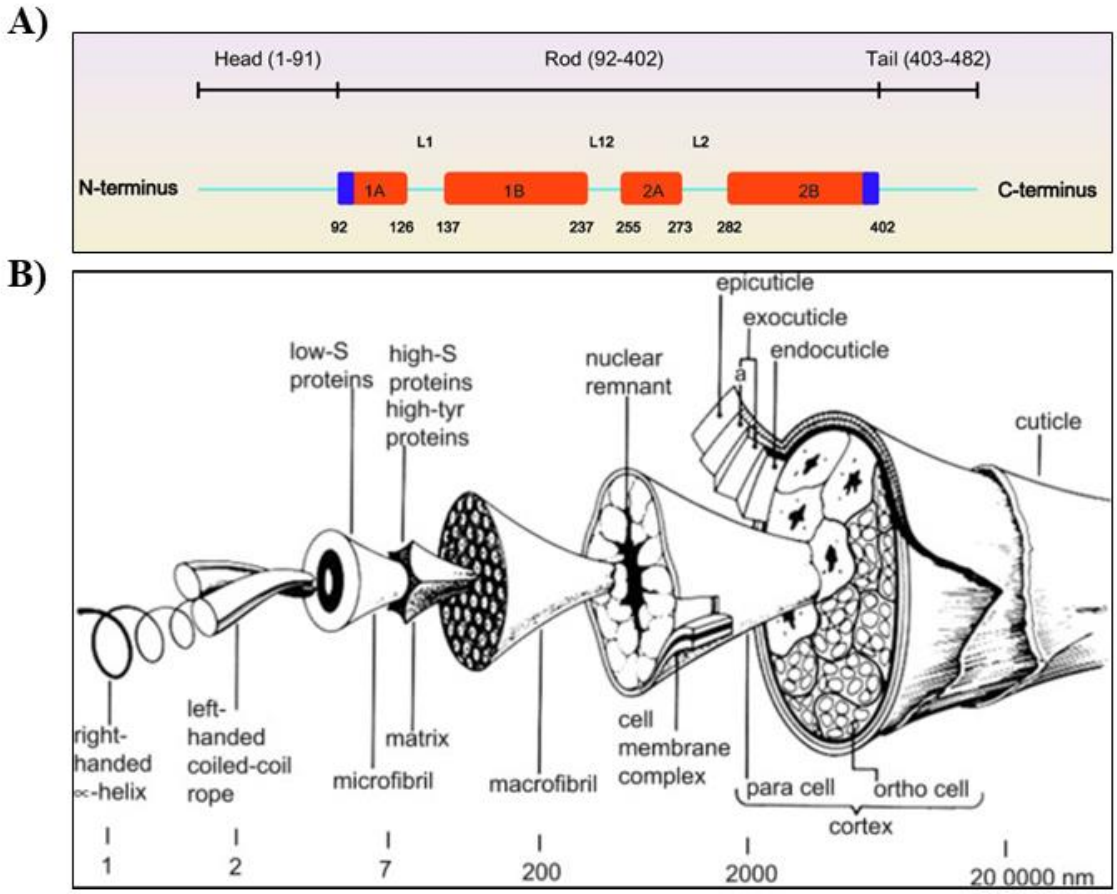

Figure 3: Keratin domains and diagram of hair fiber. **A:** Schematic representation of the domains in the structure of keratin 8. An inner rod domain is separated by a N-terminal and C-terminal head domain. The inner rod domain is composed of four subdomains separated by linkers. *Image credits: Kim HJ, Choi WJ, Lee CH. Phosphorylation and Reorganization of Keratin Networks: Implications for Carcinogenesis and Epithelial Mesenchymal Transition. Biomol Ther (Seoul). 2015 Jul;23(4):301-12. doi: 10.4062/biomolther.2015.032* [50]. **B:** Diagram of keratin molecules associating to form a hair fiber. Image credits: *Hill P, Brantley H, Van Dyke M. Some properties of keratin biomaterials: kerateines. Biomaterials. 2010 Feb;31(4):585-93. doi: 10.1016/j.biomaterials.2009.09.076* [51].

Keratin derived from human hair is used as a structural biomaterial due to its ability to promote cell adhesion and proliferation in tissue culture models and mouse models [51, 52]. The proliferative properties of keratin have been attributed to repeated amino acid sequences (leucine-aspartic acid-valine and glutamic acid-aspartic acid-serine) that enhance cell attachment by serving as a binding site for integrin proteins on the surface of the cell [51, 52, 53]. The increased cell binding capacities of keratin underly its usefulness as a biomaterial in cell culture studies and *in vivo* studies. For example, application of keratin hydrogel fillers to nerve conduits placed at peripheral nerve injuries resulted in a greater recovery of the electrophysiological function of the nerves compared to empty conduit and autograft models [54]. Similarly, complementing a keratin scaffold with Schwann cells to create an artificial nerve graft increased sciatic nerve function and nerve regeneration in a sciatic nerve injury animal model [55]. An additional study found that application of keratin hydrogels to a lethal model of liver injury facilitated hemostasis by stabilizing blood loss, mean arterial pressure, and shock index. The authors speculate that keratin prompted blood clot formation, physically sealed the site of injury, and acted as a scaffold for cell permeation [56].

Keratin has also been studied for its protective effects upon cells exposed to stress. One study investigated keratin's ability to modulate gene expression in an *in vitro* burn model. Exposure to high temperatures can result in cell necrosis, apoptosis, or autophagy, depending on the severity of the burn and proximity of the cells to the heat source [3]. Poranki and Van Dyke investigated the ability of keratin to regulate gene expression of necrosis, apoptosis, and autophagy-related genes in fibroblasts exposed to heat shock. They reasoned that the upregulation of autophagy by keratin, in contrast to the upregulation of necrosis and apoptosis,

could potentially contribute to the increased survival of these cells. At 12 and 18 hours post heat shock, the greatest change in gene expression was noted specifically in autophagy genes, suggesting increased autophagy activity in the cells exposed to keratin [3]. However, no follow-up studies were undertaken to further probe whether autophagy proteins were being generated as a result of the increased gene expression or whether those proteins were active in the autophagy pathway. Additional studies regarding the expression and modulation of autophagy-specific proteins are needed to further understand the relationship between autophagy and keratin.

A small body of research suggests that other structural biomaterials such as gelatin and chitosan also have the ability to modulate autophagic activity. Chitosan is a polymer formed by the deacetylation of chitin [57]. Several studies investigating chitosan suggest that chitosan is capable of stimulating the autophagy pathway in cell cultures and rat models treated with chitosan. Sutthasupha et al. (2022) use chitosan oligosaccharide to investigate the impacts of the biomaterial on the expression of autophagy-related markers in prediabetic rats. They found that the administration of chitosan increased autophagic markers such as BECN1, ATG5, and LC3, thus suggesting an increase in autophagy activity [58]. Yang et al. (2015) grew adipose derived stem cells on chitosan substrates and observed an increase in autophagic activity as evidenced by increased LC3-II/GAPDH ratios. They also observed an increase in the mRNA levels of ULK1 with the treatment of chitosan, a protein involved in autophagosome formation [57]. Pan et al. (2021) also observed an increase in autophagy and apoptosis in osteosarcoma cell lines treated with chitosan [59].

Similar to chitosan, one study investigated the impact of gelatin on L929 cell morphology, growth, and response to the inflammatory mediator Tumor Necrosis Factor α

(TNFα). Gelatin is a protein and is the denatured form of collagen [60]. In this study, the authors claim that western blot analysis and monodansylcadaverine (MDC) positive ratio analysis suggested that the application of gelatin alone and gelatin combined with TNFα increased autophagy activity in the cells [60]. MDC is a dye that collects in autophagic vesicles, and an increase in autophagic activity is thought to result in an increase in MDC positive structures. However, the authors of this study did not quantify the intensities of their LC3 bands, calculate LC3-II/LC3-I or LC3-II/loading control ratios, or use controls to distinguish between blocked autophagy and increased autophagy in their data set. In addition, the MDC dye is not specific to autophagic vesicles alone and can localize to other compartments, such as endosomes. Although MDC fluorescence can suggest an increase in autophagic activity, it must be combined with additional methods to accurately understand autophagic activity [61]. In addition, this method alone is also unable to distinguish between increased autophagic activity and dysfunctional autophagosome-lysosome fusion. Although these studies seem to point to a clear increase in autophagic activity in cells grown with these biomaterials, these studies suffer from a lack of positive and negative controls that are necessary to draw conclusions about autophagy in cells. Without these controls, there is no reference to determine whether autophagic activity is truly increased or whether there is a blockage in autophagosome-lysosome fusion. Therefore, the link between autophagy and structural biomaterials needs to be further clarified.

To follow up on Poranki and Van Dyke's (2014) study on autophagy and keratin, our lab has performed experiments with HEK 293 cells grown with crude keratin extract to test keratin's potential relationship to the autophagy pathway and cell degradation and recycling pathways [3, 62, 63]. Crude keratin is the insoluble fraction of keratin that contains the large, alpha keratins

discussed earlier in this introduction, in addition to the keratin-associated proteins (gamma keratins). Crude keratin is often used for cell attachment and is considered to be less bioactive relative to other forms of keratin. Gamma keratins are small (10-16 kDa), globular proteins that are soluble and compose the keratin-associated proteins. These keratins appear to be more bioactive and may be cytoprotective in nature [3].

Our experiments with crude keratin used transfection and fluorescent imaging as previously described in this introduction to measure both autophagy activity and protein degradation. In protein degradation experiments, cells were transfected with a plasmid coding for the GFP-250 protein, which forms aggregates when expressed by the cell [64]. Protein aggregation experiments showed that cells treated with crude keratin at the 30-minute timepoint contained fewer aggregates compared to untreated cells, suggesting the more rapid clearance of these aggregates in the presence of keratin. Experiments with keratin and starvation also revealed a potential relationship to autophagy. During these experiments, cells were transfected with the mCherry-EGFP-LC3B construct and treated with total starvation for 4 hours. Dual-reporter fluorescence images were taken at various timepoints during this four-hour time period. At two hours post treatment with starvation, cells treated with keratin displayed higher levels of early and late-stage autophagy compared to cells treated with keratin alone or heat shock alone. These experiments suggest a relationship between keratin and autophagy in HEK 293 cells, but more experimentation is necessary to elucidate keratin's relationship to autophagy.

CHAPTER 3: THESIS AIMS

In order to further investigate keratin's impact on autophagy, our lab has need of a method for the analysis of autophagy that sidesteps the challenges inherent with western blotting and dual-reporter fluorescent imaging. *Therefore, the first aim of my thesis is to develop an in-gel fluorescence technique to analyze the autophagy pathway and compare its usability to western blotting and dual-reporter fluorescence.* The method expanded on and refined the well-documented autophagy-tracking technique discussed previously that used a dual fluorescence autophagy reporter system transfected into cultured cells [65]. This method was compared to western blotting and fluorescent imaging to determine if it could serve as a surrogate for these methods. In addition, the ability of this method to report color changes due to different stages of autophagy was assessed and compared to fluorescent imaging.

The second aim of my thesis is to investigate the relationship between keratin biomaterials and the autophagy pathway in Human Embryonic Kidney 293 (HEK 293) cells. Cell stress via exposure to starvation was complimented with the treatment of crude keratin extract. Keratin treatment with cells was compared to the positive autophagy modulators rapamycin and starvation, in addition to the late-stage autophagy blocker chloroquine to verify autophagy activity. Western blot analysis of LC3-II/LC3-I ratios and LC3-II/GAPDH ratios were used to measure levels of autophagy.

MATERIALS & METHODS

HEK 293 Cell Thawing

HEK 293 cells were stored in liquid nitrogen in 10% dimethylsulfoxide (DMSO) (ATCC, 62854788) and 90% Dulbecco's Modified Eagle Medium (DMEM) (Gibco, 11995-065) supplemented with 10% Fetal Bovine Serum (FBS) (Gibco, A31606-01). Cells needed for experiments were thawed in a water bath at 37°C and transferred to 10 mL pre-warmed DMEM supplemented with 10% FBS. The cell suspension was centrifuged (Beckman Coulter, Allegra X-14 Centrifuge, 7600306) at 800 rpm for five minutes. The resulting cell pellet was resuspended in two mL of DMEM supplemented with 10% FBS. 1 mL of the suspension was added to a sterile 10-cm cell culture dish with 9 mL of DMEM (10% FBS) and grown in a humidified incubator at 37°C and 5% CO2.

HEK 293 Cell Culture and Maintenance

HEK 293 cells were cultured in Dulbecco's Modified Eagle Medium (DMEM) supplemented with 10% Fetal Bovine Serum (FBS). Cells were seeded at a density of 1.5x10^5 cells/mL in a 6-well dish and incubated for 24 hours before experimentation.

Cell Seeding for Experiments

Cells were grown to 80% confluency (confluency indicates the percentage of the culture dish that is covered by cells) and detached from the 10-cm culture dish with 1.5 mL TrypLe (Gibco, 12604-021). Detached cells were centrifuged (Beckman Coulter, Allegra X-14 Centrifuge, 7600306) at 800 rpm for five minutes and resuspended in two mL of DMEM

supplemented with 10% FBS. 12 µL of the cell suspension were removed and combined with 12 µL of Trypan Blue dye (Corning, 25-900-CI). 12 µL of the cell-dye suspension was dispensed onto a hemocytometer, and cells contained in the four-quadrant grid were counted. The average of the cells contained in the grid was calculated according to the following equation:

(*Average of cell counts*) x (2) x 10,000 = cells/mL

The number "2" in the above equation is the dilution factor of cells in Trypan Blue dye. In addition, the cells are multiplied by 10,000 because each square in the hemocytometer has a volume of 0.3 mm^3 [66]. Multiplication by 10,000 results in units of cells/mL [66]. The following equation was then used to determine the volume of cell suspension needed to achieve a desired seeding density:

$$C_1V_1 = C_2V_2$$

C_1 refers to the starting concentration of the solution. V_1 signifies the volume needed to reach a desired concentration of a given volume. C_2 signifies the desired final concentration, and V_2 the desired final volume. Cells were seeded to obtain a final concentration of 150,000 cells/mL in a 6-well dish for further experiments.

Plasmid Prep

LB-agar plates were made by combining 7.5 g agar (Alfa Aesar, A10752), 12.5 g LB broth powder (Fisher BioReagents, BP1426-2), and 500 mL distilled water. The mixture was sterilized via autoclave. Appropriate antibiotics were then added (100 µg/mL ampicillin and 50 µg/mL kanamycin). Recombinant *E. coli* cultures expressing the plasmid pBABE-puro mCherry-EGFP-LC3B (a gift from Jayanta Debnath; Addgene, plasmid # 22418;

http://n2t.net/addgene:22418; RRID: Addgene 22418) were grown on LB-agar plates with 100 µg /mL ampicillin (BIORAD, 166-0407). Recombinant E. coli cultures expressing the plasmid mApple-GFP (a gift from Dr. Robert Youker) were grown on LB-agar plates (Alfa Aesar, A10752; Fisher Scientific, BP1426-2) with 50 µg/mL kanamycin (Sigma, K1377-5G). The plates were incubated overnight at 37°C. The next day, individual cultures were inoculated in LB liquid broth with 50 µg/mL kanamycin for mApple-GFP or 100 µg/mL ampicillin for mCherry-EGFP-LC3B. Liquid cultures were grown for 24 hours at 37°C with shaking at 220 RPM. Plasmids were extracted from the liquid cultures using an Invitrogen™ Purelink™ Quick Plasmid Miniprep kit (Thermo Fisher Scientific, K210010). The purity and concentration of plasmid isolates were verified using the NanoDrop spectrophotometer. Plasmids were stored at 4°C.

Plasmid Transfection of HEK 293 cells

A 6-well dish was seeded to protocol and grown to approximately 80% confluency. Plasmids were prepared according to the following procedure: 1000 ng per well of mCherry-EFGP-LC3B (a gift from Jayanta Debnath; Addgene, plasmid # 22418; http://n2t.net/addgene:22418; RRID: Addgene 22418) was combined with 100 µL/well of Opti-MEM reduced serum media (Thermo Scientific, 31985062). TurboFect transfection reagent (Thermo Scientific, R0533) was vortexed for 5 seconds and 2 µL/well was added to each plasmid solution. The solutions were incubated for 30 minutes at room temperature under the laminar flow hood. 100 µL of each plasmid solution was added to each well. The dish was incubated for 24 hours at 37°C and 5% CO2. After incubation, transfection was verified via imaging with the EVOS FL Auto epifluorescence microscope.

Treatment of Transfected Cells

Transfected cells were treated with 0.3 μM rapamycin (EMD Millipore, 553210-5MG) to stimulate autophagy. Transfected cells were treated with 40 μM chloroquine diluted in phosphate-buffered saline (PBS) to block autophagosome-lysosome fusion (Acros Organics, 455240250; Cytiva, SH30256.02). Cells are also treated with 0.1 mg/mL crude keratin (a gift from Dr. Mark Van Dyke) extract to test the effects of keratin treatment on autophagy activity.

Epifluorescence Imaging of Treated Cells

Images of treated and control cell cultures were taken at multiple timepoints using the EVOS™ FL Auto epifluorescence microscope. 16-bit monochromatic images were taken using the green (GFP light cube) channel and red (Texas Red light cube) channel. Each image contained a scale bar. For every designated time point, 3 replicate image sets were taken of each well of the six well dish, each from different areas of the culture.

Cell Lysis Protocol

Culture medium was first aspirated from the cell culture dish. Each well was washed with one mL of ice-cold PBS (Cytiva, SH30256.02). The PBS washes were saved in respective 15-mL conical tubes and kept on ice. Cells were detached from the dish by applying 0.5 mL TrypLe/well and incubated at 37°C for 5 minutes. Trypsinized cells were then aspirated from the dishes and added to 15-mL conical tubes. The tubes were centrifuged (Beckman Coulter, Allegra X-14 Centrifuge, 7600306) for 5 minutes at 800 rpm. The TrypLe was removed from the pellets and the cell pellets were resuspended in 200 μL of protease inhibitor/RIPA lysis buffer (Sigma,

S8820-2TAB, Thermo Scientific, J63306.AK) and kept on ice for 20 minutes. After 20 minutes, the cell suspension was centrifuged in the cold room at 12,000 rpm for 10 minutes. The resulting supernatant was removed and aliquoted into Eppendorf tubes. The samples were flash frozen in liquid nitrogen and stored at -80°C.

Transfected Protein Quantification Assay

A serial dilution of each sample was performed by diluting samples in PBS (Cytiva, SH30256.02). The samples were added in duplicates to the wells of a black 96-well plate (Corning, 3915). The fluorescence of each sample was calculated using an iD5 Molecular Devices fluorescent plate reader with an excitation wavelength of 485 nm and an emission wavelength of 535 nm. The second setting has an excitation wavelength of 587 nm and an emission wavelength of 630 nm.

Total Protein Quantification Assay

Bovine serum albumin (BSA) standards were prepared according to the following concentrations from a 2 mg/mL stock (Thermo Scientific, 23210): 0.1 mg/mL, 0.2 mg/mL, 0.3 mg/mL, 0.5 mg/mL, 0.8 mg/mL, and 1.0 mg/mL. Each standard was diluted with a cell lysis buffer composed of 12.5 mL RIPA buffer and ¼ protease inhibitor tablet (Sigma, S8820-2TAB; Thermo Scientific, J63306.AK). Each standard was then further diluted 1:4 in PBS (Cytiva, SH30256.02). Cell lysates were then thawed on ice and diluted 1:40 in PBS (Cytiva, SH30256.02). 20 uL of each diluted standard and diluted sample was added in duplicate to the wells of a flat bottomed clear well 96 well dish (Corning, 353075). 200 uL of G-250 Coomassie Blue assay dye was then added to each well. The plate was incubated for 15 minutes at room

temperature. The absorbance of the samples was then measured at 595 nm using the SpectraMax 190 (Molecular Devices) plate reader. A standard curve was then prepared based on the absorbance values of the standards. The protein concentration of samples was determined by taking the equation for the standard curve and solving for *x* using the absorbance values of the samples as *y* values.

SDS-PAGE Gel Casting Protocol

12% SDS-PAGE resolving gels were cast as follows. 3.4 mL of distilled water was combined with 2.4 mL 40% acrylamide/Bis solution 29:1 (Bio-Rad, 1610146), 2.4 mL 1.5 M Tris pH 8.8, 80 µL 10% SDS (Fisher Scientific, BP166-500), 80 µL 10% APS (Fisher BioReagents, BP 179-100), and 5 µL TEMED (Fisher BioReagents, BP150-20). The solution was dispensed into a gel-casting device. 300 µL of water-saturated butanol (Fisher Science Education, 593100) was dispensed over the top of the gel and left to polymerize for 10 minutes.

15% SDS-PAGE resolving gels were cast as follows. 2.8 mL of distilled water was combined with 3 mL 40% acrylamide/Bis solution 29:1 (Bio-Rad, 1610146), 2 mL 1.5 M Tris pH 8.8, 80 µL 10% SDS (Fisher Scientific, BP166-500), 80 µL 10% APS (Fisher BioReagents, BP 179-100), and 5 µL TEMED (Fisher BioReagents, BP150-20). The solution was dispensed into a gel-casting device. 300 µL of water-saturated butanol (Fisher Science Education, 593100) was dispensed over the top of the gel and left to polymerize for 10 minutes.

4% SDS-PAGE stacking gels were cast as follows. 3 mL of distilled water was combined with 660 µL 40% acrylamide/Bis solution 29:1 (Bio-Rad, 1610146), 1.26 mL 0.5 M Tris pH 6.8, 50 µL 10% SDS (Fisher Scientific, BP166-500), 25 µL 10% APS (Fisher BioReagents, BP 179-

100), and 5 µL TEMED (Fisher BioReagents, BP150-20). The solution was dispensed on top of a 12% or 15% resolving gel, and a well comb was inserted into the solution. The gel was left to polymerize for 10 minutes. All gels were wrapped in moist paper towels and stored at 4°C.

In-gel Fluorescence Protocol

Cell lysates were removed from the -80°C freezer, thawed on ice, and combined with 2x Laemmli sample buffer (Bio-Rad, 161-0737) without beta-mercaptoethanol. Samples were not heated before loading onto the gel. Running buffer stock (15.1 g Tris base, FisherBiotech, BP152-1; 94 g electrophoresis grade glycine, Thermo Scientific, J64365.A1; 50 mL 10% SDS, Fisher Scientific, BP166-500; pH 8.3) was diluted to 5% in distilled water and poured over a 12% SDS-PAGE gel. Samples were added to the gel, and the gel was run at 120 volts for 25 minutes. After 25 minutes, the voltage was increased to 200 volts for 1 hour. After the protein ladder reached the bottom of the gel, the gel was imaged with the BIORAD ChemiDoc Imaging System. The following filters were used to acquire images: Alexa488, Alexa546, and Alexa647. See Figure 4 below for an illustration of this process.

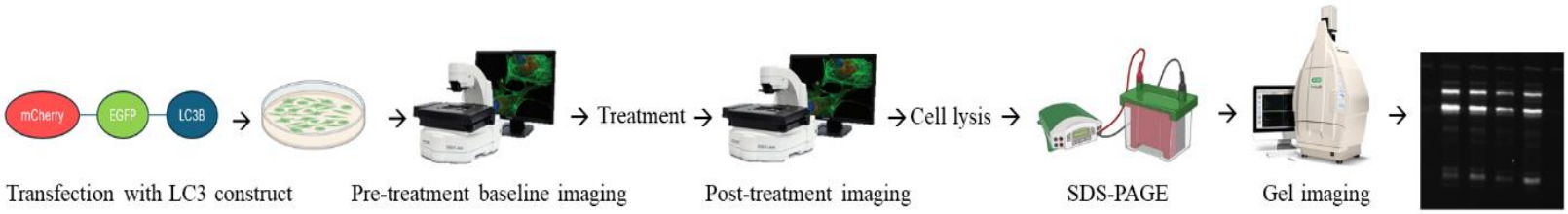

Figure 4: Illustration of the in-gel fluorescence procedure. Cells were transfected with the mCherry-EGFP-LC3B construct. 24 hours later, transfection was confirmed via widefield fluorescence imaging. Cells were treated and imaged at appropriate timepoints. Cells were lysed, and lysates were subject to a semi-native form of SDS-PAGE. After SDS-PAGE, the SDS-PAGE gel was analyzed with the BIORAD ChemiDoc Imaging System under three filters (Alexa 488, Alexa 546, and Alexa 647) to obtain images.

Western Blotting

Cell lysates were removed from the -80°C freezer and thawed on ice. Lysates were combined 1:3 with reducing buffer (12% SDS w/v, Fisher Scientific, BP166-500; 6% beta-mercaptoethanol v/v, MP Biomedicals, 194834; 30% glycerol w/v, 0.05% Coomassie Brilliant Blue 6-250, Thermo Scientific, 20278; and 150 mM Tris-HCl pH 6.8). Samples were heated to 95°C for five minutes using a heat block. Samples were cooled for five minutes and briefly centrifuged to collect evaporated moisture. Samples were loaded on a 12% SDS-PAGE gel alongside the Spectra Multicolor Broad Range Protein Ladder (Thermo Scientific, 26634) and inserted into the BIORAD Mini Tetracell gel electrophoresis apparatus (Thermofisher, 26634).

The gel was run at 120 volts for 25 minutes. After 25 minutes, the voltage was increased to 200 volts for 1 hour. After SDS-PAGE was complete, a blotting sandwich was assembled with the 12% gel in transfer buffer stock (30.385 g Tris Base, FisherBiotech, BP152-1; 144.134 g electrophoresis grade glycine, Thermo Scientific, J64365.A1; 1 liter of water) diluted to 10% in distilled water. A 0.2 µm pore size PVDF membrane (Novex, LC2002) was used for the transfer of endogenous protein. A 0.45 µm pore size PVDF membrane (Millipore IPVH20200) was used for the transfer of transfected protein. Transfer was run at 100 volts for 70 minutes. Transfer was verified by detecting the protein ladder on the membrane. The membrane was then blocked overnight in the cold room with 50 mL of 3% nonfat milk in PBST (10% phosphate buffered saline, distilled water, 0.1% Tween-20, Fisher Scientific Company, CS-279-3). Detection of LC3 and GAPDH proteins was performed by incubating the blot in 15 mL of 2.5% BSA supplemented with primary antibody titers of 1:1000 for endogenous LC3 (Novus Biologicals, NB100-2220), 1:10,000 for transfected LC3, and 1:10,000 for GAPDH (Cell Signaling

Technology, D16H11). Membranes were incubated with primary antibodies for 1 hour at room temperature with rocking. Membranes were then washed four times for five minutes and one time for 40 minutes in PBST. 15 mL of 2.5% BSA (Thermo Scientific, J65731.22) supplemented with secondary antibodies at a titer of 1:5000 (BIORAD, 170-6515) was applied to the membrane for one hour at room temperature with rocking. Membranes were washed five times for five minutes in PBST. 1 mL SuperSignal™ West Pico PLUS Chemiluminescent Substrate (Thermo Scientific, 34577) was then applied to each membrane and incubated for five minutes. The membrane was then imaged using the BIORAD ChemiDoc Imaging System. If multiple proteins were probed for a single blot, a stripping protocol was used after imaging. The blot was rinsed in distilled water to remove excess chemiluminescent substrate. The blot was then incubated in 15 mL of stripping buffer (15 g electrophoresis grade glycine, Thermo Scientific, J64365.A1; 1 g SDS, Fisher Scientific, BP166-500; 10 mL Tween-20, 1 Liter distilled water, pH 2.2) with shaking at room temperature. The blot was washed three times in PBST for five minutes each. The blot was blocked for a second time in 3% nonfat milk for 1 hour at room temperature.

Western Blot Densitometry Analysis

Western blot band densitometry was performed using FIJI (FIJI Is Just ImageJ) software. Western blot images were opened in ImageJ and inverted. Regions of interest (ROIs) were generated for each protein type on the blot. The size of each ROI was adjusted to accommodate the largest band of each protein type and was then saved. The intensity of each band in the ROI was then measured. A background measurement for each band was also taken using the same ROI. The background measurement was subtracted from its corresponding band intensity value.

The ratio of band intensities between LC3-II/LC3-I was then calculated by first normalizing each value to the corresponding GAPDH band. The normalized LC3-II band was then divided by the dividing the LC3-I band. The ratio of band intensities between LC3-II and GAPDH were calculated by dividing the LC3-II value by the corresponding GAPDH value. Ratios were graphed using GraphPad Prism software.

Statistical Analysis and Experimental Replicates

Each treatment group was composed of cells grown in 3 wells of a 6-well dish seeded to 150,000 cells/mL and combined into one lysate. Each experiment was replicated for a total of 3 replicates per experiment. T-tests and analyses of variance using Tukey's post hoc test were performed in GraphPad Prism software to determine statistical significance. Tukey's post hoc test compares all mean values to every other mean value [67]. Each figure legend denotes the statistical test used for each data set. A p-value of less than 0.05 was considered to be statistically significant.

RESULTS

1. Response of HEK 293 Cells to Autophagy Modulators

In order to establish a baseline for evaluating autophagic activity in our specific cell line, we dosed HEK 293 cells with 0.3 μM Rapamycin for 24 hours to stimulate autophagy and analyzed cell lysates with a western blot (Figure 5.A). Western blot densitometry analysis of LC3 bands obtained from 3 experiments revealed that there was a statistically significant change between the LC3-II/LC3-I ratios of the no treatment group compared to the rapamycin-treated group (rapamycin-treated groups had an average LC3-II/LC3-I ratio of 2.57 +/- 0.3090 compared to 0.6 +/- 0.1506 in the no treatment group) (Figure 5.B). In addition, the LC3-II/GAPDH ratios demonstrated a statistically significant change in the group dosed with rapamycin compared to the no treatment group (Figure 5.C). Rapamycin-treated groups had an average LC3-II/GAPDH ratio of 0.89 +/- 0.1146 compared to 0.44 +/- 0.1576 in the no treatment group. These results provide a framework for the changes in LC3 ratios we would expect in HEK 293 cells dosed with rapamycin to stimulate autophagy.

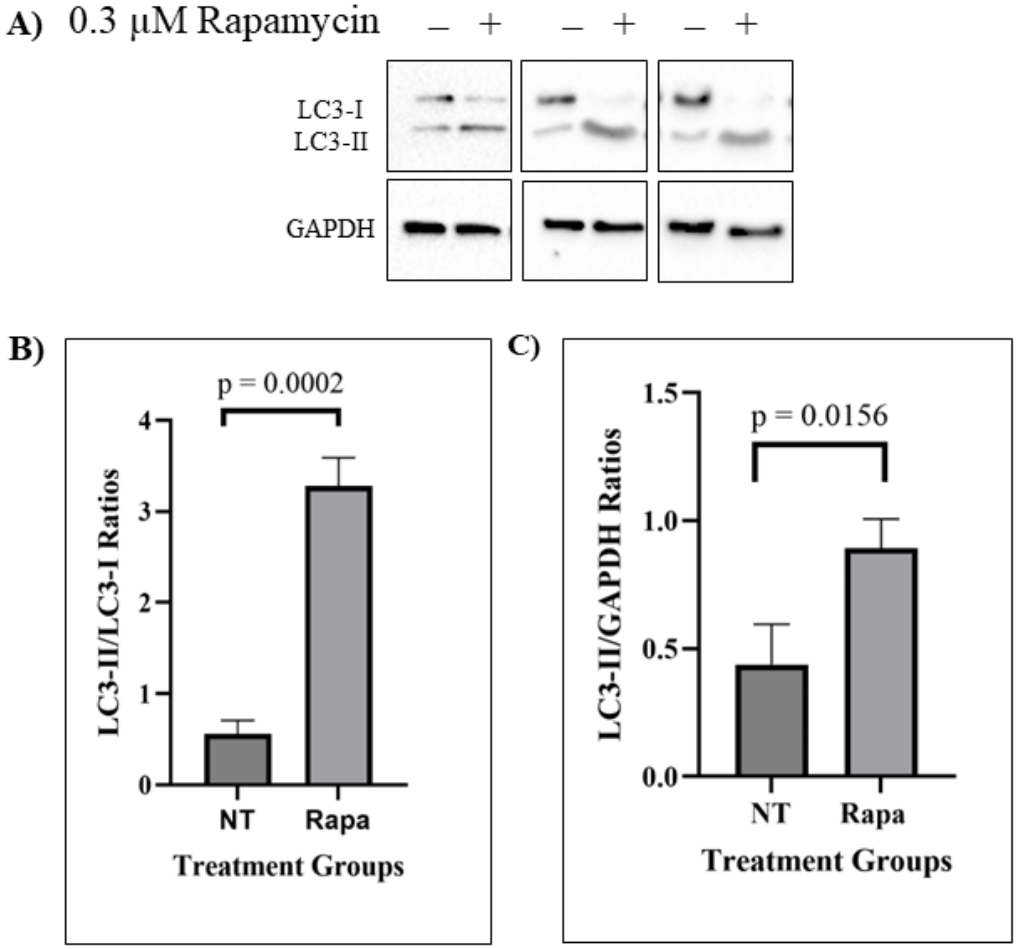

Figure 5: Effects of rapamycin treatment on HEK 293 cells. The ratios shown here are averaged from three sets of experiments. **A:** Triplicate sets of HEK 293 cells were treated with 0.3 μM rapamycin for 24 hours. Endogenous LC3-I, LC3-II, and GAPDH bands were analyzed via western blotting. **B:** LC3-II/LC3-I ratios for no treatment and rapamycin-treated groups were calculated 22via densitometry analysis in ImageJ. Statistical significance was determined using a T-Test. A p value of $p < 0.05$ indicates statistical significance. *$p = 0.0002$.* **C:** LC3-II/GAPDH ratios for no treatment and rapamycin-treated groups were calculated via densitometry analysis in ImageJ. Statistical significance was determined using a T-Test. A p value of $p < 0.05$ indicates statistical significance. *$p = 0.0156$.*

In addition to testing the effects of rapamycin on HEK 293 cells, we treated HEK 293 cells with a reduced nutrient treatment to stimulate a starvation environment (50% phosphate buffered saline and 50% DMEM) for 24 hours to stimulate autophagy. For the sake of brevity, this treatment will be referred to as starvation for the remainder of this study. 50% starvation was chosen based on previous experiments showing that 50% starvation as a cell stressor maintained cell viability and attachment over a 24-hour period of time compared to 75% starvation and 100% starvation [68]. We chose to analyze the cells 24 hours post-treatment because our positive control, rapamycin, generated the greatest autophagy response at 24 hours post treatment. We performed a western blot of cell lysates treated with 50% starvation (Figure 6.A). Western blotting and densitometry analysis revealed that there was not a statistically significant difference between the LC3-II/LC3-I ratios of the negative control group and the starvation treated group (an average ratio of 0.65 +/- 0.1489 for the negative control group and an average ratio of 0.73 +/- 0.3590 for the starvation treated group) (Figure 6.B). In addition, there was not a statistically significant difference between the LC3-II/GAPDH ratios of the negative control group and starvation treated group (an average ratio of 0.4 +/- 0.1475 for the negative control group and an average ratio of 0.27 +/- 0.09349 for the starvation treated group) (Figure 6.C).

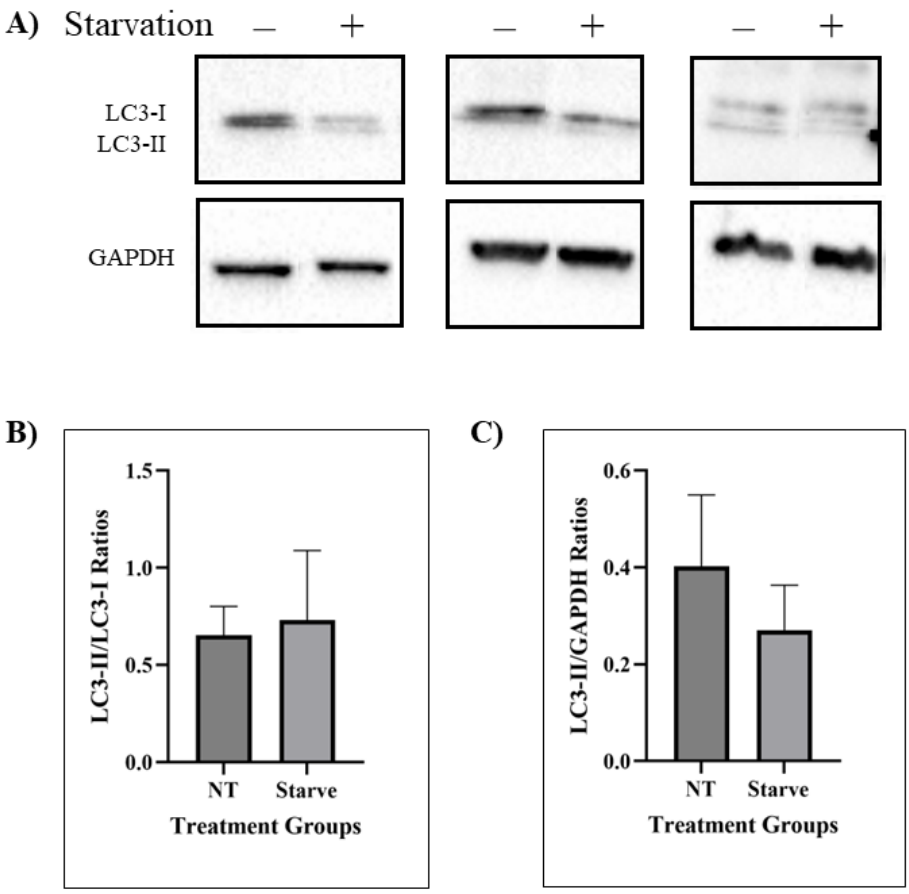

Figure 6: Effects of starvation treatment on HEK 293 cells. The ratios shown here are averaged from three sets of experiments. **A:** Triplicate sets of HEK 293 cells were treated with 50% starvation (1 mL phosphate-buffered saline, 1 mL DMEM) for 24 hours. Endogenous LC3-I, LC3-II, and GAPDH bands were analyzed via western blotting. **B:** LC3-II/LC3-I ratios for no treatment and starvation-treated groups were calculated via densitometry analysis in ImageJ. Statistical significance was determined using an ANOVA test with Tukey's post hoc analysis. A p value of $p < 0.05$ indicates statistical significance. $p > 0.9999$. **C:** LC3-II/GAPDH ratios for no treatment and starvation-treated groups were calculated via densitometry analysis in ImageJ. Statistical significance was determined using an ANOVA test with Tukey's post hoc analysis. A p value of $p < 0.05$ indicates statistical significance. $p = 0.9957$.

In addition, we dosed nontransfected HEK 293 cells with 40 μM chloroquine, a late-stage autophagy inhibitor. When cells are dosed with a combination of chloroquine and an autophagy stimulator, it serves as a control for a situation in which autophagy has been stimulated but cannot proceed through to its final stages. To determine the impact of chloroquine treatment upon LC3 ratios in HEK 293 cells, we treated cells with chloroquine alone and chloroquine and starvation together and performed a western blot (Figure 7.A). LC3-II/LC3-I ratios were then calculated via western blotting and densitometry analysis. In cells treated with chloroquine alone, there was a statistically significant difference between the LC3-II/LC3-I ratios of the negative control group and the chloroquine only group, indicating the efficacy of the chloroquine compound. The average LC3-II/LC3-I ratio for the no treatment group was 0.65 +/- 0.1489, while the average ratio for the chloroquine-only treated group was 2.09 +/- 0.4875 (Figure 7.B). In addition, there was a statistically significant difference between the negative control group and the group dosed with a combination of starvation and chloroquine. The average LC3-II/LC3-I ratio for the no treatment group was 0.65 +/- 0.1489, compared to the average ratio of 2.25 +/- 0.9874 for the chloroquine and starvation treated group (Figure 7.C).

There was also a statistically significant difference in the LC3-II/GAPDH ratios between the no treatment group and chloroquine-treated groups, as well as the no treatment group compared to the starvation and chloroquine-treated group (Figure 7.D). The average LC3-II/GAPDH ratio for the no treatment group was 0.4 +/- 0.1475, compared to an average ratio of 1.9 +/- 0.2502 in the chloroquine-only group and 1.43 +/- 0.5439 in the chloroquine and starvation treated group.

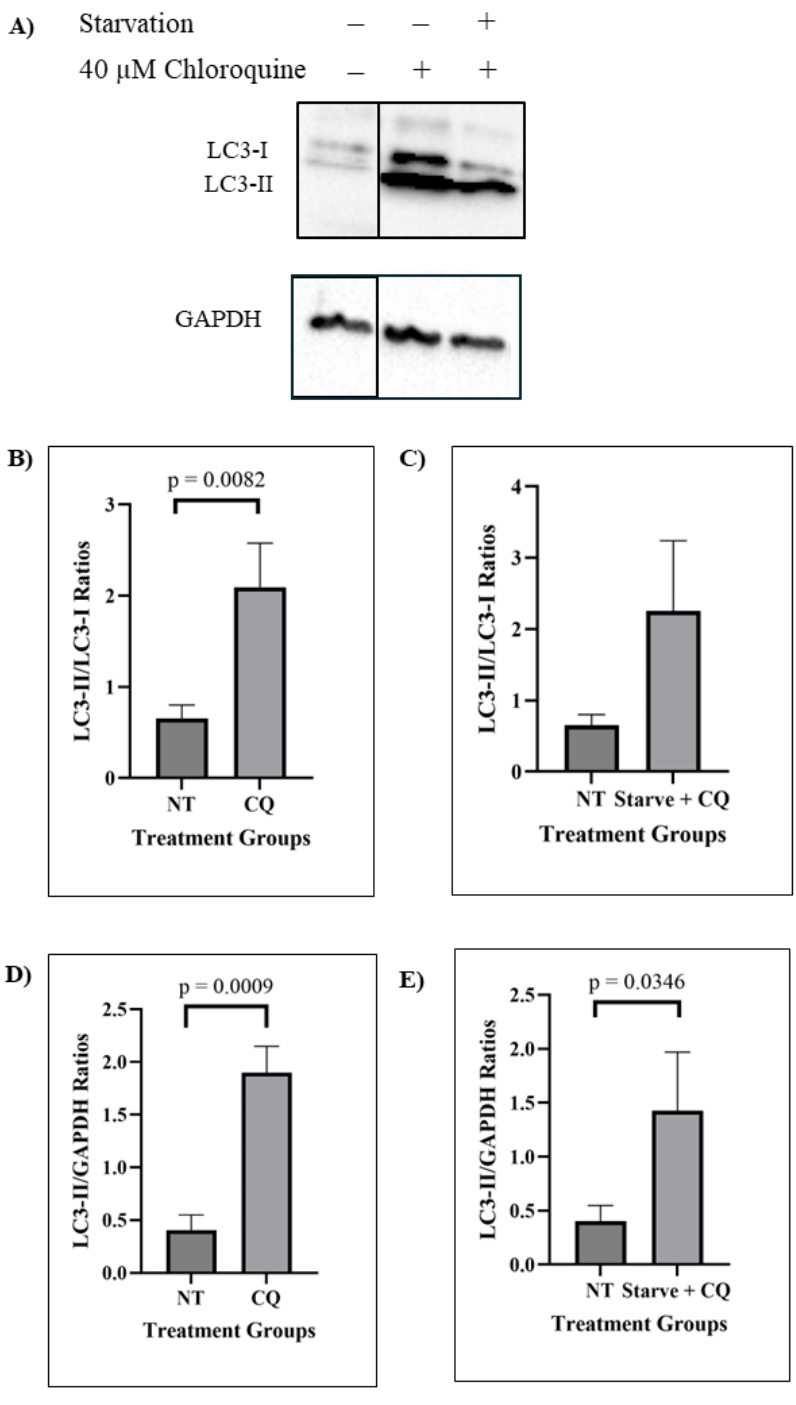
A)
Starvation – – +
40 μM Chloroquine – + +
LC3-I
LC3-II
GAPDH
B)
p = 0.0082
LC3-II/LC3-I Ratios
NT
CQ
Treatment Groups
C)
LC3-II/LC3-I Ratios
NT Starve + CQ
Treatment Groups
D)
p = 0.0009
LC3-II/GAPDH Ratios
NT
CQ
Treatment Groups
E)
p = 0.0346
LC3-II/GAPDH Ratios
NT Starve + CQ
Treatment Groups

Figure 7: Effects of chloroquine treatment on HEK 293 cells. The ratios shown here are averaged from 3 sets of experiments. **A:** Triplicate sets of HEK 293 cells were treated with 40 μM chloroquine for 24 hours. Endogenous LC3-I, LC3-II, and GAPDH bands were analyzed via western blotting. **B:** LC3-II/LC3-I ratios for no treatment and chloroquine-treated groups were calculated via densitometry analysis in ImageJ. Statistical significance was determined using a T-test. A p value of $p < 0.05$ indicates statistical significance. **C:** LC3-II/LC3-I ratios for no treatment and starvation plus chloroquine-treated groups were calculated via densitometry analysis in ImageJ. Statistical significance was determined using a T test. $p = 0.0501$. **D.** LC3-II/GAPDH ratios for no treatment and chloroquine-treated groups were calculated via densitometry analysis in ImageJ. Statistical significance was determined using a T test. $p = 0.0009$. **E.** LC3-II/GAPDH ratios for no treatment and starvation plus chloroquine-treated groups were calculated via densitometry analysis in ImageJ. Statistical significance was determined using a T test. $p = 0.0346$.

In addition to establishing a baseline for how HEK 293 cells respond to autophagy modulating drugs, we sought to understand how HEK 293 cells respond to variations in incubation times. The transfection process requires an extra 24-hour incubation period for each experiment. We wanted to know whether adding an extra day of incubation modulated autophagy activity in nontransfected HEK 293 cells. We grew nontransfected cells for either three days or four days and dosed them with 0.3 μM rapamycin for 24 hours. We analyzed these cells with western blotting and calculated the LC3-II/LC3-I ratios and LC3-II/GAPDH ratios (Figure 8.A). Cells dosed with rapamycin and grown for three days showed the expected statistically significant change in LC3-II/LC3-I ratios compared to the no treatment control (an average ratio of 0.6 +/- 0.1506 in the no treatment group compared to 2.57 +/- 0.3090 in the rapamycin-treated group) (Figure 8.B). However, cells dosed with rapamycin and grown for four days did not show the statistically significant difference in the LC3-II/LC3-I ratios between the negative and positive control groups (an average ratio of 1.3 +/- 0.4783 in the no treatment group compared to 0.98 +/- 0.09386 in the rapamycin-treated group) (Figure 8.C). There was a similar trend in the LC3-II/GAPDH ratios. Cells grown for three days showed the expected statistically significant change in LC3-II/GAPDH ratios compared to the no treatment control (an average ratio of 0.44 +/- 0.1576 in the no treatment group compared to 0.89 +/- 0.1146 in the rapamycin-treated group) (Figure 8.D). On the other hand, cells dosed with rapamycin and grown for four days did not demonstrate statistically significant changes in the LC3-II/GAPDH ratios (an average ratio of 0.64 +/- 0.1321 in the no treatment group compared to 0.42 +/- 0.1347 in the rapamycin-treated group) (Figure 8.E).

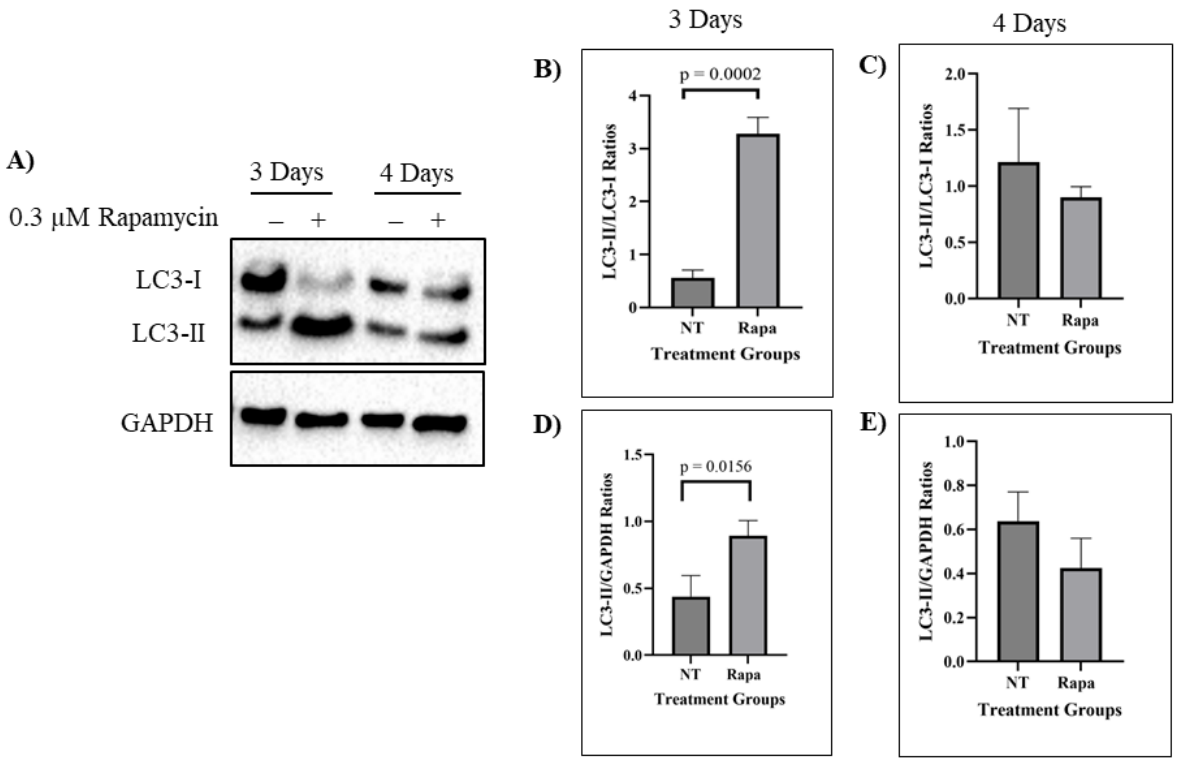

Figure 8: Effects of 3 and 4 days of incubation on HEK 293 cells. The ratios shown here are averaged from 3 sets of experiments. **A:** HEK 293 cells were dosed with 0.3 μM rapamycin for 24 hours and incubated for 72 hours or 96 hours. Endogenous LC3-I, LC3-II, and GAPDH bands were analyzed via western blotting. **B:** LC3-II/LC3-I ratios for 3-day treatment groups were calculated via densitometry analysis in ImageJ. Statistical significance was determined using a T-Test. A p value of $p < 0.05$ indicates statistical significance. *$p < 0.0001$.* **C:** LC3-II/LC3-I ratios for 4-day treatment groups were calculated via densitometry analysis in ImageJ. Statistical significance was determined using a T-Test. *$p = 0.4436$.* **D:** LC3-II/GAPDH ratios for 3-day treatment groups were calculated via densitometry analysis in ImageJ. Statistical significance was determined using a T-Test. *$p = 0.0156$.* **E:** LC3-II/GAPDH ratios for 4-day treatment groups were calculated via densitometry analysis in ImageJ. Statistical significance was determined using a T-Test. *$p = 0.1214$.*

Because cells that were incubated for an extra 24 hours showed an unexpected autophagy response to no treatment and treatment with rapamycin, we attempted to restore the expected responses by changing out the media on our cells at day 3 of incubation. Previous experiments in our lab suggested that the stressor of an extra day of incubation could be mitigated by changing out the cell culture media at 24 hours post-dosing and 72 hours post-dosing [69]. In this experiment, cells were transfected with the mCherry-EGFP-LC3B plasmid to visualize the LC3 protein during different stages of autophagy. The cells were then dosed with rapamycin, chloroquine, or a combination of rapamycin and chloroquine and imaged at set timepoints during a 65-hour time period. Late-stage autophagy levels were determined by calculating the percentage of cells containing yellow and red puncta, respectively. At 24 hours post-dosing before a media change, there was no statistically significant difference between the percentage of cells containing red puncta (indicative of late-stage autophagy) in the negative and positive control groups (Figure 9). After a media change at 28.5 hours post-dosing, there was a statistically significant difference between the percentage of cells containing red puncta in the negative and positive control groups (Figure 9).

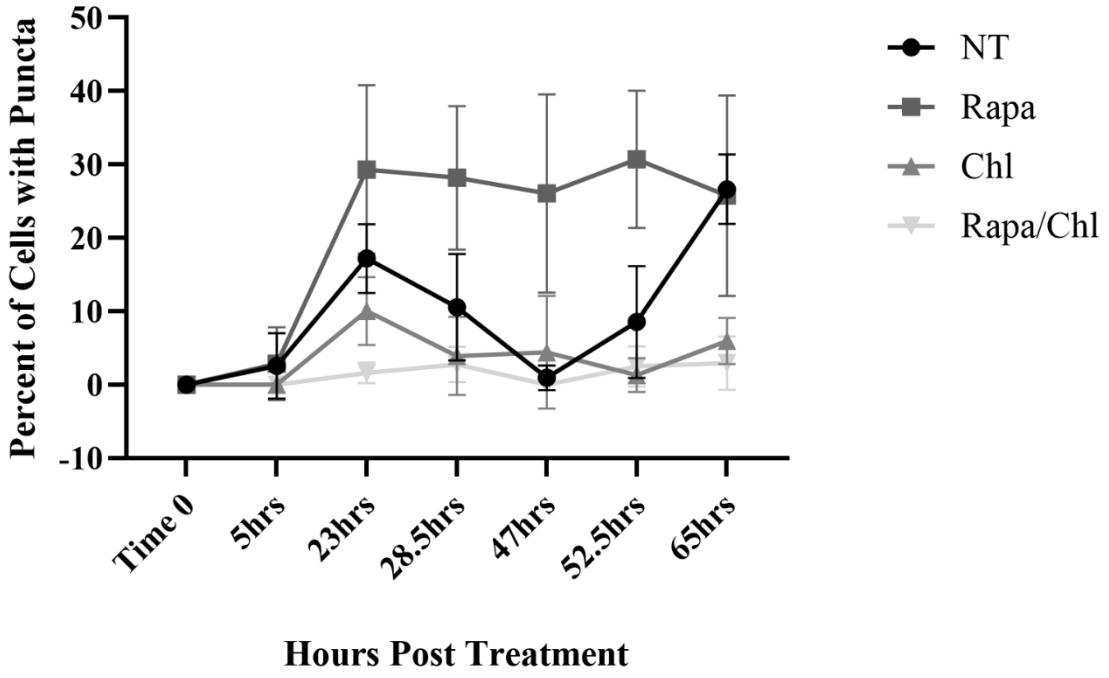

Figure 9: Percent of transfected cells undergoing late-stage autophagy. Cells were transfected and dosed with rapamycin, chloroquine, or a combination of rapamycin and chloroquine. Dosed cells were compared to a no treatment group. Images of fluorescing cells were taken at the timepoints indicated on the X-axis. The cell media was replaced after timepoint 23 hours post treatment and 47 hours post treatment.

We reasoned that a media change at 3 days of incubation may produce a similar response in nontransfected cells analyzed with western blotting. We tested whether changing the media in nontransfected cells would restore the expected changes in the LC3-II/LC3-I ratios in cells grown for four days. We performed a western blot and compared the LC3-II/LC3-I ratios of a negative control group and a rapamycin-treated group when treated with a media change and without a media change (Figure 10.A). Cells without a media change did not show a statistically significant difference in the ratios between the negative and positive control at four days (an average LC3-II/LC3-I ratio of 1.0 +/- 0.1083 in the negative control group compared to 1.0 +/- 0.3400 in the rapamycin-treated group) (Figure 10.B). However, cells treated with a media change showed a statistically significant difference in the ratios between the no treatment group and rapamycin-treated group (an average ratio of 0.46 +/- 0.1057 in the negative control group compared to 1.22 +/- 0.4348 in the rapamycin-treated group) (Figure 10.C).

We also compared the LC3-II/GAPDH ratios of cells treated with a media change and without a media change. There was no statistically significant change between the LC3-II/GAPDH ratios of cells grown for four days without a media change (an average ratio of 0.72 +/- 0.3243 in the no treatment group compared to 0.37 +/- 0.2247 in the rapamycin-treated group) (Figure 10.D). In addition, there was no statistically significant change in the ratios of cells grown for four days with a media change, although there was a trend towards an increased ratio in the rapamycin-treated group (an average ratio of 0.46 +/- 0.2760 in the no treatment group compared to 0.73 +/- 0.2224 in the rapamycin-treated group) (Figure 10.E).

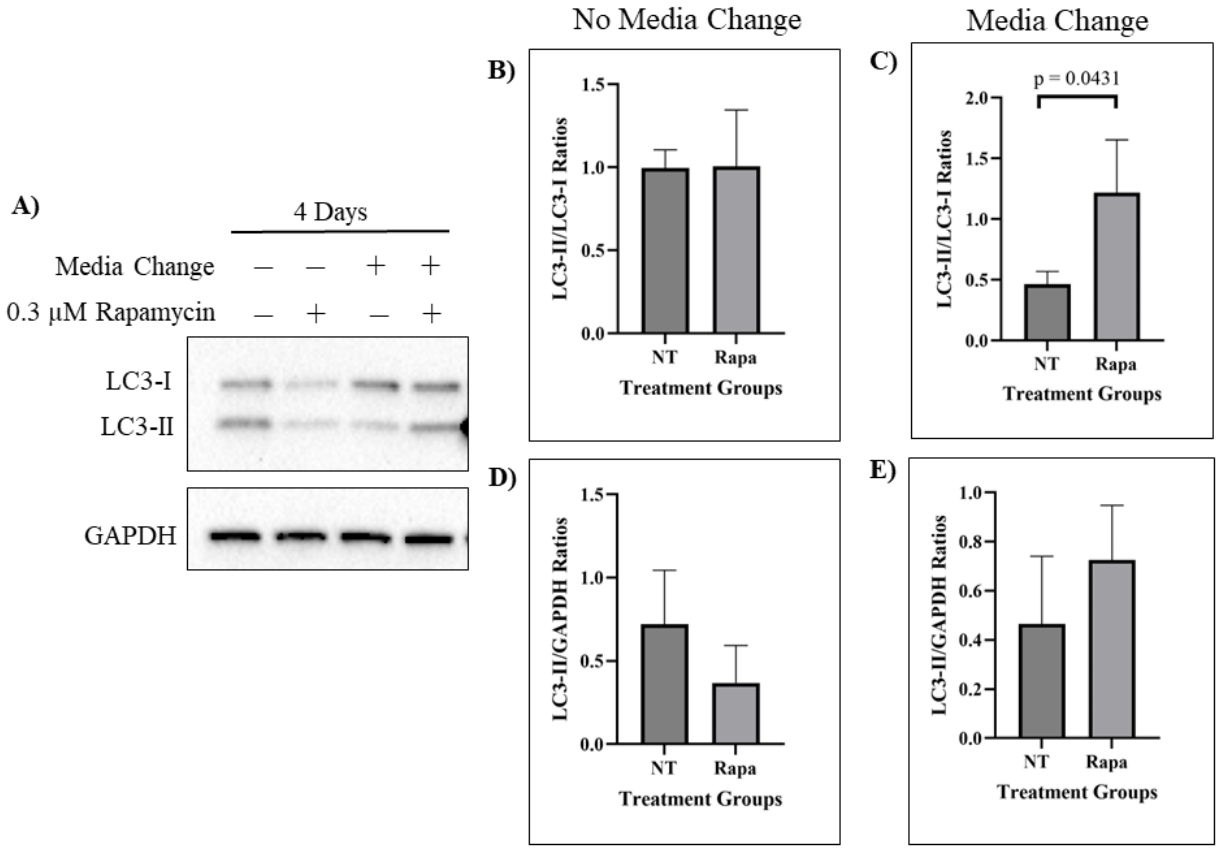

Figure 10: Effects of media change on HEK 293 cells. **A:** HEK 293 cells were dosed with 0.3 µM rapamycin for 24 hours and incubated for 96 hours. LC3-I, LC3-II, and GAPDH bands were analyzed via western blotting. **B:** Endogenous LC3-II/LC3-I ratios for 4-day treatment groups without a media change were calculated via densitometry analysis in ImageJ. Statistical significance was determined using a T-Test. A p value of $p < 0.05$ indicates statistical significance. *p = 0.9690.* **C:** LC3-II/LC3-I ratios for 4-day treatment groups with a media change were calculated via densitometry analysis in ImageJ. Statistical significance was determined using a T-Test. *p = 0.0431.* **D:** LC3-II/GAPDH ratios for 4-day treatment groups without a media change were calculated via densitometry analysis in ImageJ. Statistical significance was determined using a T-Test. *p = 0.1981.* **E:** LC3-II/GAPDH ratios for 4-day treatment groups with a media change were calculated via densitometry analysis in ImageJ. Statistical significance was determined using a T-Test. *p = 0.2721.*

2. In-Gel Fluorescence and Autophagy

After determining the expected responses of our cells to the autophagy modulators rapamycin, starvation, and chloroquine, we sought to determine whether in-gel fluorescence was capable of being used for the analysis of autophagy. During in-gel fluorescence, cells were transfected with a mCherry-EGFP-LC3 plasmid construct that coded for a recombinant protein of approximately 68.9 kDa in weight (mCherry = 28 kDa, EGFP = 26.9 kDa, and LC3 = 14-17 kDa, depending on the LC3-I or LC3-II form) (Figure 11.A). When imaged under the microscope, transfected cells undergoing autophagy display fluorescent puncta corresponding to the LC3 protein being converted from LC3-I to LC3-II (Figure 11.B). We reasoned that in-gel fluorescence would allow us to visualize the change from LC3-I to LC3-II as protein bands when transfected cell lysates were resolved with SDS-PAGE and imaged with light filters to detect the green and red portions of the transfected construct. In-gel fluorescence of cells transfected with the LC3 plasmid showed two distinct protein bands at approximately 70 kDa in weight under both the Alexa 488 filter and the Alexa 546 filter (Figure 11.C). The Alexa 488 filter allows users to detect the EGFP portion of the construct, and the Alexa 546 filter allows users to detect the mCherry protein of the construct. The SDS-PAGE gel was then further analyzed via western blotting to confirm the location of the LC3 protein. Western blotting analysis to probe for LC3 revealed a set of two protein bands at approximately 70 kDa in weight, corresponding to the bands observed with in-gel fluorescence (Figure 11.D).

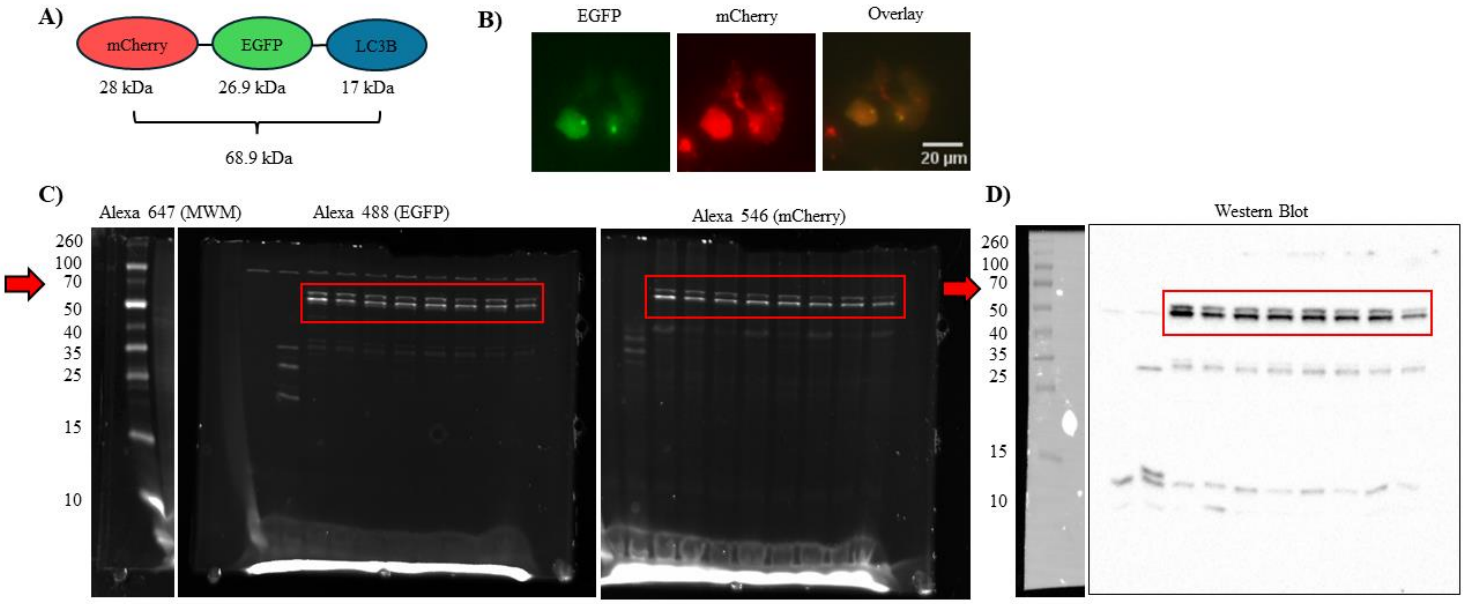

Figure 11: In-gel fluorescence allows users to detect the transfected LC3 protein. A: Illustration of the transfected protein construct and expected molecular weight. B: Example of fluorescent puncta observed in transfected cells undergoing autophagy. C: In-gel fluorescence of transfected cell lysates. The LC3 construct is highlighted in the red box under the Alexa 488 and Alexa 546 filters. The red arrow indicates the expected molecular weight of the construct. D: Western blot of transfected cell lysates. The LC3 construct is highlighted in the red box. The red arrow indicates the expected molecular weight of the construct.

Rapamycin treatment in transfected HEK 293 cells

After confirming the presence of the transfected LC3 protein with in-gel fluorescence, we dosed cells with autophagy modulators rapamycin, starvation, and chloroquine in order to determine whether the responses of transfected cells corresponded to the responses of nontransfected cells analyzed previously. The LC3-II/GAPDH ratios for transfected cells were not calculated because we did not transfect cells with a plasmid to make fluorescent GAPDH. First, we dosed HEK 293 cells with 0.3 μM Rapamycin for 24 hours to stimulate autophagy and analyzed these cells with both western blotting and in-gel fluorescence (Figure 12.A). Transfected cells dosed with 0.3 μM Rapamycin for 24 hours did not demonstrate a statistically significant change in the LC3-II/LC3-I ratios with either western blotting or with in-gel fluorescence (Figure 12.B-D). The average LC3-II/LC3-I ratios for samples analyzed with western blotting were 1.15 +/- 0.1026 for the no treatment group and 1.28 +/- 0.2242 for the rapamycin-treated group. The average ratios for samples analyzed with the Alexa 488 filter were 1.44 +/- 0.1250 for the no treatment group and 1.60 +/- 0.2498 for the rapamycin-treated group. Finally, the average ratios for samples analyzed with the Alexa 546 filter were 2.14 +/- 0.4210 for the no treatment group and 2.28 +/- 0.4149 for the rapamycin-treated group.

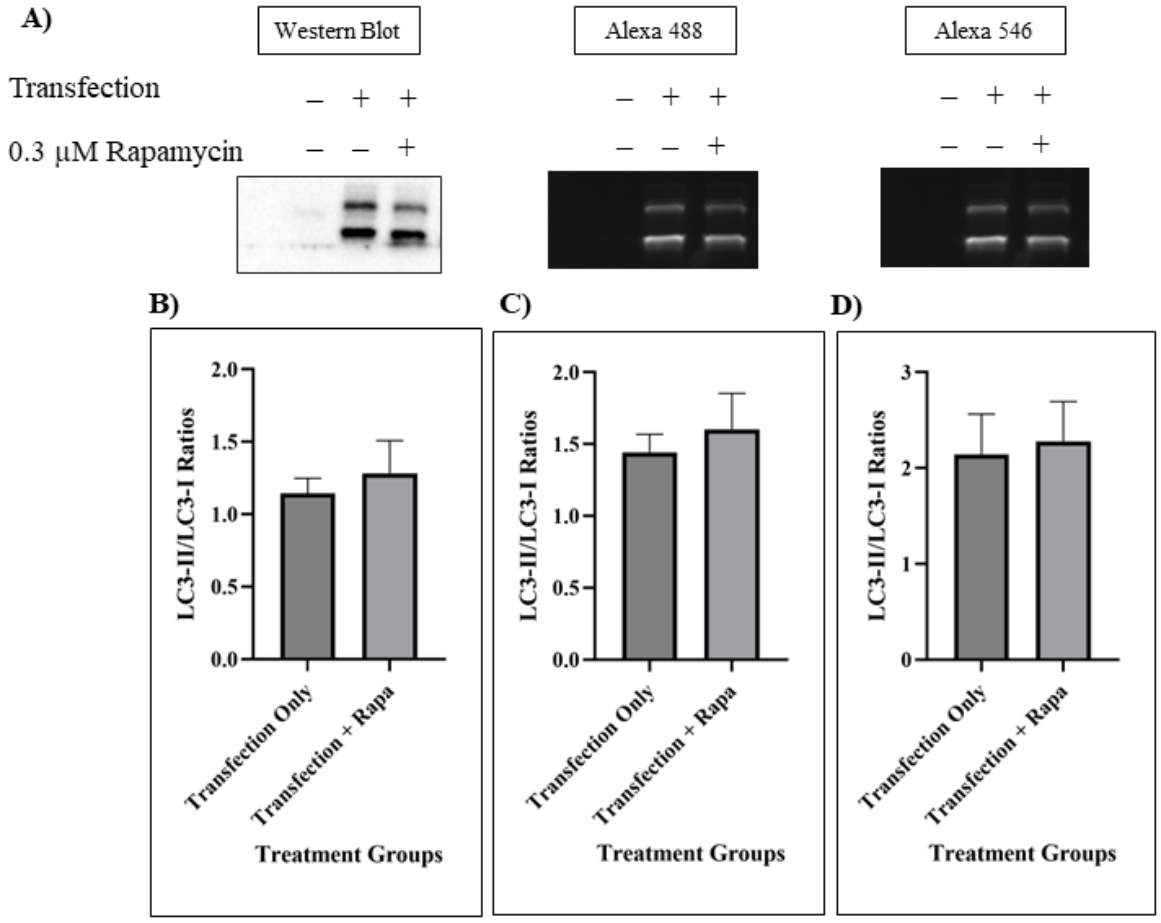

Figure 12: Effects of rapamycin treatment on transfected HEK 293 cells. The ratios shown here are averaged from 3 sets of experiments. **A:** HEK 293 cells were transfected with the EGFP-LC3B-mCherry plasmid and treated with 0.3 μM rapamycin for 24 hours. LC3-I and LC3-II bands were analyzed via western blotting and in-gel fluorescence. **B:** Western blot LC3-II/LC3-I ratios for no treatment and rapamycin-treated groups were calculated via densitometry analysis in ImageJ. Statistical significance was determined using a T-Test. A p value of $p < 0.05$ indicates statistical significance. *$p = 0.3869$.* **C:** Alexa 488 LC3-II/LC3-I ratios for no treatment and rapamycin-treated groups were calculated via densitometry analysis in ImageJ. Statistical significance was determined using a T-Test. *$p = 0.3766$.* **D:** Alexa 546 LC3-II/LC3-I ratios for no treatment and rapamycin-treated groups were calculated via densitometry analysis in ImageJ. Statistical significance was determined using a T-Test. *$p = 0.7112$.*

Starvation treatment in HEK 293 cells

To determine whether a different autophagy stimulator would provoke a similar response in transfected cells analyzed with western blotting or fluorescent imaging, we transfected cells and treated them with 50% starvation, as previously described. We then analyzed the LC3-II/LC3-I ratios with western blotting and in-gel fluorescence (Figure 13.A). In transfected cells, treatment with starvation did not result in a statistically significant change in the ratios for western blotting or in-gel fluorescence (Figure 13.B-D). The average LC3-II/LC3-I ratios for samples analyzed with western blotting were 1.23 +/- 0.06640 for the no treatment group and 1.31 +/- 0.2010 for the starvation-treated group. The average ratios for samples analyzed with the Alexa 488 filter were 1.44 +/- 0.2468 for the no treatment group and 1.47 +/- 0.06555 for the starvation-treated group. Finally, the average ratios for samples analyzed with the Alexa 546 filter were 1.67 +/- 0.3341for the no treatment group and 1.78 +/- 0.08746 for the starvation-treated group.

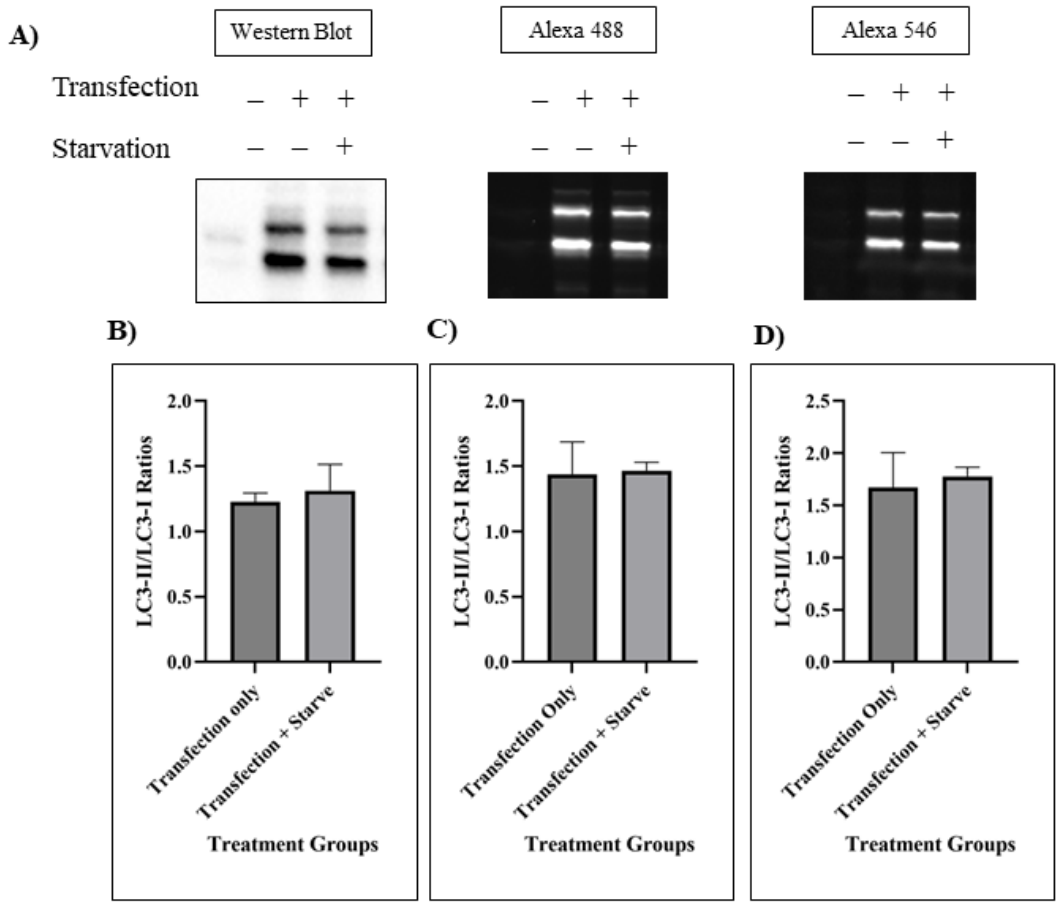

Figure 13: Effects of starvation treatment on transfected HEK 293 cells. The ratios shown here are averaged from 3 sets of experiments. **A:** HEK 293 cells were transfected with the EGFP-LC3B-mCherry plasmid and treated with 50% starvation (1 mL phosphate buffered saline with 1 mL DMEM media) for 24 hours. LC3-I and LC3-II bands were analyzed via western blotting and in-gel fluorescence. **B:** Western blot LC3-II/LC3-I ratios for no treatment and starvation-treated groups were calculated via densitometry analysis in ImageJ. Statistical significance was determined using a T-Test. A p value of $p < 0.05$ indicates statistical significance. *$p = 0.5275$.* **C:** Alexa 488 LC3-II/LC3-I ratios for no treatment and rapamycin-treated groups were calculated via densitometry analysis in ImageJ. Statistical significance was determined using a T-Test. *$p = 0.8641$.* **D:** Alexa 546 LC3-II/LC3-I ratios for no treatment and rapamycin-treated groups were calculated via densitometry analysis in ImageJ. Statistical significance was determined using a T-Test. *$p = 0.6254$.*

Chloroquine treatment in HEK 293 cells

Transfected cells dosed with rapamycin or starvation to stimulate autophagy showed no differences in the LC3-II/LC3-I ratios compared to the negative control groups. We then tested the effects of chloroquine on the LC3-II/LC3-I ratios of transfected HEK 293 cells. We dosed cells with 40 μM chloroquine and 50% starvation to both stimulate autophagy and block autophagosome-lysosome fusion and analyzed these samples with western blotting and in-gel fluorescence (Figure 14.A). We did not observe a statistically significant change in the chloroquine and starvation treated group compared to the no treatment group or the rapamycin-treated group in either western blotting or in-gel fluorescence (Figure 14.B-D). The average LC3-II/LC3-I ratios for samples analyzed with western blotting were 1.5 +/- 0.2826 for the no treatment group, 2.02 +/- 0.3528 for the rapamycin-treated group, and 1.93 +/- 0.3776 for the chloroquine-treated group. The average ratios for samples analyzed with the Alexa 488 filter were 1.56 +/- 0.05382 for the no treatment group, 2.12 +/- 0.2459 for the rapamycin-treated group, and 1.46 +/- 0.2916 for the chloroquine-treated group. Finally, the average ratios for samples analyzed with the Alexa 546 filter were 2.12 +/- 0.5010 for the no treatment group, 3.00 +/- 0.8858 for the rapamycin-treated group, and 1.86 +/- 0.7083 for the chloroquine-treated group.

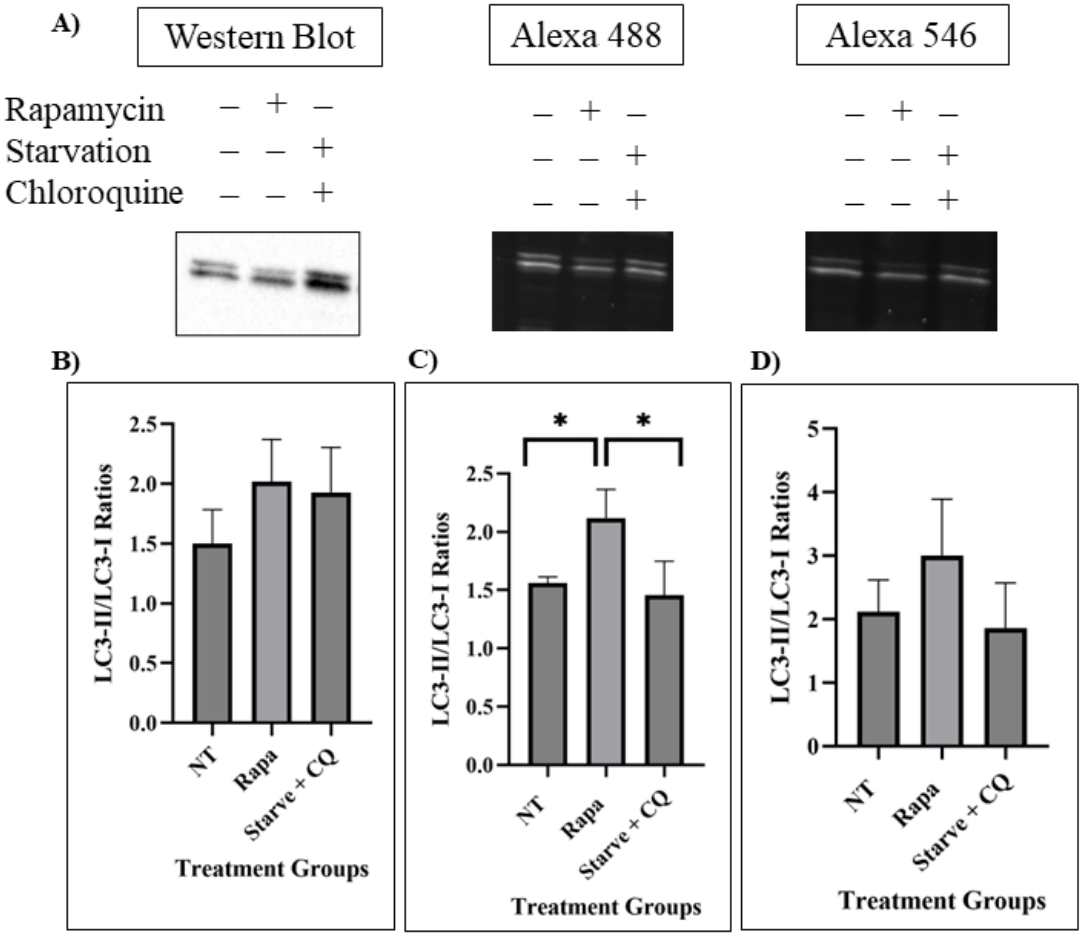

Figure 14: Effects of chloroquine treatment on transfected HEK 293 cells. The ratios shown here are averaged from 3 sets of experiments. **A:** HEK 293 cells were transfected with the EGFP-LC3B-mCherry plasmid and treated with 0.3 μM rapamycin, 50% starvation, and 5 mM chloroquine for 24 hours. LC3-I and LC3-II bands were analyzed via western blotting and in-gel fluorescence. **B:** Western blot LC3-II/LC3-I ratios were calculated via densitometry analysis in ImageJ. Statistical significance was determined using a one-way ANOVA test and a Tukey's post hoc analysis. A p value of $p < 0.05$ indicates statistical significance. *NT vs. Rapa, p = 0.2294; NT vs Starve + CQ, p = 0.3414; Rapa vs. Starve + CQ, p = 0.9431.* **C:** Alexa 488 LC3-II/LC3-I ratios were calculated via densitometry analysis in ImageJ. Statistical significance was determined using a one-way ANOVA test and a Tukey's post hoc analysis. *NT vs. Rapa, p = 0.0496; NT vs Starve + CQ, p = 0.8446; Rapa vs. Starve + CQ, p = 0.0253.* **D:** Alexa 546 LC3-II/LC3-I ratios were calculated via densitometry analysis in ImageJ. Statistical significance was determined using a one-way ANOVA test and a Tukey's post hoc analysis. *NT vs. Rapa, p = 0.3477; NT vs Starve + CQ, p = 0.9024; Rapa vs. Starve + CQ, p = 0.2044.*

The Effect of Plasmid Concentrations on LC3 Ratios

During the process of determining why transfected cells showed no statistically significant difference in the LC3-II/LC3-I ratios when dosed with rapamycin, we performed one experiment in which we transfected cells with a lower plasmid concentration to determine if lowering the plasmid concentration would augment the differences between the no treatment group and rapamycin-treated group. Cells were transfected with 1000 ng plasmid/well and 600 ng plasmid/well and treated with rapamycin. LC3-II/LC3-I ratios were analyzed with in-gel fluorescence. There was no statistically significant difference between the LC3-II/LC3-I ratios of the no treatment group and rapamycin-treated group. The resulting in-gel fluorescence images of these LC3 bands and graphs of the ratios can be found in Appendix 2 (Figure S2.1).

The Effect of Wavelength Changes on the Fluorescent intensity of LC3 bands

In addition, we asked whether in-gel fluorescence would allow us to observe changes in the signal intensities of the EGFP and mCherry tags that would correspond to different stages of autophagy. During fluorescence imaging, cells are transfected with a plasmid coding for the LC3B protein conjugated to two fluorescent tags (EGFP and mCherry). The EGFP-LC3-mCherry construct allows researchers to observe different stages of autophagy indicated by pH fluctuations in the cell. As the pH changes in the autophagosomes and lysosomes throughout the course of autophagy, the fluorescence intensity emitted by the GFP-mCherry-LC3B construct follows a predictable pattern that can yield information about the autophagic state of the cell. Low autophagic activity results in the diffuse fluorescence of both EGFP and mCherry (Figure 2.A). Early stimulation of autophagy results in the formation of green and red puncta (Figure

2.B). Late-state autophagy results in the presence of red puncta only, as the low pH of the autophagolysosome quenches the green signal from the EGFP tag (Figure 2.C). We asked whether samples undergoing autophagy would also show a decrease in the green signal of the LC3-II bands relative to a no treatment group. We also asked whether the red LC3-II band signal would be increased in samples undergoing autophagy compared to the green LC3-II band signal. We measured the intensities of individual LC3 bands imaged with in-gel fluorescence in a negative control group and a group dosed with rapamycin (Figure 15.A). We did not observe a statistically significant difference between the intensity values of the LC3-II bands between the no treatment group and rapamycin-treated group of each respective filter (Figure 15.B). We also did not observe a statistically significant difference between the intensity values of samples undergoing autophagy imaged with the Alexa 488 and Alexa 546 filter (Figure 15.B). In addition, we measured the fluorescence intensity of total lysates transfected with the EGFP-mCherry-LC3B plasmid to determine A) if there was a decrease in green signal in samples dosed with rapamycin compared to the green signal of the no treatment group, and B) if there was an increase in red signal in samples dosed with rapamycin compared to the green signal of samples dosed with rapamycin. Although there was a trend toward a decrease in green signal in samples dosed with rapamycin, there was no statistically significant difference in the fluorescent intensities of any of the treatment groups (Figure 15.C).

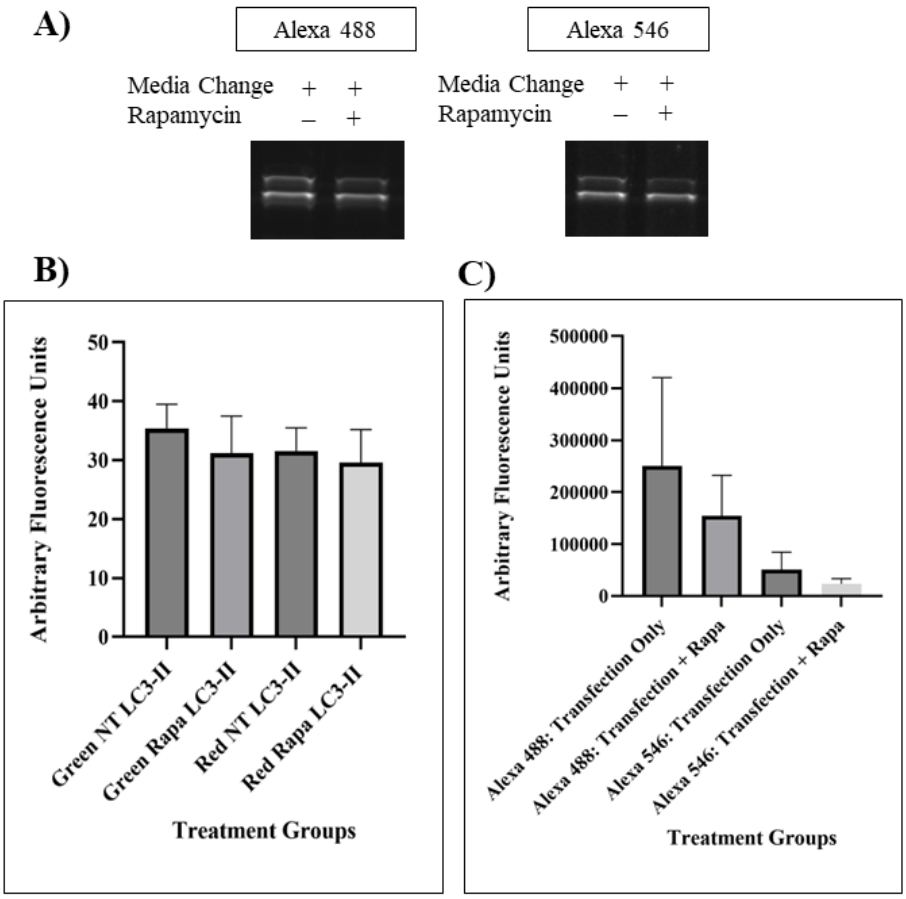

Figure 15: Fluorescent intensity of transfected samples. Ratios are averages from a triplicate set of experiments. A: In-gel fluorescence images of cells treated with a media change and rapamycin. B: Fluorescent intensities of LC3 bands imaged with the Alexa 488 filter. Statistical significance was assessed with an ANOVA test and a Tukey's Multiple Comparisons Test. A p-value of <0.05 was considered to be statistically significant. *NT LC3-I vs Rapa LC3-I*: *P = 0.3973; NT LC3-II vs Rapa LC3-II: P = 0.6127.* C: Fluorescent intensities of total lysates imaged with wavelengths corresponding to the Alexa 488 filter and the Alexa 546 filter. Statistical significance was assessed with an ANOVA test and a Tukey's Multiple Comparisons Test. A p-value of <0.05 was considered to be statistically significant. *Alexa 488: Transfection Only vs Alexa 488: Transfection + Rapa, p = 0.6208; Alexa 488 Transfection Only vs Alexa 546 Transfection Only, p = 0.1224; Alexa 488: Transfection + Rapa vs. Alexa 546: Transfection Only, p = 0.5730; Alexa 488: Transfection + Rapa vs. Alexa 546: Transfection + Rapa, p = 0.3918.*

Effect of Alexa Filters on Fluorescent Intensity of Lysates

We consistently observed that the fluorescent intensities of protein bands imaged with the Alexa 546 filter (detects mCherry) were lower in comparison to the fluorescent intensities of protein bands imaged with the Alexa 488 filter (detects EGFP). We wondered whether the Alexa 546 filter was not optimized for the mCherry tag, and we asked whether using a different combination of excitation and emission wavelengths would yield higher signal intensities from our lysates. We performed one experiment in which we measured the total fluorescence of no treatment and rapamycin-treated lysates with a fluorescent plate reader at three wavelength combinations: excitation/emission wavelengths of 488 nm/535 nm corresponding to the Alexa Fluor 488 dye, excitation/emission wavelengths of 546 nm/590 nm corresponding to the Alexa Fluor 546 dye, and excitation/emission wavelengths of 587 nm/630 nm corresponding to the optimal wavelengths for mCherry fluorescence. This experiment was performed once, and there was a trend towards lower fluorescence intensities when the Alexa 546 wavelengths were used compared to the Alexa 587 wavelengths. The resulting graph of the fluorescent intensities can be found in Appendix 2 (Figure S2.2).

The Effect of Media Change on LC3-II/LC3-I Ratios in Transfected Cells

Nontransfected cells treated with a media change on day 3 of a 4-day experiment showed statistically significant differences in the LC3-II/LC3-I ratios of no treatment groups and rapamycin-treated groups. To determine whether this effect could be replicated in transfected cells, we changed the media on transfected cells 24 hours after transfection, or 3 days after seeding. Cells were then dosed with rapamycin and compared to a no treatment control group. Cell lysates were imaged with western blotting and in-gel fluorescence and LC3-II/LC3-I ratios were calculated (Figure 16.A). Transfected cells treated with a media change showed a statistically significant difference in the LC3-II/LC3-I ratios between the negative and positive control group in the Alexa 488 and Alexa 546 filters (an average ratio of 1.92 +/- 0.06957 in the no treatment group compared to 2.44 +/- 0.07877 in the rapamycin-treated group with the Alexa 488 filter and an average ratio of 2.75 +/- 0.3283 in the no treatment group compared to 4.16 +/- 0.6422 in the rapamycin-treated group with the Alexa 546 filter (Figure 16.C-D). However, there was no statistically significant difference in the LC3-II/LC3-I ratios of the no treatment group and rapamycin-treated groups with western blotting (an average ratio of 2.09 +/- 0.1189 in the no treatment group compared to 2.35 +/- 0.3158 in the rapamycin-treated groups) (Figure 16.B).

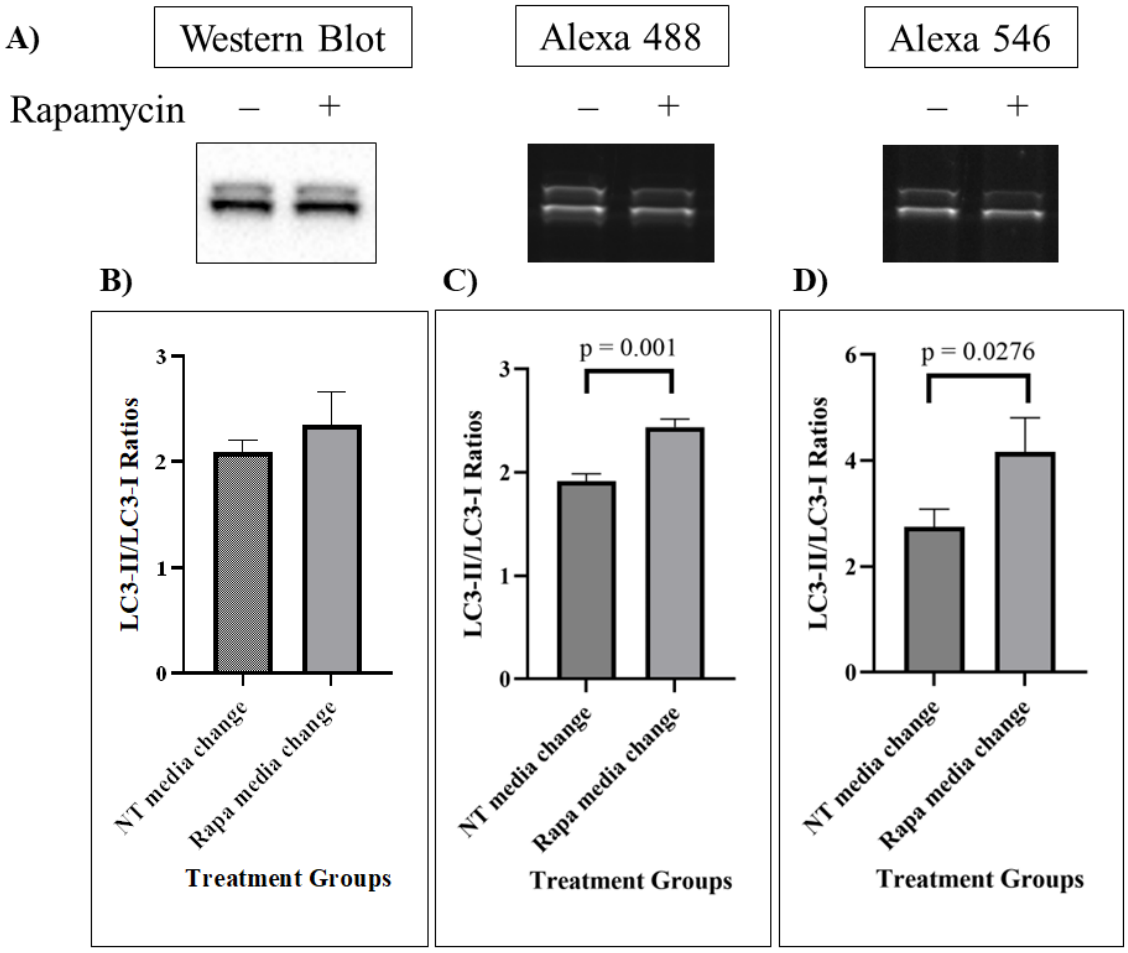

Figure 16: Effects of media change on transfected HEK 293 cells. **A:** HEK 293 cells were dosed with 0.3 µM rapamycin for 24 hours and incubated for 96 hours. LC3-I, LC3-II, and GAPDH bands were analyzed via western blotting and in-gel fluorescence. **B:** Western blot LC3-II/LC3-I ratios for 4-day treatment groups with a media change were calculated via densitometry analysis in ImageJ. Statistical significance was determined using a T-Test. A p value of $p < 0.05$ indicates statistical significance. *$p = 0.2556$.* **C:** Alexa 488 LC3-II/LC3-I ratios for 4-day treatment groups with a media change were calculated via densitometry analysis in ImageJ. Statistical significance was determined using a T-Test. *$p = 0.001$.* **D:** Alexa 546 LC3-II/LC3-I ratios for 4-day treatment groups with a media change were calculated via densitometry analysis in ImageJ. Statistical significance was determined using a T-Test. *$p = 0.0276$.*

Effects of Crude Keratin Extract on Autophagy in HEK 293 Cells

Previous data from our lab suggested that keratin in combination with an autophagy stimulator such as starvation resulted in a more pronounced autophagy response compared to cells treated with the autophagy stimulator alone. To test this, we treated cells with a combination of 0.1 mg/mL crude keratin extract and 50% starvation and analyzed cells with regular western blots. HEK 293 cells were also dosed with 50% starvation alone as a positive control, 40 μM chloroquine to block autophagosome-lysosome fusion, a combination of 50% starvation and 40 μM chloroquine to both stimulate autophagy and block its late stage, and a combination of 50% starvation, 40 μM chloroquine, and 0.1 mg/mL crude keratin extract (Figure 17.A).

The treatment groups containing keratin alone did not reveal statistically significant changes in the LC3-II/LC3-I ratios compared to the negative control group (an average ratio of 0.41 +/- 0.03131 in the keratin-treated group compared to 0.65 +/- 0.1489 in the no-treatment group) (Figure 17.B). We also combined 50% starvation with 0.1 mg/mL crude keratin extract to determine if keratin augmented the autophagy response in stressed cells. We did not observe a statistically significant change in LC3-II/LC3-I ratios in these samples compared to the starvation alone group (an average ratio of 0.84 +/- 0.2420 in the starvation and keratin treated group, compared to a ratio of 0.73 +/- 0.3590 in the starvation-only treated group) (Figure 17.B).

We also compared the LC3-II/LC3-I ratios of cells treated with chloroquine alone, cells treated with a combination of starvation and chloroquine, and cells treated with a combination of keratin, starvation, and chloroquine. There was no statistically significant difference between the

LC3-II/LC3-I ratios of cells dosed with chloroquine alone, chloroquine in combination with starvation, and chloroquine in combination with starvation and keratin (cells dosed with chloroquine alone had an average LC3-II/LC3-I ratio of 2.09 +/- 0.4875, compared to a ratio of 2.25 +/- 0.9874 in the group dosed with both starvation and chloroquine and an average ratio of 3.08 +/- 0.7389 in the group dosed with keratin, starvation, and chloroquine) (Figure 17.C). However, there was a statistically significant difference between the LC3-II/LC3-I ratios of the keratin and starvation treated group compared to the group treated with a combination of keratin, starvation, and chloroquine (an average ratio of 0.84 +/- 0.2420 in the cells treated with keratin and starvation compared to an average ratio of 3.08 +/- 0.7389 in the cells treated with a combination of keratin, starvation, and chloroquine) (Figure 17.C).

In addition to measuring the LC3-II/LC3-I ratios, we measured the LC3-II/GAPDH ratios of cells dosed with keratin, starvation, and chloroquine. Our treatment groups containing keratin alone did not reveal statistically significant changes in the LC3-II/GAPDH ratios compared to the negative control group (an average ratio of 0.16 +/- 0.02525 in the keratin-treated group compared to 0.4 +/- 0.1475 in the no-treatment group) (Figure 17.D). We also combined 50% starvation with 0.1 mg/mL crude keratin extract to determine if keratin augmented the autophagy response in stressed cells. We did not observe a statistically significant change in LC3-II/GAPDH ratios in these samples compared to the starvation alone group (an average ratio of 0.21 +/- 0.1041 in the starvation and keratin treated group, compared to a ratio of 0.27 +/- 0.09349 in the starvation-only treated group) (Figure 17.D).

There was no statistically significant difference between the LC3-II/GAPDH ratios of cells dosed with chloroquine alone or chloroquine in combination with starvation, and

chloroquine in combination with starvation and keratin (cells dosed with chloroquine alone had an average LC3-II/GAPDH ratio of 1.9 +/- 0.2502, compared to a ratio of 1.43 +/- 0.5439 in the group dosed with both starvation and chloroquine and a ratio of 1.40 +/- 0.3288 in the group dosed with keratin, starvation, and chloroquine) (Figure 17.E). However, there was a statistically significant difference between the LC3-II/GAPDH ratios of the keratin and starvation treated group compared to the group treated with chloroquine alone, chloroquine combined with starvation, and chloroquine combined with keratin and starvation (an average ratio of 0.21 +/- 0.1041 in the cells treated with keratin and starvation compared to an average ratio of 1.9 +/- 0.2502 in the cells treated with chloroquine, 1.43 +/- 0.5439 in the cells treated with chloroquine and starvation, and 1.40 +/- 0.3288 in the cells treated with chloroquine, starvation, and keratin) (Figure 17.E).

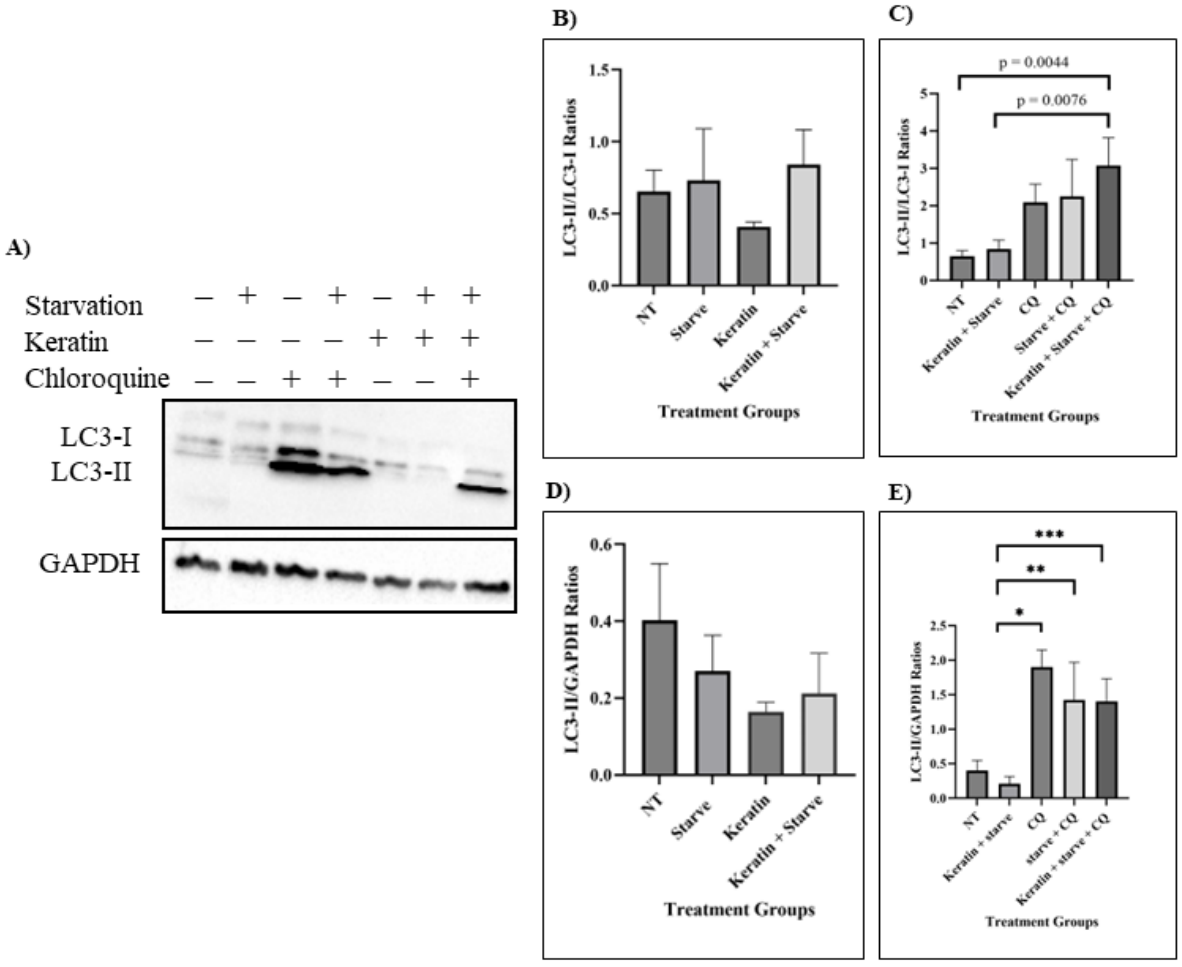
A)
Starvation
Keratin
Chloroquine
LC3-I
LC3-II
GAPDH
B)
LC3-II/LC3-I Ratios
NT
Starve
Keratin
Keratin + Starve
Treatment Groups
C)
p = 0.0044
p = 0.0076
LC3-II/LC3-I Ratios
NT
Keratin + Starve
CQ
Starve + CQ
Keratin + Starve + CQ
Treatment Groups
D)
LC3-II/GAPDH Ratios
NT
Starve
Keratin
Keratin + Starve
Treatment Groups
E)
***
**
*
LC3-II/GAPDH Ratios
NT
Keratin + starve
CQ
starve + CQ
Keratin + starve + CQ
Treatment Groups

Figure 17: Effects of crude keratin treatment on nontransfected HEK 293 cells. Ratios are averaged from triplicate sets of experiments. **A:** HEK 293 cells were dosed with 0.1 mg/mL of crude keratin extract for 24 hours and lysed. LC3-I, LC3-II, and GAPDH bands were analyzed via western blotting. **B:** LC3-II/LC3-I ratios for no treatment, starvation, keratin, and keratin + starvation groups were calculated via densitometry analysis in ImageJ. Statistical significance was determined using an ANOVA test and Tukey's post hoc analysis. A p value of $p < 0.05$ indicates statistical significance. *NT vs starve, p = >0.9999; NT vs keratin, p = 0.9970; NT vs. keratin + starve, p = 0.9993.* **C:** LC3-II/LC3-I ratios for chloroquine, starvation + chloroquine, keratin + starvation + chloroquine, and keratin + starvation groups were calculated via densitometry analysis in ImageJ. Statistical significance was determined using an ANOVA test and Tukey's post hoc analysis. *CQ vs starve + CQ, p = 0.9997; CQ vs keratin + starve + CQ, p = 0.3137; starve + CQ vs keratin + starve + CQ, p= 0.5062, keratin + starve vs. keratin + starve + CQ, p = 0.0021.* **D.** LC3-II/GAPDH ratios for no treatment, starvation, keratin, and keratin + starvation groups were calculated via densitometry analysis in ImageJ. Statistical significance was determined using an ANOVA test and Tukey's post hoc analysis. *NT vs starve, p = 0.9957; NT vs keratin, p = 0.9233; NT vs keratin + starve, p = 0.9723; NT vs keratin + starve, p > 0.9999.* **E.** LC3-II/GAPDH ratios for chloroquine, starvation + chloroquine, keratin + starvation + chloroquine, and keratin + starvation groups were calculated via densitometry analysis in ImageJ. Statistical significance was determined using an ANOVA test and Tukey's post hoc analysis. *CQ vs starve + CQ, p = 0.3779; CQ vs keratin + starve + CQ, p = 0.3312; starve + CQ vs keratin + starve + CQ, p > 0.9999, keratin + starve vs. keratin + starve + CQ, p = 0.0014.*

Keratin's Effect on Cytotoxicity in Cell Cultures

In addition to testing the impact of keratin treatment on starved cells, we performed a WST-1 assay to test whether keratin impacted the toxicity of cells treated with various degrees of starvation (50%, 75%, and 100% starvation). Cells were treated with 0.5 mg/mL crude keratin extract and phosphate-buffered saline (PBS) to starve cells. Raw absorbance values from the WST-1 assay were expressed as fold change compared to a no treatment control and displayed in a box plot. The box plot shows a decrease in fold change as starvation treatment increased from 50% to 75% to 100% (Figure 18). In addition, the box plot revealed that there was no change in the cytotoxicity of cells dosed with 50% starvation compared to cells dosed with keratin and 50% starvation. In addition, there was no difference in cells dosed with 75% starvation compared to cells dosed with 75% starvation and keratin. Finally, there was no difference between cells dosed with 100% starvation compared to cells dosed with 100% starvation and keratin (Figure 18).

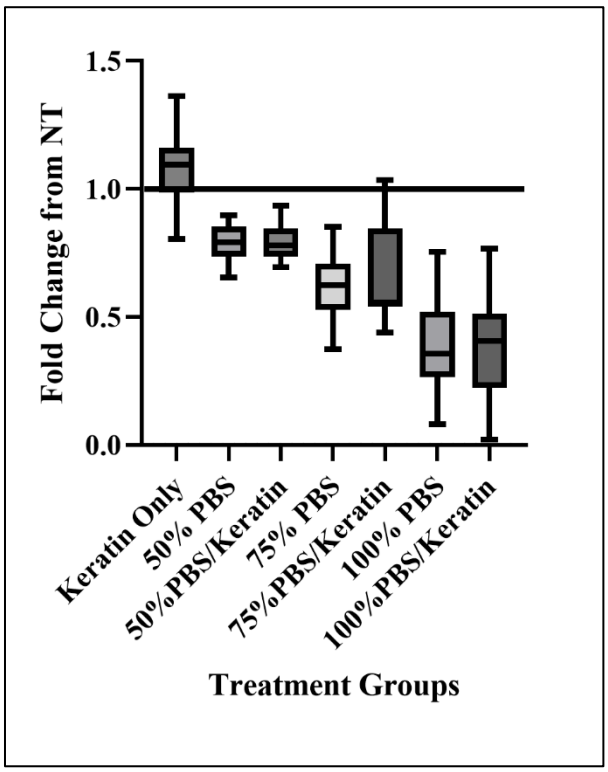

Figure 18: Cytotoxicity of cells dosed with starvation and keratin. Cells were dosed with varying degrees of phosphate-buffered saline (PBS) alone or in combination with crude keratin extract. Fold change is measured in reference to the no treatment (NT) control, which is expressed as a value of 1.0 on this graph.

DISCUSSION

Autophagy is a recycling pathway that is used by cells to adapt to stressors such as nutrient starvation and oxidative stress. Because of its role as a cytoprotective response, autophagy is a popular target among researchers looking to enhance cell viability and survival with biomaterials. Research suggests that the biomaterial keratin has cytoprotective effects via activation of cell recycling pathways, but more research is necessary to further elucidate the link between keratin and autophagy.

In order to study autophagy and how it relates to keratin, our lab has relied on using western blotting or fluorescent imaging analysis to track changing levels of the LC3 protein in cells. However, both of these methods have presented many challenges to the Coan lab. Western blotting is expensive and difficult for a primarily undergraduate-based lab to maintain. In addition, although fluorescent imaging is a helpful screening tool and serves as a complement to other data-collecting methods, fluorescent imaging is not a quantitative method, and interpretation of images is often subjective and prone to error. Therefore, the first aim of this thesis was to develop a method for analyzing autophagy in cell cultures that sidestepped some of the drawbacks of using western blotting and fluorescent imaging by being cheaper, easier, and more quantitative. We then compared the usability of in-gel fluorescence to western blotting and fluorescent imaging. The second aim of this thesis was to investigate the relationship between keratin and autophagy in HEK 293 cells.

Aim 1: In-gel Fluorescence and Autophagy Modulators

Before we could use in-gel fluorescence to study autophagy, it was necessary to establish a baseline for how HEK 293 cells respond to various autophagy modulators. One of the

characteristics of the HEK 293 cell line is the high degree of variability within the HEK cell genotype depending on the laboratory culturing the cells. Stepanenko & Dmitrenko (2015) describe a wide range of variability in the reported chromosome numbers and aberrations of HEK 293 cell lines cultured and sold by different suppliers such as the American Type Culture Collection and the European Collection of Cell Cultures. They argue that long-term propagation of HEK 293 cells can lead to the accumulation of mutations and thus distinct differences in the behavior of cells grown in different labs [70]. Similarly, Lin et al. (2014) suggest that the long-term culturing of HEK cells in different labs has led to genomic changes that could underlie the sometimes conflicting results obtained when HEK cells are used for experiments [71]. Therefore, it is possible that the HEK 293 cells grown in the Coan lab have a distinct genetic profile from other HEK cells and may respond to autophagy modulators differently from other HEK cells, thus requiring us to characterize the responses of our HEK cells before moving into the study of autophagy.

Positive Autophagy Controls. We began categorizing the responses of our HEK 293 cells to autophagy modulators by dosing nontransfected HEK 293 cells with the autophagy stimulators rapamycin and starvation, as well as the late-stage autophagy blocker chloroquine. Treatment with rapamycin resulted in the expected high LC3-II/LC3-I ratios and high LC3-II/GAPDH ratios indicating autophagy activity in those cells. Even so, we noted that the negative control groups in these experiments displayed prevalent levels of LC3-II in western blots. We attribute the prevalence of LC3-II in our no treatment groups to the higher basal autophagy levels typical of immortalized cell lines [27]. In addition to treatment with rapamycin, we also treated cells with 50% starvation (1 mL phosphate-buffered saline and 1 mL DMEM) for 24 hours to

stimulate autophagy. 24 hours as a timepoint was used because it was determined to be the optimal time point to measure autophagy with rapamycin and chloroquine, our autophagy controls. In contrast to the groups dosed with rapamycin, we did not observe a statistically significant increase in the LC3-II/LC3-I ratios or LC3-II/GAPDH ratios in starved cells compared to the no treatment group. This is not completely unexpected, as previous experiments in our lab have also shown a decreased presence of LC3 in cells treated with starvation at 24 hours post-treatment [62]. In addition, reports of lower levels of LC3-II in cells treated with starvation have been noted by several groups. For example, Nash et al. (2017) treated microglial cells with starvation for four hours and observed a steady decrease in LC3 levels from the time of initial starvation to four hours post treatment [72]. In addition, Tanida et al. (2005) used starvation to induce autophagy in HEK 293 cells and HeLa cells. In HeLa cells, they report a decrease in the LC3-II levels compared to the negative control when starvation was administered for 2 hours. The authors reason that the decrease in LC3-II was due to high levels of turnover in the autophagy pathway once it had been induced via starvation [73]. On the other hand, Husak and Dworzak (2017) argued that the decrease in LC3-II/LC3-I ratios observed upon the treatment of human bone marrow stromal cells with a prolonged hypoxia and starvation was indicative of a decrease in autophagy activity. This conclusion was supported by the decreased presence of other autophagy-related proteins studied, such as ATG13 [74]. Finally, Klionsky et al. (2021) in the *Guidelines for the Use and Interpretation of Assays to Monitor Autophagy* admit that starvation in mammalian cells often results in diminished levels of LC3-II as observed via western blotting [27]. Although these reports lend validity to the lack of statistically significant change we observed in the LC3-II/LC3-I ratios and LC3-II/GAPDH ratios of cells dosed with starvation compared to a no treatment group, we also reasoned that the 24-hour time point may

have been too late for us to observe changes in these ratios. 50% starvation had been used previously in our lab to study autophagy at 2- and 4-hours post-treatment, but these were much earlier timepoints than those used in the current experiments, and autophagy may have resumed basal levels of operation by the time 24 hours has passed. For example, Poranki & Van Dyke (2014) studied the gene expression profiles of cells treated with heat shock in the presence of gamma keratin, and they found that the upregulation of autophagy genes noted at 12 and 18 hours post heat shock had decreased by the time 24 hours had passed [3]. Future work with starvation as an autophagy stimulator in this lab should investigate earlier time points to determine if starvation induces an initial change in the LC3-II/LC3-I ratios and LC3-II/GAPDH ratios which then resolves at a later time point.

An additional explanation as to the lack of change in the ratios when cells were treated with starvation is that 50% starvation was not an adequate stimulator of autophagy activity in HEK 293 cells. Previous experiments in our lab had used 100% starvation (2 mL phosphate buffered saline) to stimulate autophagy for 4-hour experiments [63]. Treatment with 100% starvation in these experiments resulted in the expected increase in autophagy activity. In the current study, we aimed to compare the effects of starvation to the effects of rapamycin treatment at a much later timepoint than previous experiments (24 hours). This was because rapamycin treatment had shown to have its greatest impact at 24 hours post treatment in our HEK 293 cells. However, 100% starvation for 24 hours led to cell detachment from the culture dish and a decrease in cell viability. One possibility this occurred is because of the lack of calcium and magnesium in the PBS used for these experiments. To prevent excess detachment and maintain the viability of cells, we chose 50% starvation as an alternative to 100% starvation [68]. Analysis

of autophagy at 24 hours in the 50% starvation group showed a negligible change in the LC3-II/LC3-I ratios compared to the negative control. Different results may be observed if a higher percentage of starvation was used to study autophagy in addition to an earlier timepoint, although this may require additional mechanisms to prevent cell detachment, such as the application of poly-L-Lysine to cell culture dishes prior to cell seeding.

Negative Autophagy Controls. In addition to testing the use of autophagy stimulators on HEK 293 cells, we also dosed HEK 293 cells with the late-stage autophagy blocker chloroquine to determine its effects upon LC3 ratios in our cells. The application of chloroquine results in the increased buildup of the LC3-II protein, which manifests as an increased LC3-II/LC3-I ratio and LC3-II/GAPDH ratio when compared to a no treatment group and a positive control group. Blocked autophagosome-lysosome fusion has been observed in disease states such as osteoarthritis and can also be induced with drugs such as chloroquine [22, 27]. When chloroquine is used to block autophagy, the LC3-II/LC3-I ratios in the chloroquine group should be higher than the LC3-II/LC3-I ratios in the positive control group [27]. A lower ratio in the positive control group indicates LC3 turnover is occurring properly in the final stages of autophagy. A higher or equal ratio in the positive control group or the treatment group compared to the chloroquine-treated group indicates there is a blockage in the ability of autophagy to proceed through its final stages. The LC3-II/LC3-I ratio of the treatment group can be subtracted from the same ratio in the chloroquine control group to determine whether autophagy is blocked or whether autophagy is truly occurring. Researchers commonly combine the treatment of chloroquine with an autophagy stimulator like rapamycin or starvation to simulate a situation in which autophagic activity is occurring but is blocked in its late stages due to dysfunction in the

pathway. We dosed cells with a combination of starvation and chloroquine and did not see a statistically significant change in the LC3 ratios compared to cells dosed with chloroquine alone. Because the LC3 ratios were not augmented in this group compared to the group with chloroquine alone, this may suggest that the method of starvation we used was not sufficient to stimulate an autophagy response in our cells. At the same time, some evidence exists that chloroquine alone is capable of stimulating autophagy activity, so it is possible that both chloroquine-treated groups had active autophagy occurring, which would explain the lack of difference between the LC3 ratios of the two groups [75]. Despite these ambiguities, when we dosed cells with chloroquine, we observed a statistically significant change in the LC3-II/LC3-I ratios and LC3-II/GAPDH ratios in this group compared to the no treatment group and starvation-treated group, allowing us to categorize the expected changes in LC3 when chloroquine is added to cells. In addition, we combined the treatment of chloroquine with the treatment of starvation to both initiate autophagy and stimulate an autophagy blockage and also observed a statistically significant increase in the LC3-II/LC3-I ratios and LC3-II/GAPDH ratios compared to the negative control groups and starvation-treated groups.

The mechanism of action of chloroquine has been a subject of debate in recent years. Although it has widely been accepted that the basic properties of chloroquine inhibit late-stage autophagy by raising the pH of the lysosome and thus preventing the degradation of intralysosomal components, recent studies report conflicting results regarding the ability of chloroquine to raise the lysosomal pH [75]. These studies use LysoTracker Red dye to estimate changes in the pH of the lysosome when cells are treated with chloroquine. One study by Jacquin et al. (2017) used LysoTracker Red dye to monitor the acidity of lysosomes after treatment with

chloroquine. When the cells were dosed with chloroquine, the fluorescence intensity of the LysoTracker Red dye decreased, indicating that chloroquine raised the pH of the lysosomes [76]. However, a study by Lu et al. (2017) found that this decrease in LysoTracker Red dye was transient, peaking at 30 minutes of treatment and resolving to control levels at 1-hour post-treatment [77]. Similarly, Mauthe et al. (2018) used LysoTracker Red to probe the impacts of chloroquine on lysosomal acidity and did not report a decrease in fluorescence intensity following treatment with chloroquine. Mauthe et al. (2018) note that the lack of clarity regarding the ability of chloroquine to raise the pH of the lysosome is due to the different time points used for the measuring of LysoTracker Red intensity. The authors also acknowledge the limitations of using LysoTracker Red as an indicator of pH [75]. Although LysoTracker Red can give an estimation of pH in cellular compartments by losing fluorescence intensity around pH > 6.5, the fluorescence intensity of LysoTracker Red does not correlate to changes in pH [75]. Thus, studies relying on LysoTracker red are unclear regarding the effect chloroquine has on the pH of the lysosome.

Because of the lack of clarity regarding chloroquine's ability to alter lysosomal pH, Mauthe et al. (2018) suggest that chloroquine instead acts by inhibiting autophagosome-lysosome fusion [75]. They performed a colocalization analysis to study the impact of chloroquine upon autophagosomal SNARE colocalization with the lysosomal protein LAMP2A. Increased colocalization of the two proteins inferred that autophagosome-lysosome fusion was occurring. When cells were treated with chloroquine, the authors observed a decreased colocalization of the SNAP29 SNARE protein with LAMP2A. They reasoned that chloroquine inhibited the ability of the cells to recruit SNAP29 and speculate that this failure to recruit

SNAP29 could be due to the large-scale remodeling of the Golgi complex they also observed upon treatment with chloroquine [75]. Thus, the authors propose that chloroquine inhibits late-stage autophagy by preventing autophagosome-lysosome fusion.

Another additional autophagy modulator that we hope to use in future studies is the autophagy inhibitor 3-MA. While chloroquine is often used to block late-stage autophagy, the compound 3-methyladenine (3-MA) is used to block early-stage autophagy and is thus included in studies as a negative control [29]. 3-MA inhibits autophagy by targeting one of the complexes necessary for formation of the autophagosome, the PI3KC3 complex. This lipid kinase works together with the BECN1 protein to phosphorylate phosphoinositol and create PI3P [29]. By blocking the action of PI3KC3, the production of PI3P is decreased. PI3P is important for the recruitment of ATG machinery, and without its action, the autophagosome cannot be synthesized [29]. This prevents the conversion of LC3-I to LC3-II. Treatment with 3-MA would thus be expected to result in a low LC3-II/LC3-I ratio or a low LC3-II/GAPDH ratio. Future studies in our lab will attempt to establish a baseline for the response of HEK 293 cells to 3-MA. This will be beneficial in helping us answer questions about the relatively high levels of background autophagy we note in some of our no treatment groups in both nontransfected cells and transfected cells.

LC3 Ratios. In order to determine the effects of rapamycin, starvation, and chloroquine on our HEK 293 cells, we performed western blots and measured the LC3-II/LC3-I ratios and LC3-II/GAPDH ratios as indicators of autophagy activity. These ratios are both commonly used to analyze levels of autophagy in cell cultures. However, caution must be used when interpreting these ratios for several reasons. First, turnover between LC3-I to LC3-II does not always follow

a predictable pattern. Although it is generally accepted that an increase in LC3-II relative to LC3-I or LC3-II to GAPDH is indicative of autophagy activity, it is also possible that a decrease in LC3-II relative to LC3-I can be indicative of autophagic activity, due to high levels of autophagosome-lysosome fusion and turnover and thus degradation of the LC3 protein [27]. This particular response has been noted in the response of mammalian cells to treatment with starvation [27]. In addition to decreased levels of LC3-II as an indicator of high autophagic activity, the induction of autophagy could also stimulate a decrease in the levels of both LC3-I and LC3-II. Such a response may be noted in cells undergoing high levels of background autophagy, such as in immortalized cell lines [27]. Thus, it is vital to use positive and negative controls alongside treatment groups when calculating the LC3 ratios in order to determine the expected response of a particular cell line. Klionsky et al. (2021) recommend calculating the ratio between LC3-II to GAPDH or another housekeeping protein as a measure of autophagy, although they admit that neglecting LC3-I may prevent researchers from understanding the whole measure of autophagic flux in their cell cultures [27]. Calculating the ratio between LC3-II/GAPDH may lead to incorrect conclusions about the state of autophagy, as autophagy sometimes results in the decrease of circulating levels of LC3-II. They suggest that LC3-II/GAPDH ratios be complemented with LC3-II/LC3-I ratios in the study of autophagy.

Another important note when using LC3 to study autophagy is that LC3 has been noted to participate in nonautophagy-related activities in cells. For example, LC3-II has been observed to be recruited alongside tubules emanating from lysosomes and potentially contributes to lysosomal membrane expansion [27]. Because LC3 can be recruited to assist in nonautophagic

activities, it is vital to couple LC3 analysis with the analysis of additional autophagy marker proteins in order to definitely say whether or not autophagy is happening in cells.

Measuring Autophagy via p62 Levels. One example of an autophagy marker protein used alongside the analysis of LC3 is the cargo receptor p62. p62 is capable of binding to ubiquitinated substrates within a cell and transports them to the LC3-II docking sites on the surface of autophagosomes, where it then binds and allows the entry of cargo into the autophagosome [27]. As the cargo enters the autophagosome, p62 is taken up into the autophagosome and degraded once fusion with the lysosome occurs. Thus, a decrease in the levels of p62 as seen on a western blot indicates that autophagic flux is occurring. A buildup of p62 indicates that autophagy is not occurring, or that it is inhibited [27].

Despite the potential for p62 as an indicator of autophagy, there are many context-dependent responses of p62 that must be interpreted with caution, as with the LC3 protein. Although a decrease in p62 levels generally indicate autophagy activity, some researchers have observed a transient increase in levels of p62 when autophagy is stimulated, likely due to an increased transcription of p62 as autophagy initiates [27]. On the other hand, decreased levels of p62 could also be indicative of apoptosis. p62 is cleaved by caspase 6 and caspase 8 during apoptosis, thus resulting in decreased levels of the protein detected via western blot. In order to distinguish between autophagy and apoptosis on a western blot, Klionsky et al. (2021) recommend using caspase inhibitors as controls to determine whether decreased levels are due to autophagy or apoptosis [27].

In addition to the variability of responses observed with p62 levels, it must also be remembered that p62 has been implicated in an additional cell recycling pathway (the ubiquitin-

proteasome system, or the UPS). In this pathway, p62 plays a similar role as it does in the autophagy pathway, namely, sequestration of ubiquitinated cargo and delivery of cargo to the proteasome [27]. In order to determine whether p62 levels are reflective of autophagy or the UPS, proteasome inhibitors and autophagy inhibitors should be applied to serve as controls. Therefore, p62 levels themselves should not be interpreted without the context of other autophagy proteins [27]. Because of the variability in the expected responses of LC3 and p62 to different autophagy states, future studies in the Coan lab will integrate the analysis of an additional autophagy marker protein alongside the data sets obtained in this study.

Four Days of Cell Growth and Media Changes. After establishing the expected responses of our HEK 293 cells to rapamycin, starvation, and chloroquine by measuring both LC3-II/LC3-I ratios and LC3-II/GAPDH ratios, we sought to determine whether nontransfected cells grown for 4 days showed altered autophagy levels compared to cells grown for a standard 3-day experiment. The experiments we performed with nontransfected cells take up to 3 days to complete. However, the transfection process used for the in-gel fluorescence method required an extra 24 hours added to the 3-day process. We wondered whether the extra day would change the autophagy response in our cells to treatment with rapamycin. Nontransfected cells grown for 3 days showed the expected statistically significant changes in the LC3-II/LC3-I ratios and LC3-II/GAPDH ratios of the no treatment group and rapamycin-treated group. However, nontransfected cells grown for 4 days did not show a statistically significant change between the no treatment group and rapamycin-treated group. We reasoned that the extra day of incubation was compounding the stressors our cells were subjected to, such as diminished nutrient availability and pH changes within the old media and stimulating excess autophagy in our no

treatment control group. We hypothesized that the high levels of autophagy in the no treatment group prevented us from seeing differences in autophagy levels between the no treatment control and rapamycin-treated group. In order to ameliorate the stressors placed upon our cells during the extra day of incubation required during transfection experiments, we tested whether changing the media of our cells would alter the LC3-II/LC3-I ratios and the LC3-II/GAPDH ratios. We decided to test a media change because a previous set of experiments in our lab demonstrated that changing the media on day 4 of an experiment restored the expected autophagy levels in a no-treatment group compared to a rapamycin-treated group (Figure 8). In nontransfected cells, changing the cell media at day 3 and assessing autophagy activity with western blotting after day 4 resulted in the statistically significant change in the LC3-II/LC3-I ratios of the negative and positive control groups, indicating the efficacy of a media change when it comes to restoring the expected levels of autophagy activity in cells. It is worth noting that we did not see a statistically significant change in the LC3-II/GAPDH ratios of nontransfected cells when we changed the media. This is because the LC3-II/GAPDH ratio method does not take into account changing levels of LC3-I and how this may contribute to autophagy activity. Although the levels of LC3-II were relatively similar in the no treatment control compared to the rapamycin-treated group, the presence of LC3-I was much higher in the no treatment groups compared to rapamycin-treated groups, thus indicating a decrease in the autophagy activity of the no treatment group because of the media change. This indicates that in-gel fluorescence is usable to study autophagy if a media change is incorporated to ameliorate cell stress.

Irregular Protein Bands: Western Blotting. In the process of performing western blots in nontransfected cells, we sometimes observed the presence of a protein band in between the

two LC3 proteins (Figure 16). An example of a western blot with this third protein band is included below (Figure 16). It is unclear whether this band is an intermediate form of the LC3 protein or a product of nonspecific antibody binding. We dosed cells with the late-stage autophagy blocker chloroquine and noted that the middle band did not increase in size; this suggested that the middle band itself was not LC3-II (Figure 19). In the samples treated with the late-stage autophagy blocker chloroquine, the bottom band of the three increased in size, indicating that the bottom band was LC3-II. However, it was unclear whether or not this middle band was an unprocessed form of LC3B, a different type of LC3 (LC3A or LC3C) or a different protein altogether. Similar reports of a middle band have been noted by Klionsky et al. (2021) in their characterization of the impacts of lysosomal protease inhibitors on LC3 levels, and they suggest that the middle band is a processing intermediate of the LC3-I protein [27]. One possibility is that partial lipidation of the LC3-I protein in the LC3-I to LC3-II conversion process results in the presence of a third band. In addition, one study by Wang et al. (2013) generated mutants of the LC3B protein such that the unprocessed form of LC3 (called pro-LC3) could not be cleaved and processed by the ATG4 protein to form LC3-I [78]. They performed a series of western blots to show that the pro-LC3 form of the protein migrated in a similar pattern to LC3B-II. It is possible that the middle band observed on the western blots in this study is the pro-LC3 protein that has been detected by the LC3 primary antibody. The authors show that pro-LC3 may become visible on a blot if there is an overexpression of LC3B and if there are subsequent low levels of ATG4 (such as in an ATG4 knockout cell line) [78]. It is also possible that the intermediate band observed in the western blot is a different LC3 protein, such as the unprocessed version of LC3A. Wang et al. (2013) found that pro-LC3A migrates at a similar rate to LC3B-I and could be detected using a LC3B primary antibody, although the antibody used for

this study (Novus Biologicals, NB100-2220) is a different antibody and is reported to be specific for LC3B only [78, 79].

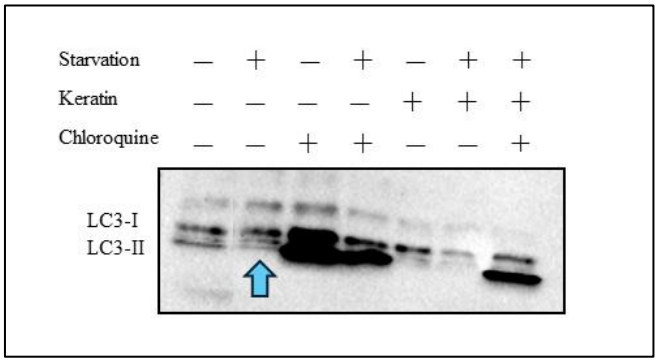

Figure 19: Western blot displaying an extra band between LC3-I and LC3-II (example indicated by blue arrow). Nontransfected cells were dosed with a combination of starvation, keratin, and chloroquine for 24 hours before lysing and analysis via western blotting.

In-Gel Fluorescence and Western Blotting. After determining the expected responses of our nontransfected HEK 293 cells to autophagy stimulators and growth conditions, we developed an in-gel fluorescence method to serve as a replacement for western blotting and fluorescent imaging and tested the response of transfected HEK 293 cells to the autophagy modulators used previously. First, we sought to determine if in-gel fluorescence was capable of detecting the LC3 protein when cells were transfected with the mCherry-EGFP-LC3B construct. Images taken with the Alexa 488 filter (to detect EGFP) and the Alexa 546 filter (to detect mCherry) contained two fluorescing protein bands at the expected molecular weight of the construct (68.9 kDa; Figure 10.C). A western blot was then performed to analyze the banding pattern of the transfected LC3 construct from the same SDS-PAGE gel. With this blot, we observed two protein bands at the same molecular weight as with in-gel fluorescence. This indicated that the proteins observed with in-gel fluorescence were the same LC3 construct

observed with western blotting. It also suggests that in-gel fluorescence is a viable alternative to western blotting, because it allows for the visualization of LC3 and the separation of LC3-I and LC3-II bands.

In addition to observing the LC3 construct with in-gel fluorescence, we regularly noticed fluorescing bands that did not correspond to the expected molecular weight of the LC3 construct. First, we noted the presence of two stacked proteins at a lower molecular weight than that of the mCherry-EGFP-LC3B construct (Figure 18.C, boxed in green). These two protein bands appear to be approximately 35 kDa in weight and are present in Alexa 488 in-gel fluorescence images and in western blots. It is possible that the proteins observed in the Alexa 488 images and western blots are cleavage products of the mCherry-EGFP-LC3B construct. In particular, these proteins may represent a cleaved version of this construct lacking the mCherry portion of the tag. This explanation is based on the observation that this cleavage product is present in images taken with the Alexa 488 filter (detects EGFP), but not in images taken with the Alexa 546 filter (detects mCherry). In addition, this product can be observed in western blots, indicating that the primary antibody detects the presence of LC3B within the protein.

Interestingly, one study found that using mCherry to tag proteins targeted to the lysosome resulted in high amounts of cleavage of the mCherry protein. In this study, Huang et al. (2014) constructed a fusion protein between mCherry and the lysosomal cholesterol binding protein NPC2 and expressed it in cells. The authors noted a significant degree of cleavage in transfected cells attributed to a flexible, 11 amino acid sequence in the N-terminal region of the mCherry protein that left it susceptible to lysosomal proteases [80]. This lends credibility to the explanation that the mCherry of our LC3 construct is being cleaved in the lysosome. However,

we still see these unknown protein bands in samples treated with the late-stage autophagy blocker chloroquine, which in theory would inhibit the ability of the lysosome to fuse to autophagosomes containing the mCherry-EGFP-LC3B construct and thus prevent the lysosome's ability to cleave the construct. The presence of this construct in cells dosed with chloroquine further suggests that this construct is not being processed in the lysosome and may instead be cleaved at an earlier stage of the pathway or as part of a different process. Future studies should investigate the use of protease inhibitors to determine if this has any effect on the presence of these protein bands.

Second, we regularly observed a single band present in the Alexa 546 images that migrates to a different location than the bands from the mCherry-EGFP-LC3B construct. This band migrates slightly higher than the unknown protein bands present in the Alexa 488 image and the western blot (40 kDa as opposed to 35 kDa), leading us to speculate that the bands in the Alexa 546 image are a different protein than the unknown bands discussed in the previous paragraph (Figure 20.C, boxed in red) Third, we also observe a protein of a high molecular weight in images taken with the Alexa 488 filter. This protein band migrates to approximately 100 kDa (Figure 20.C, boxed in blue). We do not think this band is a part of the LC3 construct, as it is present in the lanes of lipid-only transfection samples and transfection-only samples (Figure 20.C, boxed in blue). This indicates that this protein is not an aggregated form of the LC3 construct that may be unable to migrate through the gel. However, it is possible that this band represents aggregated protein that may be unable to pass through the SDS-PAGE gel due to the modified sample preparation used for the semi-native approach to SDS-PAGE. Prior to loading samples on the gel, samples were combined with Laemmli sample buffer without a

reducing agent and then were loaded to the gel without heating to denature. This procedure preserves the ability of the EGFP and mCherry tags to fluoresce when imaged but may interfere with the ability of other proteins to migrate through the gel. Fourth, the second lane of this gel shows several protein bands at lower molecular weights than the LC3 construct. These bands are apparent in the Alexa 488 image and western blot. We believe the sample loaded to this well experienced a greater than normal amount of cleavage due to a technical issue made during the preparation of the lysate. Finally, we occasionally observe the presence of two stacked protein bands at the 14-17 kDa markers in western blots of transfected cells, such as in Figure 20.D (indicated by the purple box). These protein bands are not detected with in-gel fluorescence and are only observed when primary LC3 antibodies are used for western blotting. They are at the expected molecular weight of endogenous LC3-I and LC3-II and thus are the two forms of the LC3 protein endogenously expressed by the HEK 293 cells used. These proteins are not always observed with transfected western blots because of the short exposure times required to detect transfected LC3 as opposed to endogenous LC3.

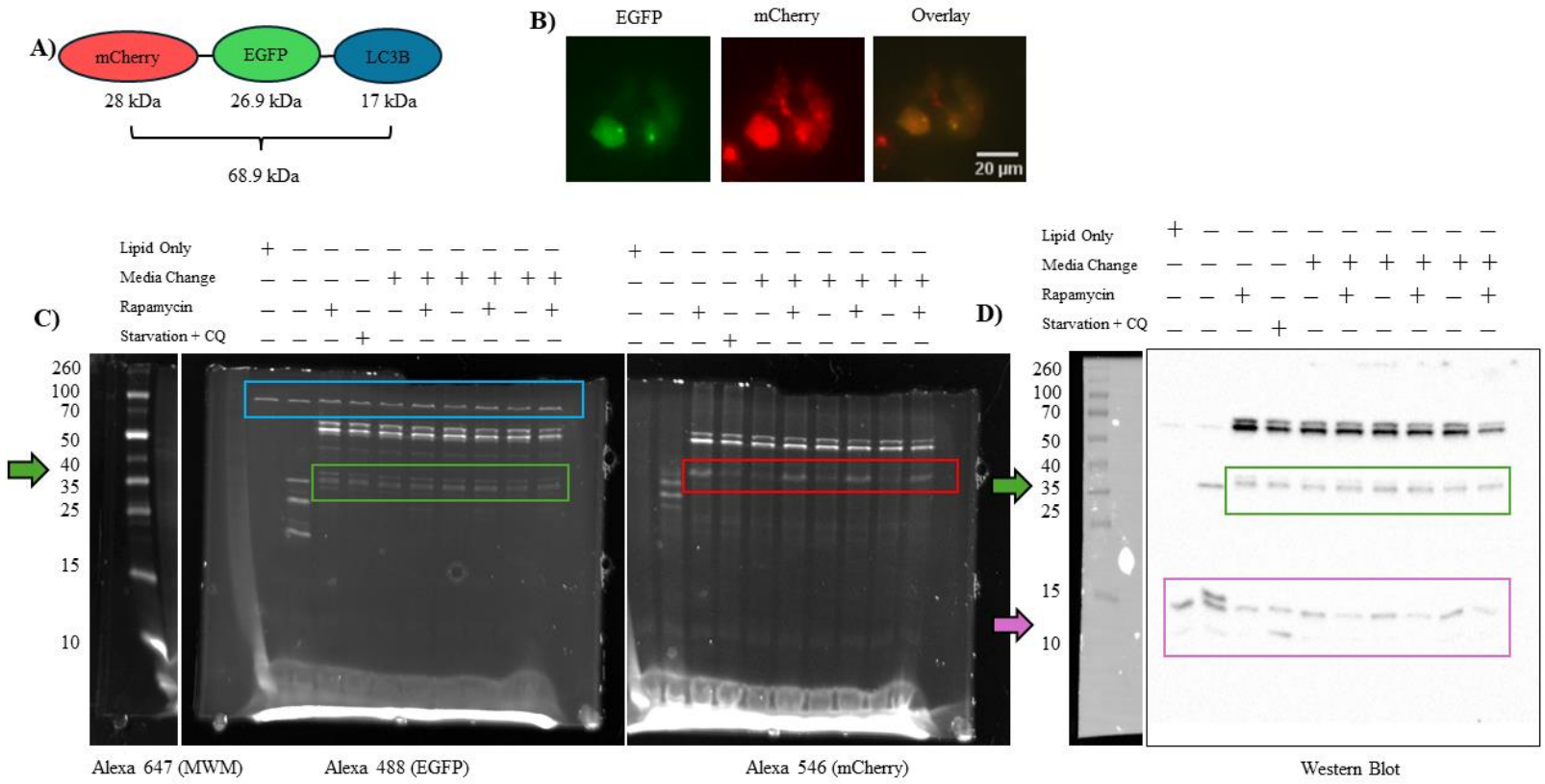

Figure 20: Abnormal bands observed with in-gel fluorescence and western blotting. A: Illustration of the transfected protein construct and expected molecular weight. B: Example of fluorescent puncta observed in transfected cells undergoing autophagy. C: In-gel fluorescence of transfected cell lysates. The LC3 construct is highlighted in the red box under the Alexa 488 and Alexa 546 filters. The red arrow indicates the expected molecular weight of the construct. D: Western blot of transfected cell lysates. The LC3 construct is highlighted in the red box. The red arrow indicates the expected molecular weight of the construct.

In-Gel Fluorescence, Autophagy Modulators, and Media Changes. After establishing the expected migration patterns of the EGFP-mCherry-LC3B construct with in-gel fluorescence, we analyzed the LC3-II/LC3-I ratios in transfected cells dosed with the autophagy modulators rapamycin, starvation, and chloroquine. We did not observe statistically significant changes in the LC3-II/LC3-I ratios dosed with any of these treatments. We reasoned that the extra day of incubation required for transient transfection stressed the cells and induced autophagy in the no treatment control group, thus preventing us from seeing the changes we expected between the treatment groups. We observed this trend in experiments with nontransfected cells that were previously discussed. When nontransfected cells were grown for 4 days, the LC3 ratios indicated that the autophagy responses of these cells had been altered compared to cells grown for 3 days.

In order to ameliorate the stressors our cells experienced due to the extra day of incubation required for transfection, we tested whether changing the media of our cells would restore the LC3-II/LC3-I ratios and the LC3-II/GAPDH ratios to the responses we see with nontransfected cells. In nontransfected cells, changing the cell media resulted in the statistically significant change in the LC3-II/LC3-I ratios of the no treatment control and rapamycin-treated groups. Similarly, when we changed the media at 72 hours of incubation in transfected cells, the LC3-II/LC3-I ratios restored to their expected relative values (an increased ratio in cells dosed with rapamycin compared to the negative control). This change was statistically significant, indicating the usability of in-gel fluorescence as a method for analyzing autophagy.

One potential drawback to using in-gel fluorescence is that the current system does not allow for protein normalization to a housekeeping control such as GAPDH. Accomplishing this would require transfection with an additional plasmid to code for a fluorescent housekeeping

control. However, the LC3 plasmid used in this study is large, requires a high amount of DNA, and requires a high seeding density. The incorporation of an additional plasmid for transfection would require a delicate balance of multiple factors to optimize the expression of both plasmids. This may be difficult given the strict requirements of the current LC3 plasmid transfection system. A more realistic option would be to stain the gel with Coomassie blue stain and normalize LC3 levels to total protein or create a stably transfected cell line with the LC3 plasmid and then probe for regular GAPDH. Future studies may attempt to normalize LC3 to total protein instead of incorporating a transfected housekeeping protein into the in-gel fluorescence method.

Incorporating a media change into the in-gel fluorescence protocol can ameliorate cell stress and preserve the expected responses to autophagy modulators in the control groups. Future studies in our lab may attempt to circumvent the need to grow HEK 293 cells for 4 days by generating a stably transfected cell line to perform three-day experiments with in-gel fluorescence. For example, one paper using in-gel fluorescence and transfection to study autophagy sidesteps the challenges we experienced by using stably transfected cell lines instead of transiently transfected cells. Yim et al. (2022) stably transfected HeLa cells to generate a HALO-LC3 construct for autophagy assays. In-gel fluorescence was then used to visualize this construct and study autophagy [81]. Stable transfection may allow users to sidestep the challenges we experienced with our transiently transfected cells responding unexpectedly to autophagy-modulating compounds.

In-Gel Fluorescence and Fluorescent Imaging. In addition to questioning whether in-gel fluorescence was a usable alternative to western blotting, we also asked whether in-gel fluorescence could serve as a replacement to dual-reporter fluorescent imaging. Dual-reporter

fluorescence imaging allows users to determine what stage of autophagy a group of cells is in by tracking the location and fluorescent intensity of the mCherry-EGFP-LC3B construct in cells. During dual-reporter fluorescent imaging, the location and intensities of the mCherry-EGFP-LC3B construct reflect different autophagic states due to pH changes that occur at different autophagic states. In fluorescent imaging, low levels of autophagy manifest as diffuse red and green fluorescence throughout the cell (Figure 2.A). When autophagy is stimulated and in its early stages, fluorescent imaging reveals the formation of red and green puncta in cells. This corresponds to the LC3-I protein turning into LC3-II and getting recruited to the membrane of the autophagosomes (Figure 2.B). When autophagy is in its late stages, fluorescent imaging reveals the presence of red puncta but the absence of green puncta. The absence of green puncta is due to the low pH of the lysosome quenching the signal from the EGFP tag, while the mCherry tag remains stable under acidic conditions (Figure 2.C). With in-gel fluorescence, we hypothesized that cells undergoing late-stage autophagy would display a decrease in the signal of the LC3-II band imaged under the Alexa 488 filter (detects EGFP) compared to the LC3-II band of the no treatment group imaged under the Alexa 488 filter. This decrease in signal would correlate to the pH of the lysosome quenching the signal of the EGFP tag. We also hypothesized that in samples undergoing late-stage autophagy, the intensity of the LC3-II band under the Alexa 546 filter (detects mCherry) would be increased compared to the intensity of the LC3-II band under the Alexa 488 filter. This increased signal would correlate to the mCherry tag fluorescing in the lysosome while the EGFP tag was quenched.

We tested whether or not we saw the appropriate changes in LC3-II fluorescent signal when cells were treated with rapamycin and compared to a no treatment group. We observed that

there was no change in the fluorescent intensities of LC3-II bands of the no treatment group and rapamycin-treated group imaged with the Alexa 488 filter (Figure 13.B). The fluorescent intensities of the rapamycin-treated LC3-II bands when imaged with the Alexa 546 filter were not increased compared to the corresponding bands in the Alexa 488 filter. In addition, we measured the total fluorescence of lysates with a fluorescent plate reader and asked whether we noted these same changes. Although there was a trend towards a decrease in green signal in samples dosed with rapamycin compared to the green signal of the no treatment group, it was not a statistically significant change. In addition, there was a trend towards a decrease in the red signal of all samples compared to the green signal of samples dosed with rapamycin, which was the opposite of what we had hypothesized to observe in the rapamycin-treated groups (Figure 13.C).

One potential reason why the fluorescent intensities of our LC3 protein bands with in-gel fluorescence do not correspond to the fluorescent intensities of our LC3 construct with fluorescent imaging is because of the limitations of our imaging equipment. The ChemiDoc imager used for in-gel fluorescence is equipped with a green filter (Alexa 488) that is optimized for the detection of the Alexa Fluor 488 dye, and a red filter (Alexa 546) that is optimized for the detection of the Alexa Fluor 546 dye. The optimal excitation and emission wavelengths for our EGFP tag are similar to that of the Alexa Fluor 488 dye (excitation/emission wavelengths of 488 nm/507 nm for EGFP and excitation/emission wavelengths of 496 nm/519 nm for Alexa Fluor 488), indicating the usability of the Alexa 488 filter for the detection of EGFP [82, 83]. However, the optimal excitation and emission wavelengths of the Alexa Fluor 546 dye do not correspond as closely to that of the mCherry tag. The mCherry tag fluoresces at an

excitation/emission wavelength of 587 nm/630 nm, while the Alexa Fluor 546 dye fluoresces at an excitation/emission wavelength of 556 nm/573 nm [82, 84]. This discordance may result in the less-than-optimal detection of mCherry signal with our current in-gel fluorescence system. To test whether or not the wavelengths used for the detection of Alexa Fluor 546 resulted in a less-than-optimal detection of mCherry, we measured the fluorescent signal of lysates with a fluorescent plate reader using three sets of wavelengths: 488 nm/535 nm (corresponding to the wavelengths for the Alexa Fluor 488 dye), 546 nm/590 nm (corresponding to the wavelengths for the Alexa Fluor 546 dye), and 587 nm/630 nm (corresponding to the optimal wavelengths for mCherry). This experiment was performed one time. The lysate measured had a higher fluorescent signal when 587 nm was used as an excitation wavelength as opposed to 546 nm, suggesting sub-optimal excitation of the mCherry protein at 546 nm. However, this experiment would need to be repeated to reach conclusions about the usability of the Alexa 546 filter for our in-gel fluorescence system.

One explanation as to why samples undergoing late-stage autophagy do not show a decrease in signal under the Alexa 488 filter is that cell lysis raises the pH of the lysosome and restores the quenched EGFP signal. Klionsky et al. (2021) describe how the quenched EGFP signal of the LC3 construct can be restored if caution is not taken when preparing cell samples with buffers of a neutral pH [27]. Klionsky et al. (2021) transfected cells with a GFP-LC3 construct, treated cells with starvation, fixed cells in a neutral pH buffer, and performed immunofluorescent staining of the lysosomal marker LAMP1. They noted a high degree of colocalization between GFP-LC3 and LAMP1, indicating that the GFP-LC3 was in the lysosome. However, the GFP signal was not quenched, suggesting that the pH of the buffer had

restored the GFP signal from its expected decrease [27]. Future studies in our lab could perform similar experiments by adjusting the pH of transfected cell lysates to determine if this impacts EGFP signal detection. In addition, future studies should rule out the possibility that EGFP is being degraded in the lysosome. Katayama et al. (2008) tested whether GFP is merely quenched in the lysosome or degraded by blocking the acidity of the lysosomes in transfected cells and measuring EGFP signal intensity. They reasoned that blocking the acidity of the lysosomes should restore EGFP signal if the molecule had been quenched. However, fluorescent imaging of transfected cells revealed that fluorescence was not restored [85]. To further test whether or not EGFP was degraded, the authors incubated EGFP in a neutral pH solution, acidic pH solution (pH = 5.0), and acidic pH solution combined with lysosomal contents. Analysis of samples with SDS-PAGE revealed that EGFP had been degraded after incubation with lysosomal contents. The authors thus concluded that EGFP is degraded within the lysosome [85]. It is possible that degradation could explain the protein bands migrating to a lower molecular weight in images taken with the Alexa 546 filter (Figure 12, boxed in red). However, this explanation is inconsistent with the high levels of EGFP signal we detect when fluorescent intensities of lysates and gels are measured. Thus, it is more likely that the EGFP signal is quenched in the lysosome until cell lysis, which restores the signal.

Aim 2: Keratin and Autophagy

In addition to assessing the usability of in-gel fluorescence as an alternative method to western blotting and fluorescent imaging, the second aim of this thesis was to test the effect of crude keratin extract on autophagy activity in HEK 293 cells. Previous experiments in the Coan lab have identified a potential link between crude keratin and autophagy activity. Furthermore,

studies have suggested that the gamma keratin fraction may be the main component of keratin responsible for modulating autophagy [3]. However, this study chose to use crude keratin in continuity with the data already garnered by our lab, and because we had relatively little work done with gamma keratin.

To test keratin's relationship to autophagy, nontransfected HEK 293 cells were treated with 50% starvation alongside 0.1 mg/mL crude keratin extract for 24 hours before lysis and analysis with western blotting. There was no statistically significant difference between the LC3-II/LC3-I ratios or LC3-II/GAPDH ratios of cells dosed with starvation and keratin in comparison to the no treatment control or starvation-only control group. These results are not unexpected based upon several factors. First, crude keratin extract was less expected to modify the autophagy activity of HEK 293 cells compared to other forms of keratin such as gamma keratin, as crude keratin is not considered to be bioactive and serves primarily as an attachment point for cell cultures [3]. Second, these results were not unexpected due to the impact of crude keratin on cytotoxicity as measured via WST-1 assay. In these assays, we observed that crude keratin treatment did not have an impact on the cytotoxicity of cells dosed with varying degrees of starvation (50%, 75%, and 100% starvation) compared to groups treated with starvation alone (Figure 18). These data correspond to the lack of change observed in the autophagy levels of cells dosed with crude keratin and starvation and suggest crude keratin has a lower degree of bioactivity.

Third, it had already been established that starvation in our HEK 293 cells did not result in the expected increase in the LC3-II/LC3-I ratios or LC3-II/GAPDH ratios. As discussed previously in this section, the unexpected response we noted to starvation treatment could be due

to the timepoints at which starvation and autophagy were measured, the degree of starvation used, or the high autophagy response of cells treated with starvation to induce autophagy. The timepoint at which autophagy was measured is of special interest in this case. As discussed previously, Poranki & Van Dyke (2014) found that certain autophagy genes were upregulated at 12 and 18 hours post heat shock, but the effect had decreased by the time 24 hours had passed [3]. Based upon the results of their work, it is possible that our experimental timepoints were not appropriate for the optimal analysis of autophagy activity in these cells. Future work with starvation as an autophagy stimulator in combination with keratin should investigate earlier time points to determine if starvation induces an initial change in the LC3-II/LC3-I ratios and LC3-II/GAPDH ratios which then resolves at a later time point. In addition to testing an array of timepoints to optimize the analysis of autophagy activity, gamma keratin extract should be incorporated into this work to determine if it has a more pronounced effect on autophagy than crude keratin.

We also measured the LC3-II/LC3-I ratios and LC3-II/GAPDH ratios of cells dosed with chloroquine, chloroquine combined with starvation, and chloroquine combined with starvation and keratin. There was no statistically significant difference between the ratios in any of these groups. In light of our previous work categorizing the response of HEK 293 cells to starvation, it is not surprising that starvation did not have a compounding effect on chloroquine treatment. The addition of keratin to starvation and chloroquine-treated groups also did not result in a statistically significant change compared to the chloroquine only group or the chloroquine plus starvation group. This was not unexpected, based upon the lack of change observed in the LC3 ratios of cells dosed with keratin alone. However, we did note a statistically significant change

between the LC3-II/LC3-I ratios and LC3-II/GAPDH ratios of groups treated with keratin and starvation in comparison to groups treated with keratin, starvation, and chloroquine. This difference may indicate the effectiveness of the chloroquine drug in blocking late-stage autophagy. It also may indicate that the combined treatment of keratin and starvation had a slight additive effect to increase the LC3 ratios.

The results obtained from both aims of this study highlight the inherent difficulties of analyzing the autophagy pathway. There is a wide range of LC3 protein banding patterns that are considered indicative of autophagy activity, and LC3 protein bands visualized via western blotting often deviate from the expected norms when dosed with autophagy modulators such as starvation. These banding display patterns are often cell line specific, such as in the case of the HEK 293 cells used in this study, and because of this, their responses to autophagy modulators must be categorized prior to autophagy analysis. Even in the case of LC3 banding patterns that conform to the expected responses, these bands can easily be misinterpreted without the application of autophagy blockers such as chloroquine to control for late-stage autophagy blockages. Further complicating this is the crucial role timepoints play in the evaluation of autophagy. Autophagy is a dynamic process that occurs in flux, and timepoints are only snapshots of the process. Unexpected LC3-II/LC3-I ratios must be interpreted with the understanding that the response at various timepoints may not be uniform based on the method of autophagy induction or inhibition.

CONCLUSION

In conclusion, the first aim of this thesis was to develop a method for analyzing autophagy in cell cultures and compare its usability to western blotting and fluorescent imaging. We established the expected responses of our nontransfected HEK 293 cells to autophagy modulators rapamycin, starvation, and chloroquine. We then showed that in-gel fluorescence allows for the detection of the autophagy protein LC3. After assessing the use of the autophagy control rapamycin with in-gel fluorescence, we conclude that the evidence strongly suggests that in-gel fluorescence can serve as a replacement for western blotting if certain parameters are met. The extra 24-hour incubation period required for transfection during in-gel fluorescence obscures the expected differences between a no treatment control and rapamycin-treated group. However, if a media change is incorporated at 24 hours post treatment in transfected cell groups, the positive and negative control groups resolve to the expected LC3 ratio levels. Thus, in-gel fluorescence requires that cell stress be mitigated using a media change at 24 hours post transfection.

Although in-gel fluorescence serves as a usable alternative to western blotting, our current system does not allow it to replace the information gained from the dual-reporter fluorescent imaging method. In particular, it does not allow users to correlate fluctuations in fluorescent intensities to different stages of autophagy. It also does not allow for the acquisition of spatial information regarding the transfected protein. In addition, a major limitation with our system is that only one of our light filters is optimized for one of our fluorescent reporters. This means that we cannot compare signal intensities between the EGFP and mCherry tags to determine the stages of autophagy based on LC3 band intensity alone or lysate intensity alone.

However, it is possible that this issue could be resolved with the use of a more appropriate filter and light source. In addition, it is unclear whether cell lysis disrupts the ability of the lysosomes to maintain the quenched signal of the EGFP reporter during late-stage autophagy. Future studies should investigate both of these questions in order to conclusively determine whether or not in-gel fluorescence can be used in this manner.

The second aim of this thesis was to investigate the relationship between keratin biomaterials and the autophagy pathway in HEK 293 cells. This study primarily evaluated keratin's impact at the 24-hour timepoint, which correlated to the optimal timepoint for observing autophagy with our positive control, rapamycin, and our late-stage autophagy blocking negative control, chloroquine. At this specific timepoint, there was no indication of keratin's impact upon cells stressed with starvation. However, it is unclear whether the starvation method used was strong enough to invoke a stress response in the cells, or whether this timepoint was appropriate for observing the starvation response. Future studies should investigate both earlier timepoints with starvation and keratin and alternative methods of inducing stress in cells (for example, treating with hydrogen peroxide to induce oxidative stress).

In conclusion, autophagy is a dynamic and complex process, and the study of autophagy requires the use of methods that are highly technical in nature. These methods are often difficult, expensive, time-consuming, and lacking in quantitative power. In addition, the experimental variables used to study autophagy – from the types of autophagy stimulators used to the timepoints at which autophagy is measured – are crucial to the ability to detect autophagy activity in cells. Honing these parameters while also using innovative techniques to detect

autophagy activity will allow our lab to continue to elucidate the relationship between biomaterials like keratin and cell recycling pathways like autophagy.

REFERENCES

1. Pohl C, Dikic I. Cellular quality control by the ubiquitin-proteasome system and autophagy. *Science.* 2019;366(6467):818-822. doi:10.1126/science.aax3769

2. Kuma A, Hatano M, Matsui M, et al. The role of autophagy during the early neonatal starvation period. *Nature.* 2004;432:1032-1036. doi:10.1038/nature03029

3. Poranki DR, Van Dyke ME. The effect of gamma keratose on cell viability in vitro after thermal stress and the regulation of cell death pathway-specific gene expression. *Biomaterials.* 2014;35(16):4646-4655. doi:10.1016/j.biomaterials.2014.02.044

4. Lőrincz P, Juhász G. Autophagosome-lysosome fusion. *J Mol Biol.* 2020;432(8):2462-2482. doi:10.1016/j.jmb.2019.10.028

5. Wang L, Klionsky DJ, Shen HM. The emerging mechanisms and functions of microautophagy. *Nat Rev Mol Cell Biol.* 2023;24:186–203. doi:10.1038/s41580-022-00529-z

6. Dikic I, Elazar Z. Mechanism and medical implications of mammalian autophagy. *Nat Rev Mol Cell Biol.* 2018;19(6):349-364. doi:10.1038/s41580-018-0003-4

7. Corona Velazquez AF, Jackson WT. So many roads: The multifaceted regulation of autophagy induction. *Mol Cell Biol.* 2018;38(21):303-318. doi:10.1128/MCB.00303-18

8. Kim J, Kundu M, Viollet B, Guan KL. AMPK and mTOR regulate autophagy through direct phosphorylation of Ulk1. *Nat Cell Biol.* 2011;13(2):132-141. doi:10.1038/ncb2152

9. Dossou AS, Basu A. The Emerging Roles of mTORC1 in Macromanaging Autophagy. *Cancers (Basel).* 2019;11(10):1422. doi:10.3390/cancers11101422

10. Jia J, Bissa B, Brecht L, et al. AMPK, a regulator of metabolism and autophagy, is activated by lysosomal damage via a novel galectin-directed ubiquitin signal transduction system. *Mol Cell.* 2020;77(5):951-969. doi:10.1016/j.molcel.2019.12.028

11. Krieg S, Lüscher B, Vervoorts J, Dohmen M. Studying the role of AMPK in autophagy. *Methods Mol Biol.* 2018;1732:373-391. doi:10.1007/978-1-4939-7598-3_24

12. Hernandez GA, Perera RM. Autophagy in cancer cell remodeling and quality control. *Mol Cell.* 2022;82(8):1514-1527. doi:10.1016/j.molcel.2022.03.023

13. Brier LW, Ge L, Stjepanovic G, et al. Regulation of LC3 lipidation by the autophagy-specific class III phosphatidylinositol-3 kinase complex. *Mol Biol Cell.* 2019;30(9):1098-1107. doi:10.1091/mbc.E18-11-0743

14. Yu L, Chen Y, Tooze SA. Autophagy pathway: Cellular and molecular mechanisms. *Autophagy.* 2018;14(2):207-215. doi:10.1080/15548627.2017.1378838

15. Tian X, Teng J, Chen J. New insights regarding SNARE proteins in autophagosome-lysosome fusion. *Autophagy.* 2021;17(10):2680-2688. doi:10.1080/15548627.2020.1823124

16. Ni H-M, Bockus A, Wozniak AL, et al. Dissecting the dynamic turnover of GFP-LC3 in the autolysosome. *Autophagy.* 2011;7:188–204. doi: 10.4161/auto.7.2.14181

17. Springhorn A, Hoppe T. Western blot analysis of the autophagosomal membrane protein LGG-1/LC3 in Caenorhabditis elegans. *Methods Enzymol.* 2019;619:319-336. doi:10.1016/bs.mie.2018.12.034

18. Amm I, Sommer T, Wolf DH. Protein quality control and elimination of protein waste: The role of the ubiquitin–proteasome system. *Biochim Biophys Acta*. 2014;1843(1):182-196. doi:10.1016/j.bbamcr.2013.06.031

19. Duncan LM, Piper S, Dodd RB, Saville MK, Sanderson CM, Luzio JP, Lehner PJ. Lysine-63-linked ubiquitination is required for endolysosomal degradation of class I molecules. *EMBO J.* 2006;25(8):1635-45. doi: 10.1038/sj.emboj.7601056.

19. Bauer B, Martens S, Ferrari L. Aggrephagy at a glance. *J Cell Sci.* 2023;136(10):jcs260888. doi:10.1242/jcs.260888

20. Bard JAM, Goodall EA, Greene ER, Jonsson E, Dong KC, Martin A. Structure and Function of the 26S Proteasome. *Annu Rev Biochem.* 2018;87:697-724. doi:10.1146/annurev-biochem-062917-011931

21. Jung, S., Jeong, H. & Yu, SW. Autophagy as a decisive process for cell death. *Exp Mol Med*. 52, 921–930 (2020). https://doi.org/10.1038/s12276-020-0455-4

22. Fan YJ, Zong WX. The cellular decision between apoptosis and autophagy. *Chin J Cancer.* 2013 Mar;32(3):121-9. doi: 10.5732/cjc.012.10106.

23. Uddin MS, Stachowiak A, Mamun AA, et al. Autophagy and Alzheimer's disease: from molecular mechanisms to therapeutic implications. *Front Aging Neurosci.* 2018;10:4. doi:10.3389/fnagi.2018.00004

24. Yan J, Shen M, Sui B, et al. Autophagic LC3+ calcified extracellular vesicles initiate cartilage calcification in osteoarthritis. *Sci Adv.* 2022;8(19):eabn1556. doi:10.1126/sciadv.abn1556

25. Funderburk SF, Marcellino BK, Yue Z. Cell "self-eating" (autophagy) mechanism in Alzheimer's disease. *Mt Sinai J Med.* 2010;77(1):59-68. doi:10.1002/msj.20161

26. Ejlerskov P, Rasmussen I, Nielsen TT, et al. Tubulin polymerization-promoting protein (TPPP/p25α) promotes unconventional secretion of α-synuclein through exophagy by impairing autophagosome-lysosome fusion. *J Biol Chem.* 2013;288(24):17313-17335. doi:10.1074/jbc.M112.401174

27. Klionsky DJ, Tong CK. Guidelines for the use and interpretation of assays for monitoring autophagy (4th edition)1. *Autophagy.* 2021;17(1):1-382. doi:10.1080/15548627.2020.1797280

28. Li J, Kim SG, Blenis J. Rapamycin: one drug, many effects. *Cell Metab.* 2014;19(3):373-379. doi:10.1016/j.cmet.2014.01.001

29. Wu YT, Tan HL, Shui G, et al. Dual role of 3-methyladenine in modulation of autophagy via different temporal patterns of inhibition on class I and III phosphoinositide 3-kinase. J Biol Chem. 2010;285(14):10850-10861. doi:10.1074/jbc.M109.080796

30. Sharifi MN, Mowers EE, Drake LE, Macleod KF. Measuring autophagy in stressed cells. *Methods Mol Biol.* 2015;1292:129-50. doi: 10.1007/978-1-4939-2522-3_10.

31. Yu W, Wang Y, Zhu J, et al. Autophagy inhibitor enhance ZnPc/BSA nanoparticle induced photodynamic therapy by suppressing PD-L1 expression in osteosarcoma immunotherapy. *Biomaterials.* 2019;192:128-139. doi:10.1016/j.biomaterials.2018.11.019

32. Beesabathuni NS, Park S, Shah PS. Quantitative and temporal measurement of dynamic autophagy rates. *Autophagy.* 2023;19(4):1164-1183. doi: 10.1080/15548627.2022.2117515.

33. BIORAD. What is real-time PCR (qPCR)? Available at: https://www.bio-rad.com/en-us/applications-technologies/what-real-time-pcr-qpcr?ID=LUSO4W8UU. Accessed June 9th, 2024.

34. Marin E, Boschetto F, Pezzotti G. Biomaterials and biocompatibility: An historical overview. *J Biomed Mater Res A.* 2020;108(8):1617-1633. doi:10.1002/jbm.a.36930

35. Prasad K, Bazaka O, Chua M, et al. Metallic Biomaterials: Current Challenges and Opportunities. *Materials (Basel).* 2017;10(8):884. doi:10.3390/ma10080884

36. Vaiani L, Boccaccio A, Uva AE, et al. Ceramic Materials for Biomedical Applications: An Overview on Properties and Fabrication Processes. *J Funct Biomater.* 2023;14(3):146. doi:10.3390/jfb14030146

37. Kalirajan C, Dukle A, Nathanael AJ, et al. A Critical Review on Polymeric Biomaterials for Biomedical Applications. *Polymers (Basel).* 2021;13(17):3015. doi:10.3390/polym13173015

38. Munonyedi KE. A fundamental review on composite materials and some of their applications in biomedical engineering. *J King Saud Univ Eng Sci.* 2021;33(8):557-568. doi:10.1016/j.jksues.2020.07.007

39. Zhao X. Introduction to bioactive materials in medicine. In: Zhao X, Courtney JM, Qian H, eds. Bioactive Materials in Medicine. Woodhead Publishing; 2011:1-13. doi:10.1533/9780857092939.1

40. Vert M, Doi Y, Hellwich KH, et al. Terminology for biorelated polymers and applications (IUPAC Recommendations 2012). *Pure and Applied Chemistry.* 2012;84(2):377-410. doi:10.1351/pac-rec-10-12-04

41. Crawford L, Wyatt M, Bryers J, Ratner B. Biocompatibility evolves: Phenomenology to toxicology to regeneration. *Adv Healthc Mater.* 2021;10(11):e2002153. doi:10.1002/adhm.202002153

42. Temenoff JS, Mikos AG. Biomaterials: The Intersection of Biology and Materials Science. Pearson/Prentice Hall; 2008.

43. Feroz S, Muhammad N, Ratnayake J, Dias G. Keratin-based materials for biomedical applications. *Bioact Mater.* 2020;5(3):496-509. doi:10.1016/j.bioactmat.2020.04.007

44. de Guzman RCD, Merrill MR, Richter JR, Hamzi RI, Greengauz-Roberts OK, Van Dyke ME. Mechanical and biological properties of keratose biomaterials. *Biomaterials.* 2011;32(32):8205-8217. doi:10.1016/j.biomaterials.2011.07.054

45. Koch SL, Tridico SR, Bernard BA, Shriver MD, Jablonski NG. The biology of human hair: A multidisciplinary review. *Am J Hum Biol.* 2020;32:e23316. doi:10.1002/ajhb.23316

46. Bragulla HH, Homberger DG. Structure and functions of keratin proteins in simple, stratified, keratinized and cornified epithelia. *J Anat.* 2009;214(4):516-559. doi:10.1111/j.1469-7580.2009.01066.x

47. Schweizer J, Bowden PE, Coulombe PA, et al. New consensus nomenclature for mammalian keratins. *JCB.* 2006;174(2):169-174. doi:10.1083/jcb.200603161

48. Kirfel J, Magin TM, Reichelt J. Keratins: a structural scaffold with emerging functions. *Cell Mol Life Sci.* 2003;60(1):56-71. doi: 10.1007/s000180300004.

49. Lazarus BS, Chadha C, Velasco-Hogan A, Barbosa JDV, Jasiuk I, Meyers MA. Engineering with keratin: A functional material and a source of bioinspiration. *iScience.* 2021;24(8):102798. doi:10.1016/j.isci.2021.102798

50. Kim HJ, Choi WJ, Lee CH. Phosphorylation and Reorganization of Keratin Networks: Implications for Carcinogenesis and Epithelial Mesenchymal Transition. *Biomol Ther (Seoul).* 2015;23(4):301-12. doi: 10.4062/biomolther.2015.032

51. Hill, P.S., Brantley, H., & Van Dyke, M.E. Some properties of keratin biomaterials: kerateines. *Biomaterials.* 2010;31(4), 585-93. doi: 10.1016/j.biomaterials.2009.09.076.

52. Reichl, S. Films based on human hair keratin as substrates for cell culture and tissue engineering. *Biomaterials.* 2009;30(36), 6854-66. doi: 10.1016/j.biomaterials.2009.08.051.

53. Rouse, J.G., & Van Dyke, M.E. A review of keratin-based biomaterials for biomedical applications. *Materials (Basel).* 2010;3(2), 999–1014. doi: 10.3390/ma3020999.

54. Hill PS, Apel PJ, Barnwell J, et al. Repair of peripheral nerve defects in rabbits using keratin hydrogel scaffolds. *Tissue Engineering Part A.* 2011;17(11-12):1499-1505. doi:10.1089/ten.tea.2010.0184

55. Qin HJ, Li H, Chen JZ, et al. Artificial nerve graft constructed by coculture of activated Schwann cells and human hair keratin for repair of peripheral nerve defects. *Neural Regeneration Research*. 2023;18(5):1118. doi:10.4103/1673-5374.355817

56. Aboushwareb T, Eberli D, Ward C, et al. A keratin biomaterial gel hemostat derived from human hair: Evaluation in a rabbit model of lethal liver injury. *J Biomed Mater Res B Appl Biomater.* 2008;90B(1):45-54. doi:10.1002/jbm.b.31251

57. Yang CM, Huang YJ, Hsu SH. Enhanced autophagy of Adipose-Derived stem cells grown on chitosan substrates. *BioResearch Open Access.* 2015;4(1):89-96. doi:10.1089/biores.2014.0032

58. Sutthasupha P, Promsan S, Thongnak L, et al. Chitosan oligosaccharide mitigates kidney injury in prediabetic rats by improving intestinal barrier and renal autophagy. *Carbohydrate Polymers.* 2022;288:119405. doi:10.1016/j.carbpol.2022.119405

59. Pan Z, Cheng DD, Wei XJ, Li SJ, Guo H, Yang QC. Chitooligosaccharides inhibit tumor progression and induce autophagy through the activation of the p53/mTOR pathway in osteosarcoma. *Carbohydrate Polymers.* 2021;258:117596. doi:10.1016/j.carbpol.2020.117596

60. Wang HJ, Li MQ, Liu W, et al. Gelatin promotes murine fibrosarcoma L929 cell detachment and protects the cells from TNFα-induced cytotoxicity. *Connective Tissue Research.* 2016;57(4):262-269. doi:10.3109/03008207.2016.1146713

61. Murugan S, Amaravadi RK. Methods for Studying Autophagy Within the Tumor Microenvironment. *Adv Exp Med Biol.* 2016;899:145-66. doi: 10.1007/978-3-319-26666-4_9.

62. Davis C, et al. Keratin affects cellular pathways associated with autophagy in human embryonic kidney cells. Presented at: NCTERMS; Nov, 2017; Winston-Salem, NC.

63. Hollars J, et al. Keratin's modulation of protein aggregation and autophagy pathways may underlie its cytoprotective effects. Presented at: The Tissue Engineering and Regenerative Medicine International Society Annual Meeting; Dec, 2019; Orlando, FL.

64. García-Mata R, Bebök Z, Sorscher EJ, Sztul ES. Characterization and dynamics of aggresome formation by a cytosolic GFP-chimera. *J Cell Biol.* 1999;146(6):1239-54. doi: 10.1083/jcb.146.6.1239.

65. N'Diaye E, Kajihara KK, Hsieh I, Morisaki H, Debnath J, Brown EJ. PLIC proteins or ubiquilins regulate autophagy-dependent cell survival during nutrient starvation. *EMBO Reports.* 2009;10(2):173-179. doi:10.1038/embor.2008.238

66. Chemometec. Spilling the secrets: How to count cells with a hemocytometer. Available at: https://chemometec.com/how-to-count-cells-with-a-hemocytometer/. Accessed June 9th, 2024.

67.Graphpad. Tukey and Dunnett methods. Available at: https://www.graphpad.com/guides/prism/latest/statistics/stat_the_methods_of_tukey_and_dunne.htm. Accessed June 9th, 2024.

68. Cox M, Price M, Coan HB. Determination of starvation conditions and timing to induce autophagy in human embryonic kidney cells. Presented at: State of North Carolina Undergraduate Research Conference, Dec, 2022; Wilmington, NC.

69. Owen M, Hatton R. Observing the autophagy process using chemical controls, fluorescent imaging, and cell toxicity assays. Presented at: SoCon Undergraduate Research Forum; Sept, 2022; Spartanburg, SC.

70. Stepanenko AA, Dmitrenko VV. HEK293 in cell biology and cancer research: phenotype, karyotype, tumorigenicity, and stress-induced genome-phenotype evolution. *Gene.* 2015;569(2):182-190. doi:10.1016/j.gene.2015.05.065

71. Lin YC, Boone M, Meuris L, et al. Genome dynamics of the human embryonic kidney 293 lineage in response to cell biology manipulations. *Nature Communications.* 2014;5(1). doi:10.1038/ncomms5767

72. Nash Y, Schmukler E, Trudler D, Pinkas-Kramarski R, Frenkel D. DJ-1 deficiency impairs autophagy and reduces alpha-synuclein phagocytosis by microglia. *Journal of Neurochemistry.* 2017;143(5):584-594. doi:10.1111/jnc.14222

73. Tanida I, Minematsu-Ikeguchi N, Ueno T, Kominami E. Lysosomal turnover, but not a cellular level, of endogenous LC3 is a marker for autophagy. *Autophagy.* 2005;1(2):84-91. doi: 10.4161/auto.1.2.1697.

74. Husak, Z., Dworzak, M.N. Chronic stress induces CD99, suppresses autophagy, and affects spontaneous adipogenesis in human bone marrow stromal cells. *Stem Cell Res Ther.* 8:83 (2017). https://doi.org/10.1186/s13287-017-0532-3

75. Mauthe M, Orhon I, Rocchi C, et al. Chloroquine inhibits autophagic flux by decreasing autophagosome-lysosome fusion. *Autophagy.* 2018;14(8):1435-1455. doi:10.1080/15548627.2018.1474314

76. Jacquin E, Leclerc-Mercier S, Judon C, et al. Pharmacological modulators of autophagy activate a parallel noncanonical pathway driving unconventional LC3 lipidation. *Autophagy.* 2017. May 4;13(5):854–867.

77. Lu S, Sung T, Lin N, et al. Lysosomal adaptation: how cells respond to lysosomotropic compounds. *PloS One.* 2017;12(3):e0173771

78. Wang W, Chen Z, Billiar TR, Stang MT, Gao W. The carboxyl-terminal amino acids render pro-human LC3B migration similar to lipidated LC3B in SDS-PAGE. *PLoS One.* 2013 Sep 10;8(9):e74222. doi: 10.1371/journal.pone.0074222.

79. Novus Biologicals. LC3B antibody - BSA free. Available at: https://www.novusbio.com/products/lc3b-antibody_nb100-2220. Accessed June 9th, 2024.

80. Huang L, Pike D, Sleat DE, Nanda V, Lobel P. Potential pitfalls and solutions for use of fluorescent fusion proteins to study the lysosome. *PLoS One.* 2014 Feb 21;9(2):e88893. doi: 10.1371/journal.pone.0088893.

81. Yim WW, Yamamoto H, Mizushima N. A pulse-chasable reporter processing assay for mammalian autophagic flux with HaloTag. *Elife.* 2022 Aug 8;11:e78923. doi: 10.7554/eLife.78923.

82. Thermo Fisher Scientific. Alexa Fluor Dyes – Across the Spectrum. Available at: https://www.thermofisher.com/us/en/home/brands/molecular-probes/key-molecular-probes-products/alexa-fluor/alexa-fluor-dyes-across-the-spectrum.html. Accessed June 9th, 2024.

83. FPBase. EGFP. Available at: https://www.fpbase.org/protein/egfp/. Accessed June 9th, 2024.

84. FPBase. mCherry. Available at: https://www.fpbase.org/protein/mcherry/. Accessed June 9th, 2024.

85. Katayama H, Yamamoto A, Mizushima N, Yoshimori T, Miyawaki A. GFP-like proteins stably accumulate in lysosomes. *Cell Struct Funct.* 2008;33(1):1-12. doi: 10.1247/csf.07011.

APPENDIX 1: UNCROPPED WESTERN BLOTS

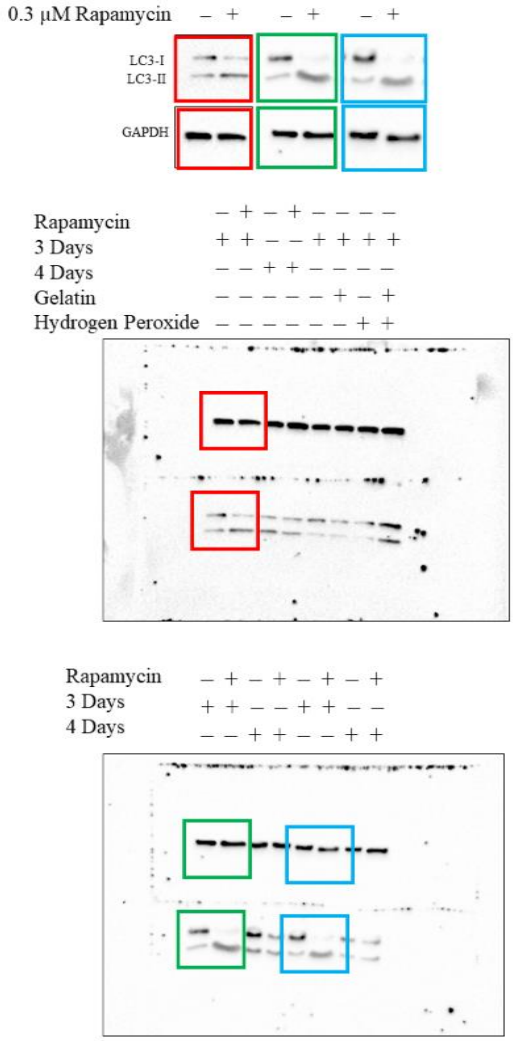

Figure S1.1: Uncropped western blots of nontransfected cells. Cells were dosed with rapamycin and grown for 3 days or 4 days and compared to a no treatment control group. LC3-I, LC3-II, and GAPDH bands of each sample are indicated by the corresponding-colored boxes.

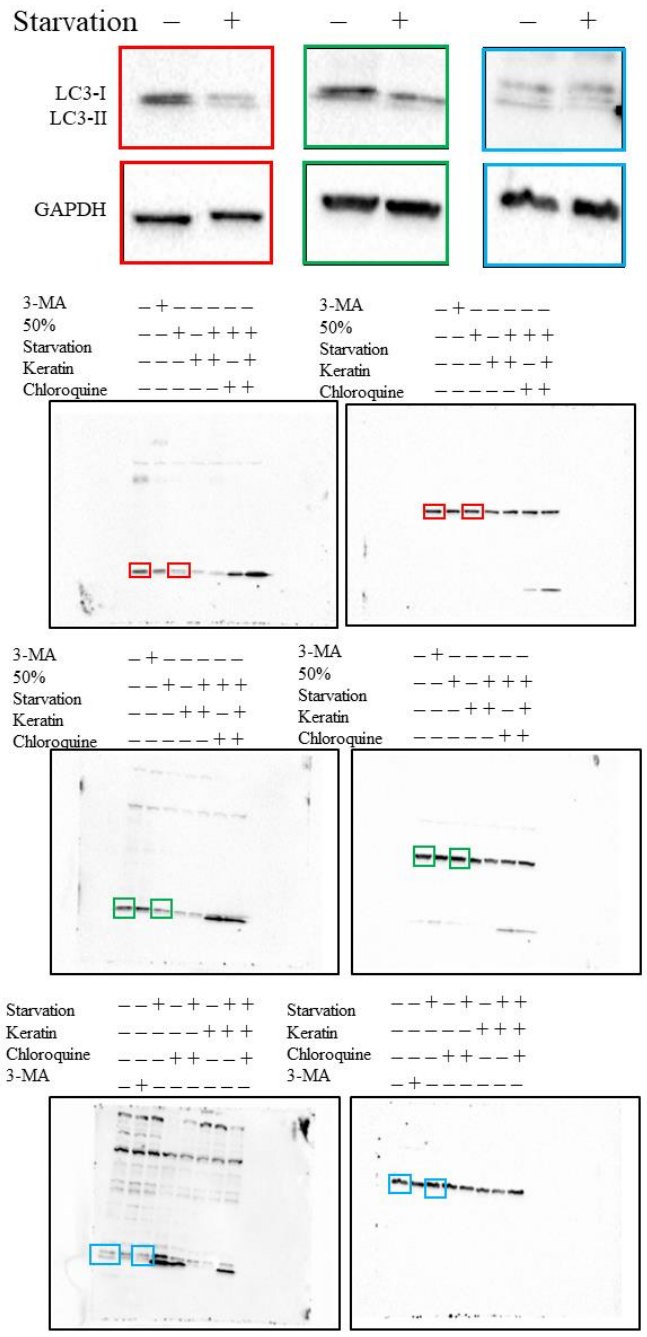

Figure S1.2: Uncropped western blots of nontransfected cells. Cells were dosed with starvation and compared to a no treatment control group. LC3-I, LC3-II, and GAPDH bands of each sample are indicated by the corresponding-colored boxes.

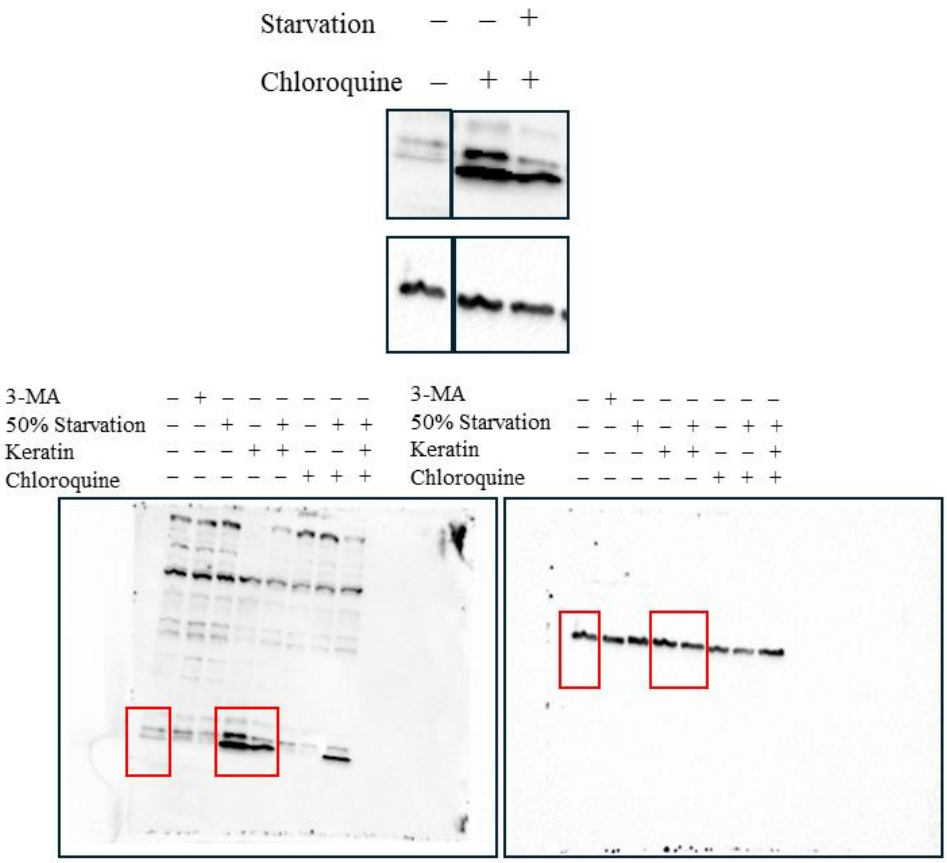

Figure S1.3: Uncropped western blots of nontransfected cells. Cells were dosed with chloroquine and chloroquine plus starvation and compared to a no treatment control group. LC3-I, LC3-II, and GAPDH bands of each sample are indicated by the corresponding-colored boxes.

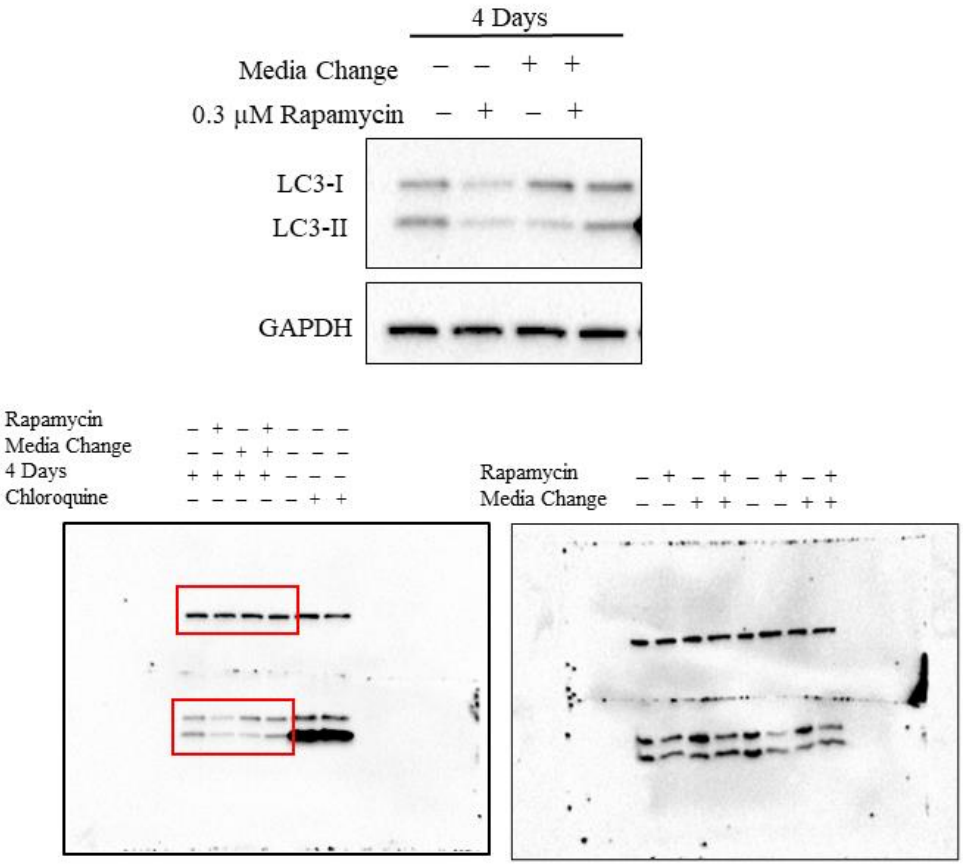

Figure S1.4: Uncropped western blots of nontransfected cells and triplicates. Cells were dosed with rapamycin and a media change. Cells were grown for 4 days and compared to a no treatment control group. LC3-I, LC3-II, and GAPDH bands of each sample are indicated by the corresponding-colored boxes.

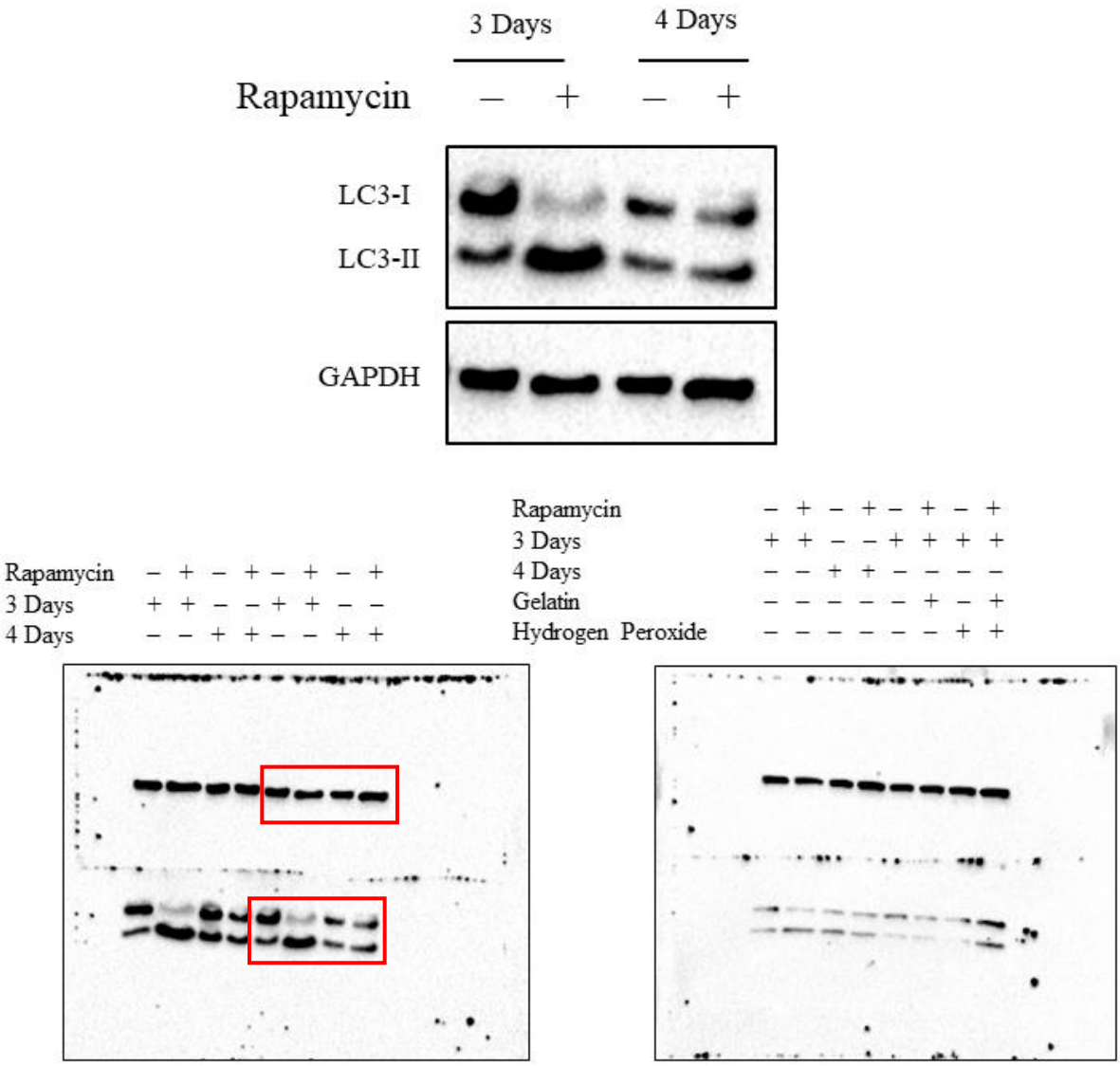

Figure S1.5: Uncropped western blots of nontransfected cells and triplicates. Cells were dosed with rapamycin and grown for 3 days or 4 days and then compared to no treatment control groups. Cropped LC3-I, LC3-II, and GAPDH bands are indicated by the red boxes.

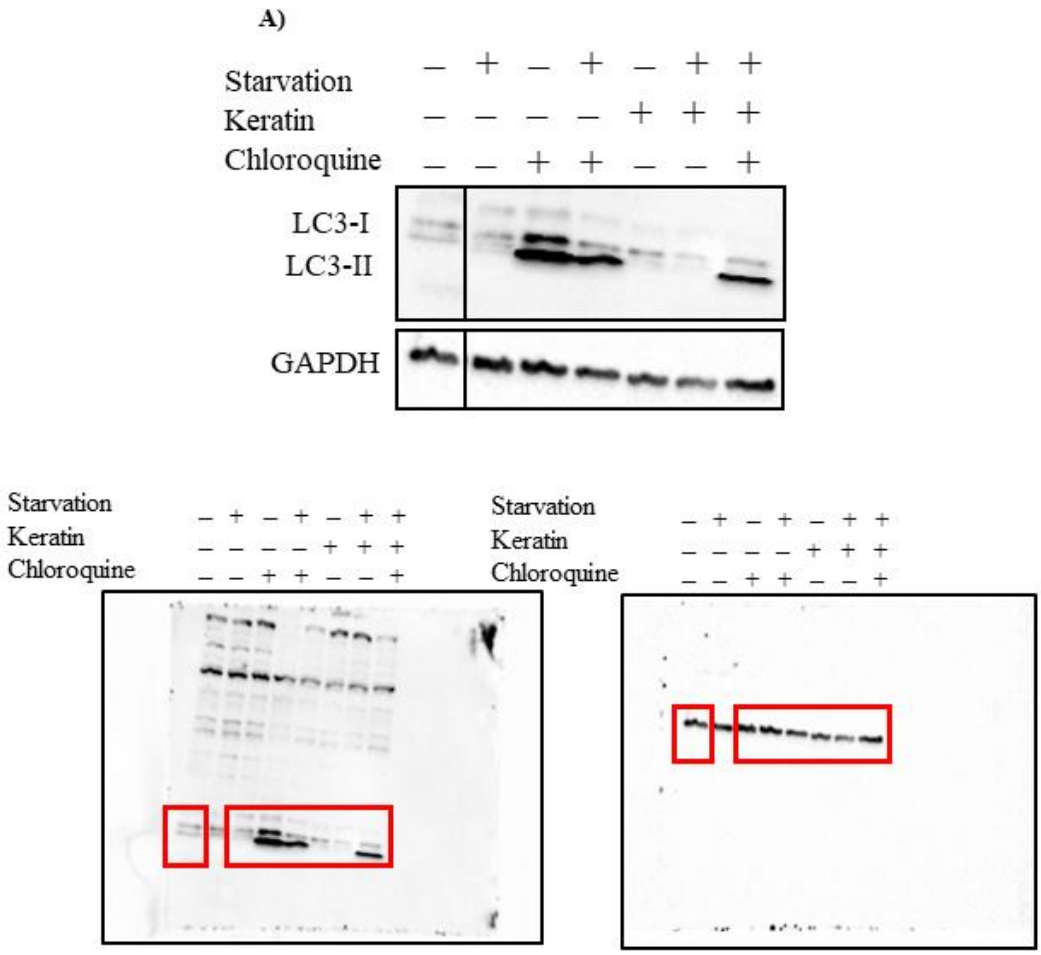

Figure S1.6: Uncropped western blots of nontransfected cells. Cells were dosed with starvation, keratin, chloroquine, or a combination and then compared to no treatment control groups. Cropped LC3-I, LC3-II, and GAPDH bands are indicated by the red boxes.

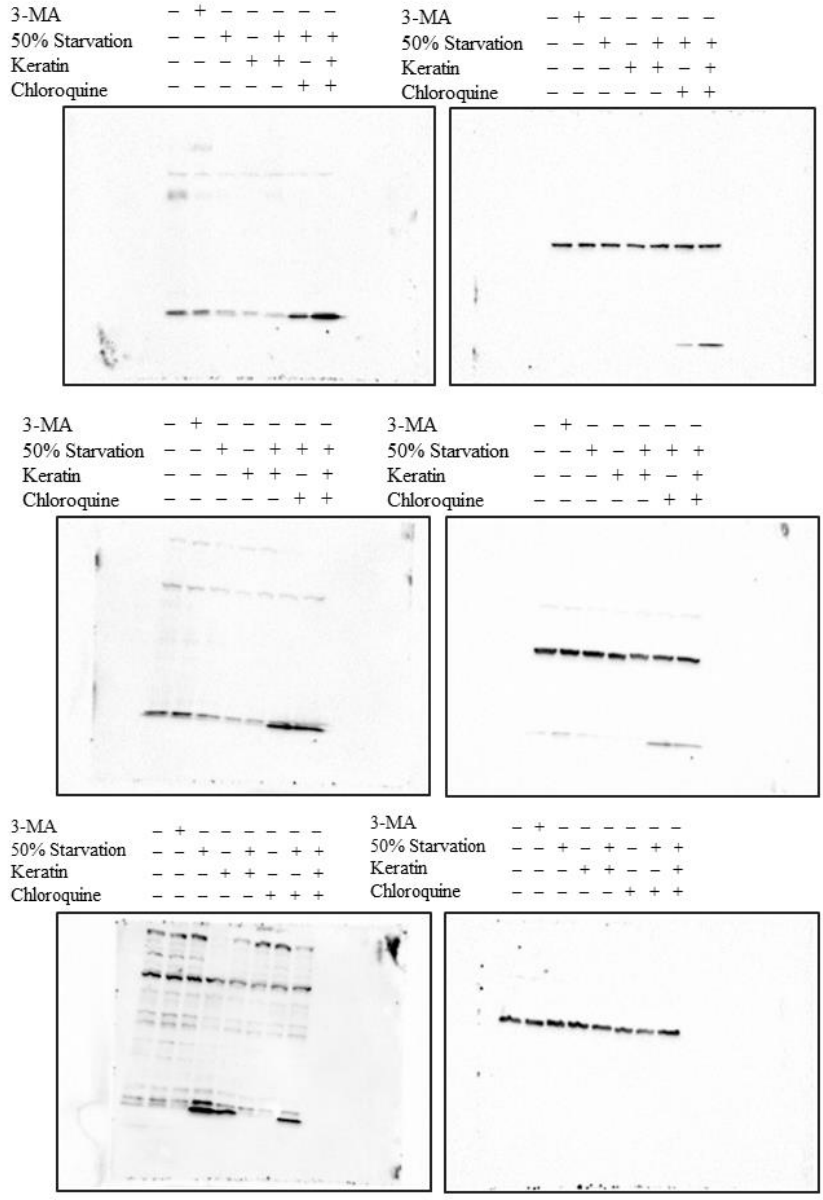

Figure S1.7: Triplicates of uncropped western blots of nontransfected cells. Cells were dosed with starvation, keratin, chloroquine, or a combination and then compared to no treatment control groups.

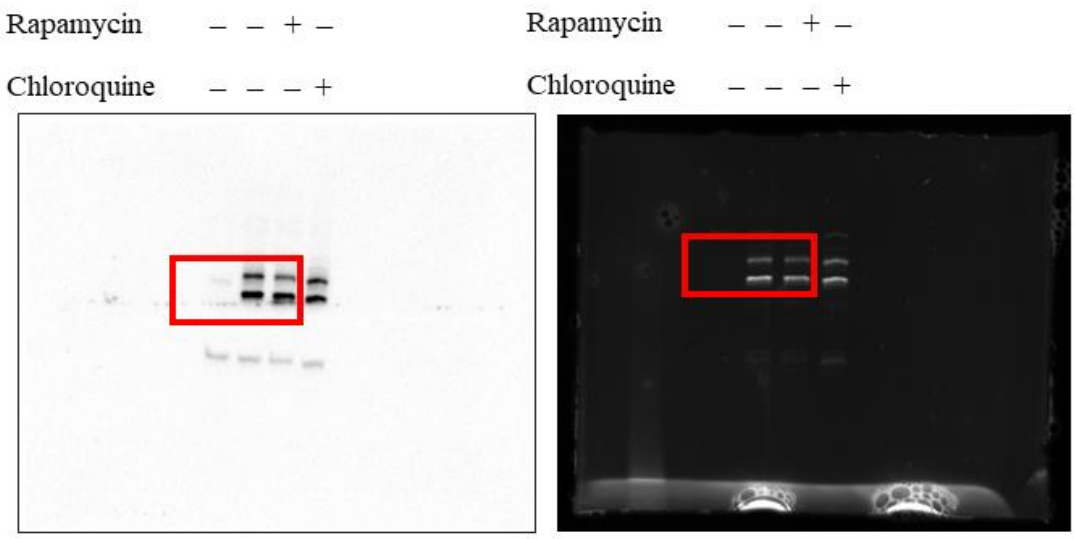

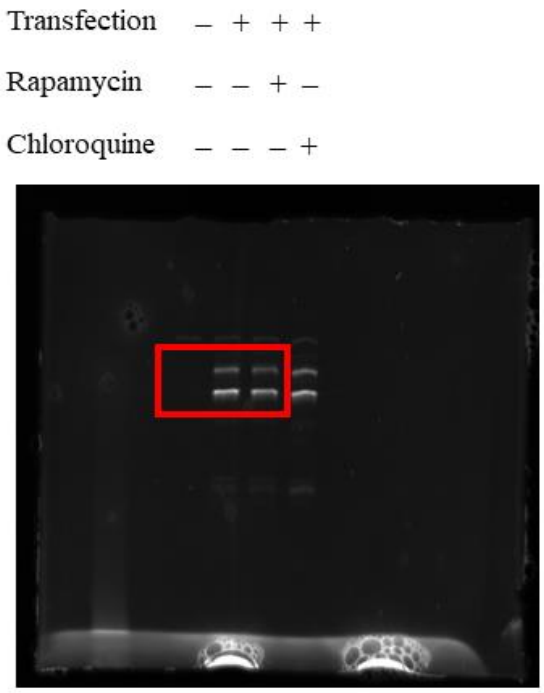

Figure S1.8: Uncropped western blots and in-gel fluorescence of transfected cells dosed with rapamycin and compared to no treatment control groups. The image on the left is a western blot of LC3 proteins. The image on the right is taken with the Alexa 488 filter, while the image in the bottom lefthand corner is taken with the Alexa 546 filter. Cropped LC3-I and LC3-II bands are indicated by the red boxes.

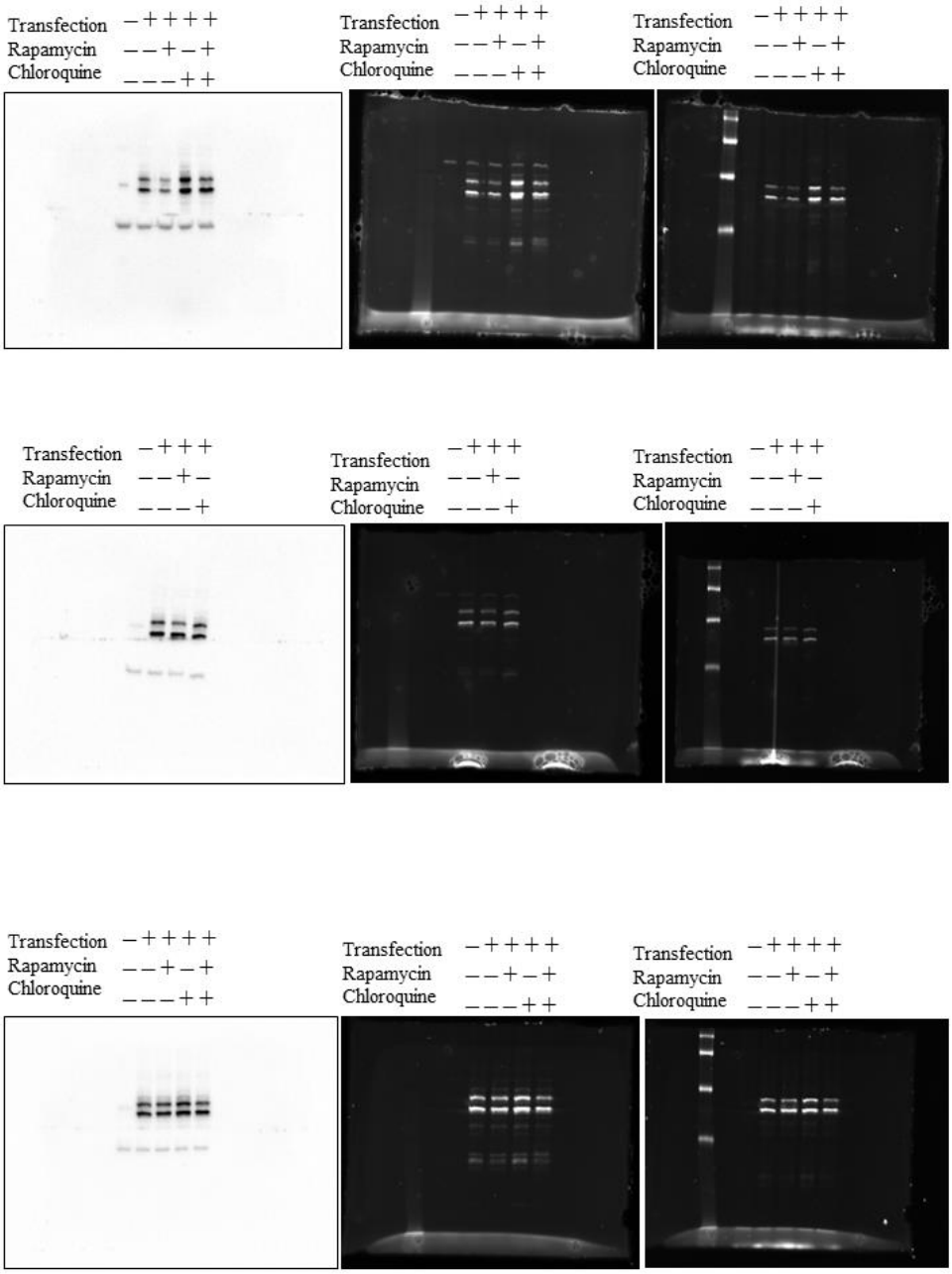

Figure S1.9: Uncropped triplicates of transfected cells treated with rapamycin. Cells were transfected and dosed with rapamycin and compared to no treatment control groups. The images on the left are western blots of LC3 proteins. The images in the middle are taken with the Alexa 488 filter, while the images on the right are taken with the Alexa 546 filter.

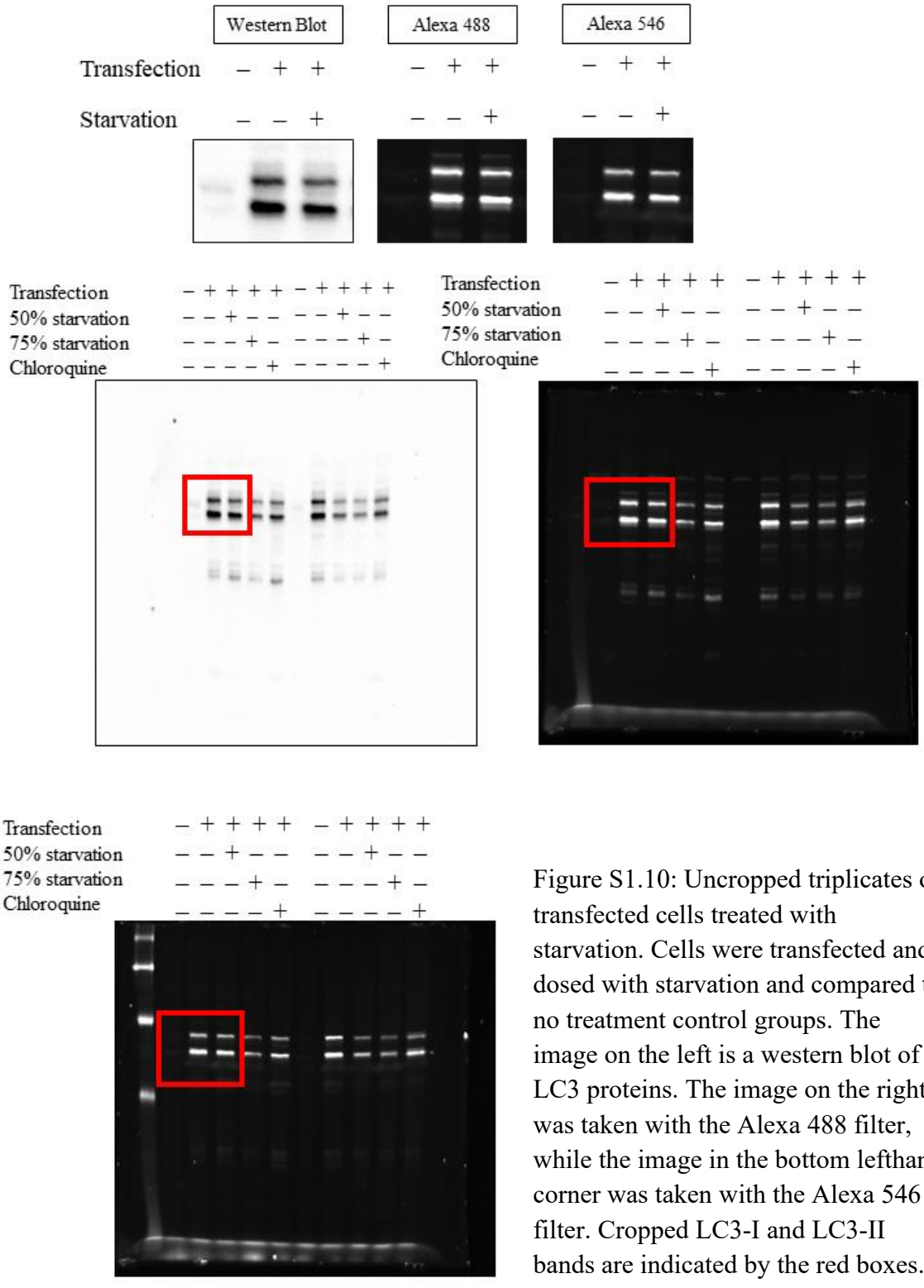

Figure S1.10: Uncropped triplicates of transfected cells treated with starvation. Cells were transfected and dosed with starvation and compared to no treatment control groups. The image on the left is a western blot of LC3 proteins. The image on the right was taken with the Alexa 488 filter, while the image in the bottom lefthand corner was taken with the Alexa 546 filter. Cropped LC3-I and LC3-II bands are indicated by the red boxes.

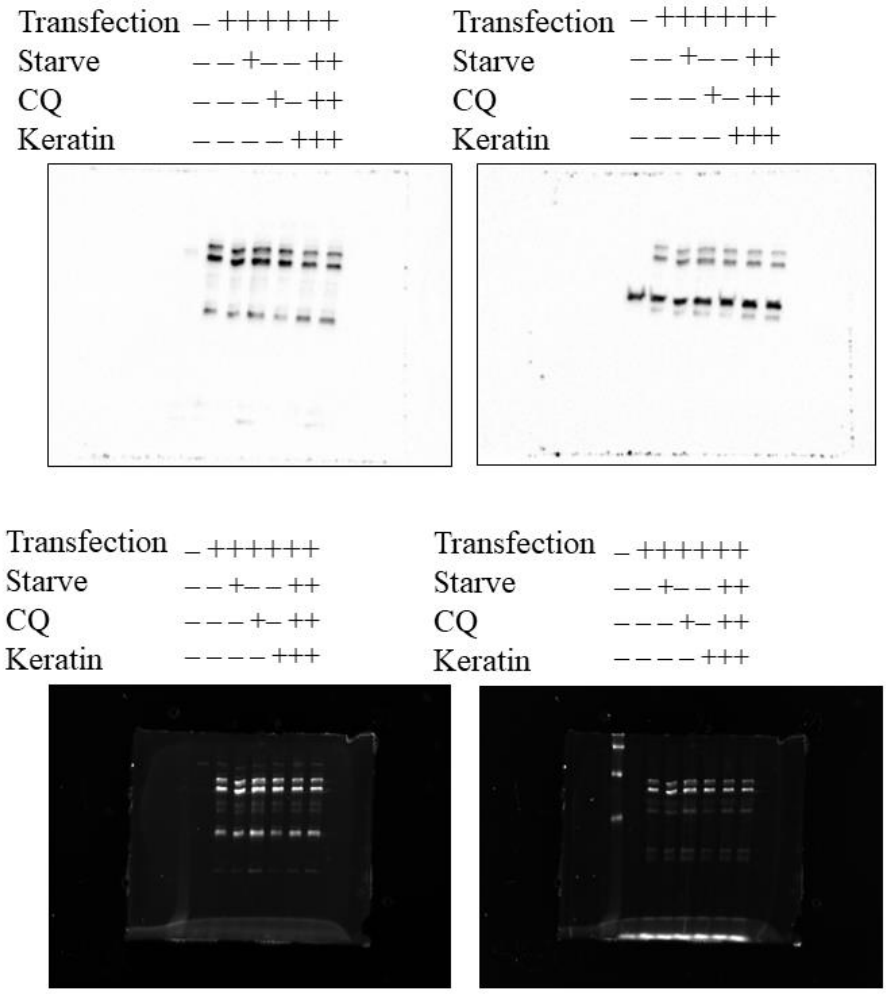

Figure S1.11: Uncropped triplicates of transfected cells treated with starvation. Cells were transfected and dosed with starvation and compared to no treatment control groups. The top row of images are western blots of LC3 proteins. The image to the left was taken with the Alexa 488 filter, while the image to the right was taken with the Alexa 546 filter.

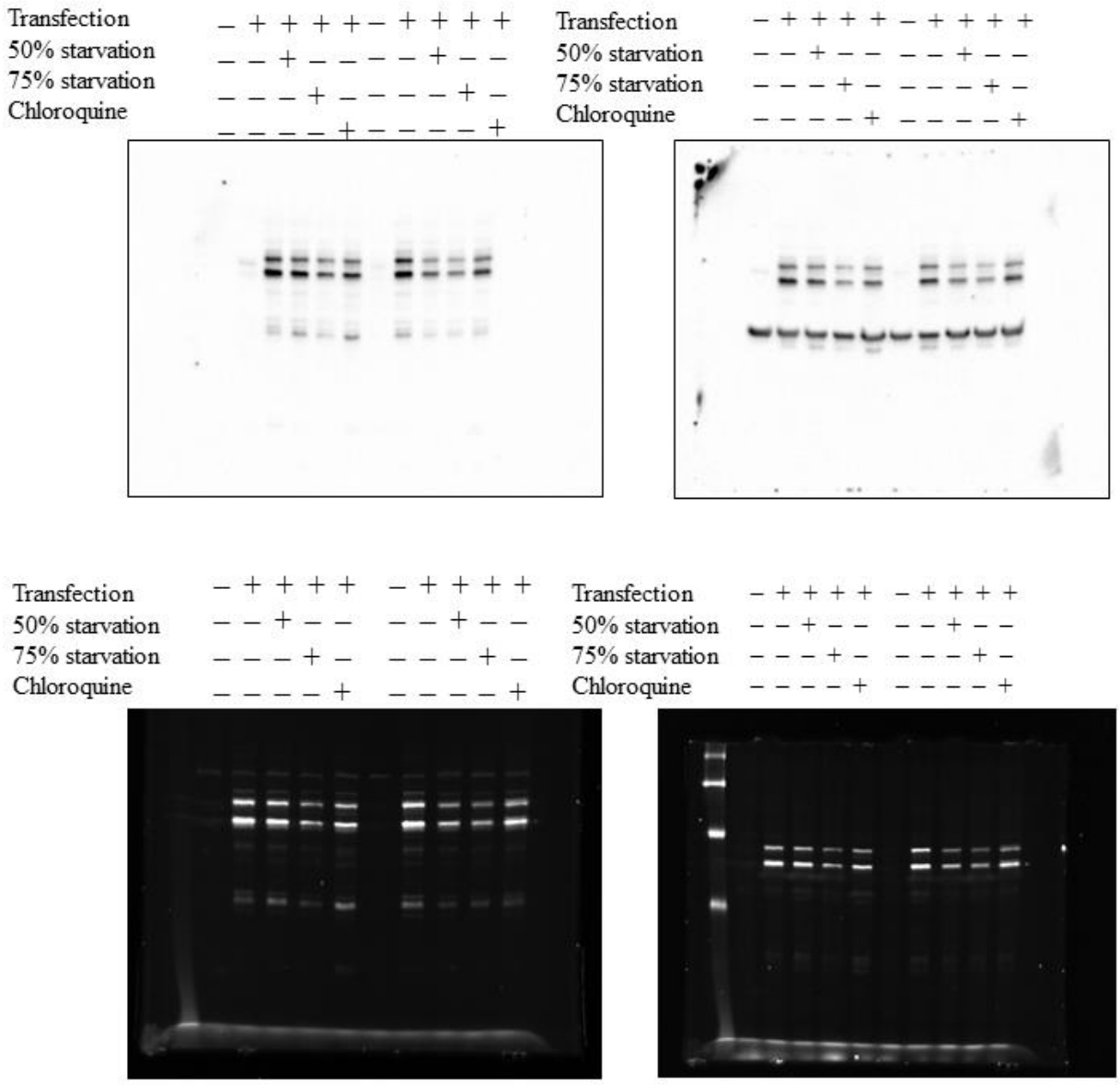

Figure S1.12: Uncropped triplicates of transfected cells treated with starvation. Cells were transfected and dosed with starvation and compared to no treatment control groups. The top row of images are western blots of LC3 proteins. The image to the left was taken with the Alexa 488 filter, while the image to the right was taken with the Alexa 546 filter.

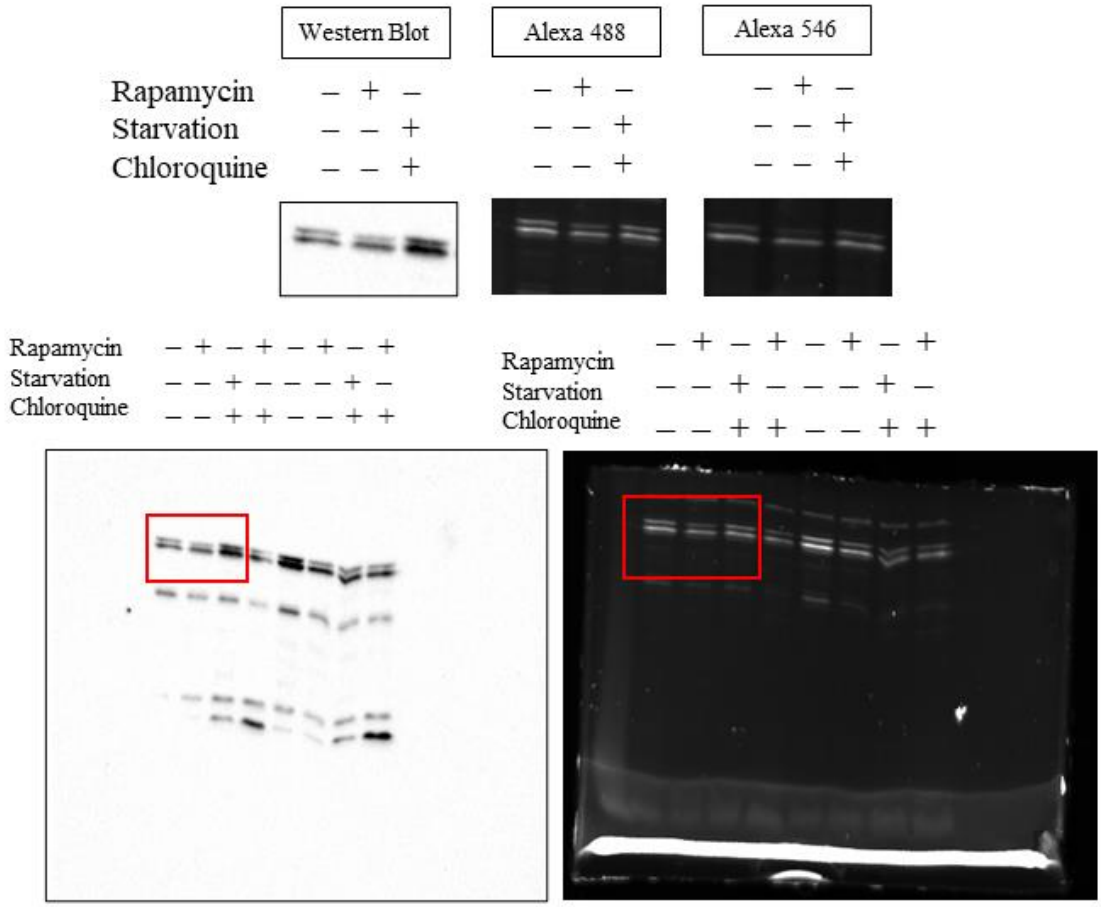

Figure S1.13: Uncropped triplicates of transfected cells treated with starvation and chloroquine. Cells were transfected and dosed with starvation and chloroquine and compared to no treatment control groups and rapamycin-treated groups. The top image to the left is a western blot of LC3 proteins. The image to the right was taken with the Alexa 488 filter, while the bottom lefthand image was taken with the Alexa 546 filter. Cropped LC3-I and LC3-II bands are indicated by the red boxes.

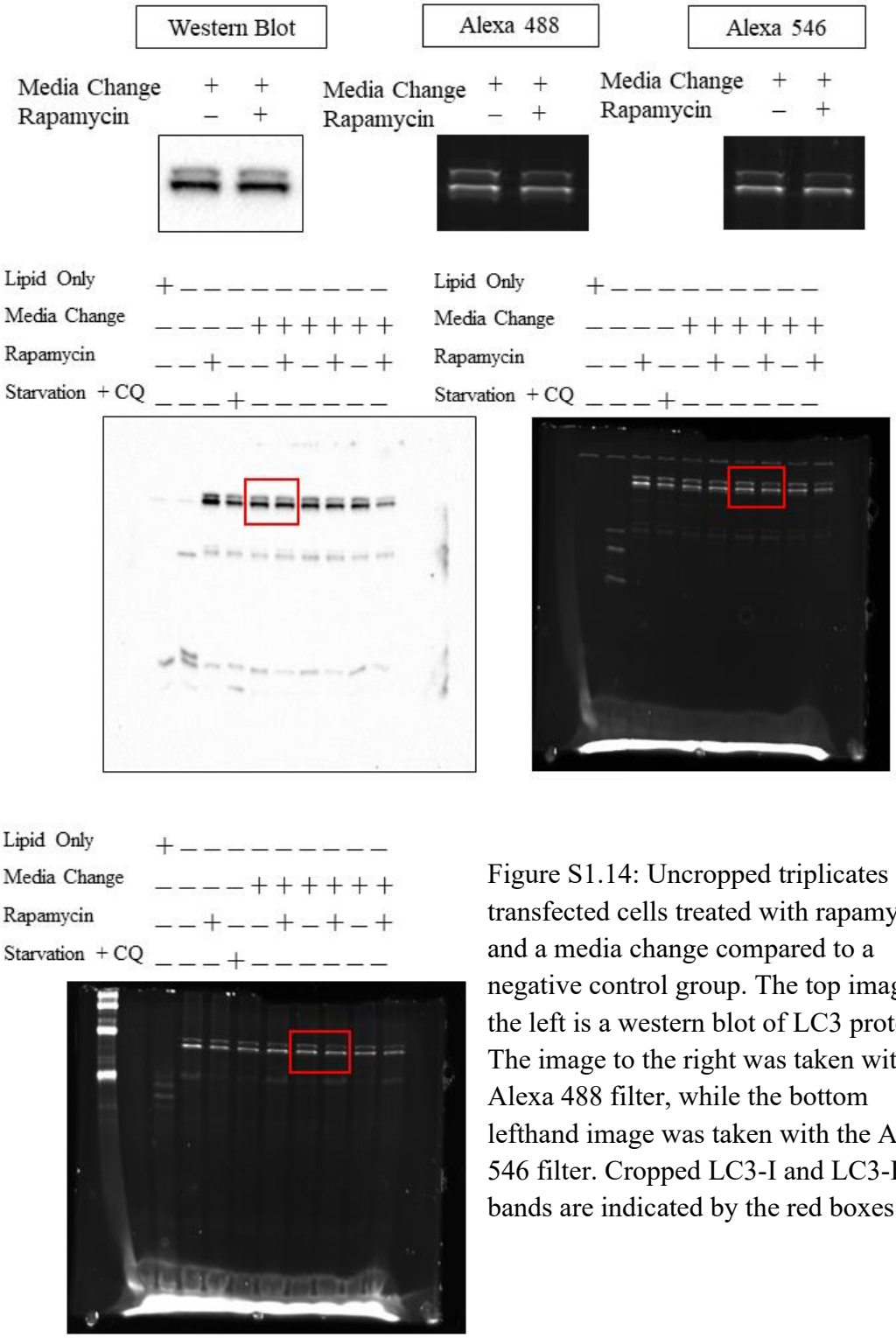

Figure S1.14: Uncropped triplicates of transfected cells treated with rapamycin and a media change compared to a negative control group. The top image to the left is a western blot of LC3 proteins. The image to the right was taken with the Alexa 488 filter, while the bottom lefthand image was taken with the Alexa 546 filter. Cropped LC3-I and LC3-II bands are indicated by the red boxes.

APPENDIX 2: IN-GEL FLUORESCENCE

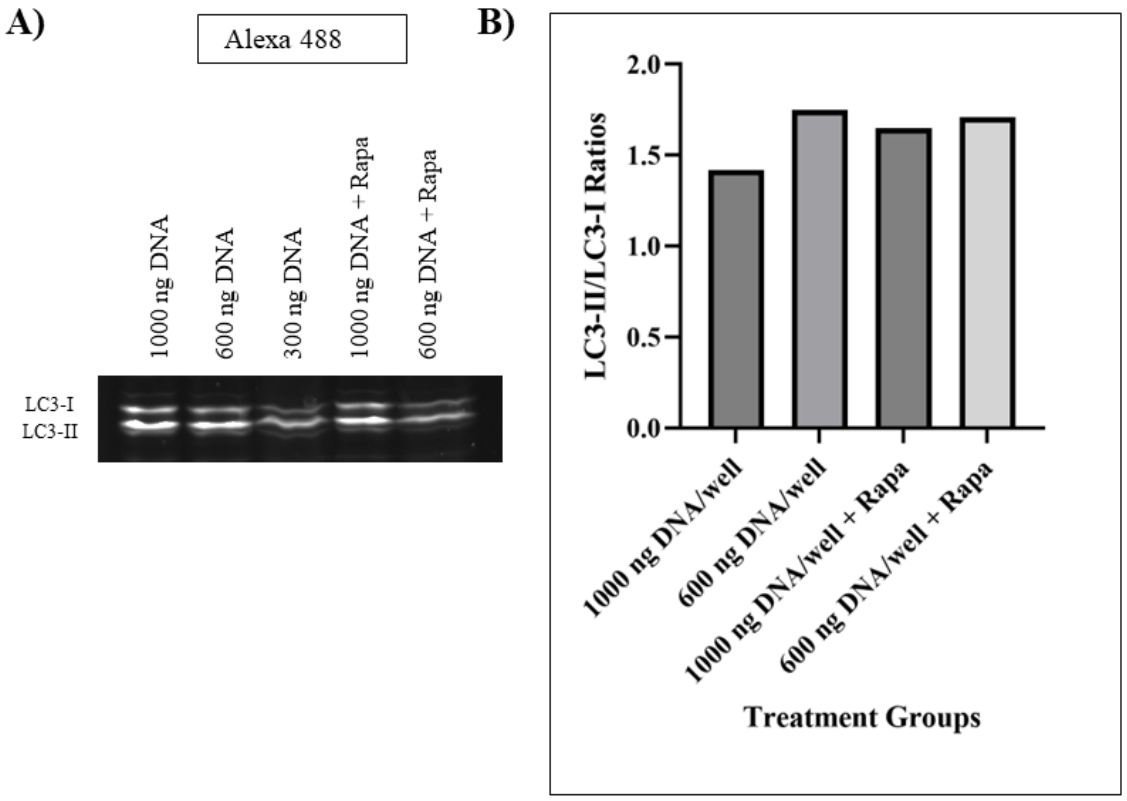

Figure S2.1: Plasmid concentrations and LC3-II/LC3-I ratios. One total experiment was performed. A: HEK 293 cells were transfected with the following plasmid concentrations and treated with rapamycin: 1000 ng DNA/well, 600 ng DNA/well, and 300 ng DNA/well. B: LC3-II/LC3-I ratios for transfected samples.

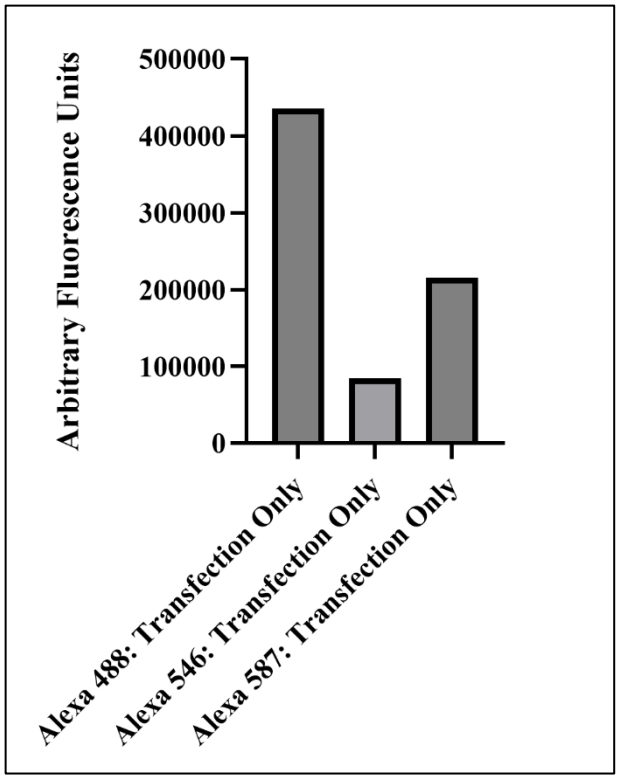

Figure S2.2: Lysate fluorescent intensity values. One total experiment was performed. A: HEK 293 cells were transfected with the mCherry-EGFP-LC3B plasmid and lysed. Fluorescent signal from the lysate was measured on a fluorescent plate reader with three wavelength settings: 488 nm/535 nm (corresponding to the wavelengths for the Alexa Fluor 488 dye), 546 nm/590 nm (corresponding to the wavelengths for the Alexa Fluor 546 dye), and 587 nm/630 nm (corresponding to the optimal wavelengths for mCherry).